SYNTHESIS AND CHARACTERIZATION OF YTTRIUM-BARIUM-COPPER-OXIDE THIN FILMS

A Dissertation

Presented to the Faculty of the Graduate School

of

Yale University

in candidacy for the degree of

Doctor of Philosophy

by

Richard Neil Steinberg

November 1992

ABSTRACT

SYNTHESIS AND CHARACTERIZATION OF YTTRIUM-BARIUM-COPPER-OXIDE THIN FILMS

Richard Neil Steinberg
Yale University
1992

In order to better understand the behavior of the copper oxide high temperature superconductors, it is important to grow high quality thin films of them. Thin film growth is also important for many of the applications that make use of superconductors. In this thesis, I report on methods of $YBa_2Cu_3O_7$ film growth, on characterization of these films, and on preliminary work on device fabrication from them. We have grown films by metal cosputtering, by on-axis high magnetic field sputtering from a composite target, and by off-axis sputtering from a composite target. The effects of oxygen ion bombardment of the growing film and of low oxygen partial pressure during growth are described. As a means of film characterization, resistive and inductive transitions, crystal structure, and critical current density are reported. Film growth through a mechanical contact mask as a means of patterning the films is also described.

Acknowledgements

My accomplishments here over the last six years here would not have been possible without the help of many people. They generously guided, assisted, and supported me and I am forever grateful.

First and foremost, I would like to thank my advisor, Professor Daniel E. Prober. His skill as a scientist is only matched by his genuine concern for the well being of his students. No words I can write here can do justice for what Dan has provided for me as a mentor, a boss, and a friend. I leave here with the deepest respect for Dan.

I thank the other members of my dissertation committee: Professors Victor E. Henrich, Nicholas Read, and Robert G. Wheeler. Their time consuming examination of this thesis and constructive feedback is greatly appreciated. I also owe a great deal of thanks to Dr. Julia M. Phillips of AT&T Bell Laboratories for generously agreeing to be my outside reader. Her careful analysis of my work and subsequent conversation with me about it before my defense was invaluable.

This research was supported by Olin Corporation and by the CT Department of Higher Education. I would like to thank Ed Cooney and Dr. Bruce Guenin of Olin Metals Research Laboratory, Professors Joseph Budnick and Fred Otter of University of Connecticut, and Dr. Michele Migliuolo of Kurt J. Lesker Co. for their collaboration on this work.

It has been a privilege to have had the opportunity to know and work with Dr. Stanley Mroczkowski. I have been very fortunate to listen to his physical insights regarding crystal chemistry and to have his energetic friendship.

It is with great pleasure that I acknowledge the countless students with whom I have had the privilege to work, discuss issues in physics, and even debate topics ranging from international politics to the meaning of life. I would like to

especially thank a few in particular. Venkat Chandrasekhar was an invaluable help during my first few years here. Whenever there was something I did not understand about anything from low temperature physics to group theory, he knew the answer and was eager to help. Steve Klepper was my officemate for four years. His friendship was enjoyable and he was always happy and able to assist me with any problem. Aaron Datesman constructed the J_c measurement apparatus with me which worked very nicely. Curt Richter also helped with this project as well as with commuting. Most of all, I would like to thank Jim McCambridge. I have benefitted from and enjoyed the many, many hours I have spent with Jim as a coworker and a friend. His smile and attitude have been pleasures I won't soon forget.

Dean Face and Elie Track are former graduate students of Dan that I have had the pleasure of knowing. They have generously provided assistance and advice regarding YBCO film growth.

I owe Dr. Edith MacMullen a great personal thanks. Her presence has been largely responsible for redirecting my career path in a direction that has me very excited. I am a much better person for having known Edie.

Above all, I thank my family. A day does not go by that I do not think that if I had merely sensational parents that I would not have come close to achieving what I have personally or professionally. Their undying love and support have made everything I have achieved possible. The birth of my son Matthew in 1990 gave me renewed spirit and energy. The joy he brings to me each day makes life a pleasure. Most of all, I thank my wife Margot. The support she has given, particularly through the last very difficult months, has been tremendous. She is my strength, my motivation, and my purpose. If all I ever have in life is the love I share with her, than I have more than any one person deserves.

Table of Contents

Acknowledgements ii

List of Common Symbols and Abbreviations vii

List of Figures ix

List of Tables xi

I. INTRODUCTION 1

A. Overview 1

B. High Temperature Superconductivity 4

C. Applications of Superconductivity 5

D. Research Goals 7

II. SUPERCONDUCTIVITY 10

III. $YBa_2Cu_3O_{7-\delta}$ 16

A. Properties of $YBa_2Cu_3O_{7-\delta}$ 16

1. Crystal Structure 16

2. Bulk Synthesis 19

3. Electronic and Magnetic Structure 21

4. Normal State Resistivity 22

5. Superconducting Properties 25

6. Substitutions and Defects 26

B. Synthesis of YBCO Thin Films 30

1. Implications of YBCO Properties 30
2. Synthesis Techniques 34

IV. FILMS GROWN BY COSPUTTERING 39
A. Deposition System Design 40
B. Post annealed films 45
C. *In situ* films 47
1. Sputtering and Resputtering 47
2. Deposition Conditions 49
3. Results 56
4. Discussion 58

V. FILMS GROWN BY COMPOSITE TARGET SPUTTERING 66
A. Sputtering with a High Strength Magnet 66
B. Off-axis Sputtering 69
1. System Modifications 69
2. Deposition Conditions 75
3. Results 77
4. Discussion 90

VI. SUPERCONDUCTING DEVICES 92
A. Superconducting Weak Links 92
B. YBCO Weak Links 94
C. Device Design/Fabrication Progress 99
1. Device Design 99

2. Advantages and Disadvantages 99
3. Progress 101
4. Remaining Work 104

VII. CONCLUSIONS 107

APPENDIX A: Measurements of Superconductivity in Small Samples 110
APPENDIX B: Cryostat Design 115
APPENDIX C: Post-Annealed Cosputtered Films 118
APPENDIX D: *In Situ* Cosputtered Films 121
APPENDIX E: Off-Axis Composite Target Sputtered Films 129

References 142

List of Common Symbols and Abbreviations

δ	Oxygen Deficiency in Formula $YBa_2Cu_3O_{7-\delta}$
δ	Normal State Skin Depth
Δ	Superconducting Energy Gap
λ	Magnetic Penetration Depth
ρ_{ab}	Resistivity in the ab Planes of YBCO
ρ_c	Resistivity in the c Direction of YBCO
Ω	Ohms
ξ	Superconducting Coherence Length
a	a Crystallographic Direction of the YBCO Crystal
ab	ab Planes of the YBCO Crystal
b	b Crystallographic Direction of the YBCO Crystal
Å	Angstroms (10^{-8} cm)
A	Amperes
Ag	Silver
Ar	Argon
Au	Gold
Ba	Barium
BaCu	Barium-Copper Alloy
BCS	Bardeen, Cooper, and Schrieffer
c	c Crystallographic Direction of the YBCO Crystal
°C	Degrees Celsius
Cu	Copper
EDS	Energy Dispersive Spectroscopy
Fe	Iron
G	Gauss
GL	Ginzburg and Landau
$\hbar$	Reduced Planck Constant
hr	hour
H_c	Critical Magnetic Field (Type I Superconductor)
H_{c1}	Lower Critical Magnetic Field (Type II Superconductor)
H_{c2}	Upper Critical Magnetic Field (Type II Superconductor)
I	Current
I_c	Critical Current

ICP	Inductively Coupled Plasma Atomic Emission Spectroscopy
J_c	Critical Current Density
k_B	Boltzman Constant
K	Kelvin
LAO	$LaAlO_3$
mil	0.001 inches
min	Minute
mT	10^{-3} Torr
O	Oxygen
P	Pressure
PBCO	$PrBa_2Cu_3O_{7-\delta}$
RBS	Rutherford Backscattering Spectroscopy
RSJ	Resistively Shunted Junction
sccm	Standard Cubic Centimeters per Minute
SIS	Superconductor - Insulator - Superconductor Junction
SNS	Superconductor - Normal Metal - Superconductor Junction
SQUID	Superconducting QUantum Interference Device
STO	$SrTiO_3$
T	Temperature
T	Tesla
T_c	Critical Transition Temperature
T_{dep}	Deposition Temperature
V	Voltage
W	Watts
Y	Yttrium
YBCO	$YBa_2Cu_3O_7$

List of Figures

Figure		Page
3.1	Unit cell of YBCO	17
3.2	Crystal structure of YBCO	18
3.3	Unit cell of perovskite crystal structure	18
3.4	Phase diagram of YBCO	23
3.5	Anisotropic resistivity of YBCO single crystal	24
3.6	Resistivity of Fe doped YBCO	29
3.7	Crystal structure of twin boundary	31
4.1	Front view of deposition system	41
4.2	Top view of deposition system	42
4.3	Resistance vs. temperature of post-annealed cosputtered film	46
4.4	Schematic of on-axis sputter deposition	48
4.5	Gas flow - electrical flow analogy	52
4.6	Schematic of off-axis sputter deposition	55
4.7	On-axis vs. off-axis cosputtered film resistive transition comparison	57
4.8	x-ray diffraction pattern of cosputtered film	59
4.9	Resistance vs. temperature for a Ba deficient cosputtered film	61
4.10	Pressure-temperature phase diagram of YBCO	62
4.11	Y:Ba ratio vs. Y sputter gun power	64
5.1	Rate vs. target-substrate distance	70
5.2	System diagram - composite target sputtering	72
5.3	Resistance vs. temperature for Fe contaminated film	74

5.4	Ba:Y vs. deposition pressure	80
5.5	R = 0 temperature vs. substrate temperature	81
5.6	Ba:Y vs. gun angle	82
5.7	R = 0 temperature vs. gun angle	84
5.8	Rate vs. gun angle	85
5.9	Resistance vs. temperature for off-axis composite target film	87
5.10	Mutual inductance vs. temperature for off-axis composite target film	88
5.11	x-ray diffraction pattern for off-axis composite target film	89
5.12	Schematic of J_c measurement apparatus	91
6.1	YBCO weak links	96
6.2	Weak link processing steps	100
6.3	Mechanical mask design	103
6.4	Resistance vs. temperature for YBCO stripe	105
6.5	Mutual inductance vs. temperature for YBCO stripe	106
A.1	Small sample T_c measurement apparatus schematic	111
A.2	V_0 vs. frequency for small sample T_c measurement	113
A.3	V_0 vs. temperature showing superconducting transition	114
B.1	Schematic of sample measurement cryostat	116

List of Tables

Table		Page
3.1	Superconducting parameters	27
3.2	Crystal properties of YBCO compared to substrates used	33
4.1	Definition of variables in gas flow/electrical analogy	53
5.1	Summary of high strength magnet sputtering	68
5.2	Orthogonal table - example	76
5.3	Orthogonal table - off-axis sputtering	78
C.1	Post-annealed cosputtered films	119
D.1	*In Situ* Cosputtered Films	122
E.1	Off-Axis Composite Target Sputtered Films	130

I. INTRODUCTION

A. Overview

Since the discovery of superconductivity in 1911 [Onnes (1911)], the field has been scientifically interesting and technologically applicable. In 1986, superconductivity was discovered at record temperatures in a new class of superconductors [Bednorz and Mueller (1986)]. In 1987, for the first time superconductivity was possible at temperatures above the boiling point of liquid nitrogen (77 K). Wu *et al.* (1987) reported finding superconductivity above 90 K in what was later identified [by Cava *et al.* (1987)] as $YBa_2Cu_3O_7$ (YBCO). Before 1987, no material superconducted above 23 K. Since the breakthroughs in 1986-87, many in the scientific community have devoted their efforts to advancing the understanding of these new materials, improving the ability to process them, and attempting to exploit their properties in practical and/or interesting ways. Tremendous attention has been paid by the general public to these high temperature superconductors, particularly in the first few years following the initial discoveries. Results have been reported by The New York Times, The Wall Street Journal, Business Week, and CNN. While many of the early predictions for applications were exaggerated, some applications for the new class of superconductors seem imminent, and the potential for more spectacular uses persists. Furthermore, no conclusive theory describing these scientifically fascinating materials has yet emerged. For these reasons, in 1987, we set out to further study the properties of YBCO.

When I began my research in the summer of 1987, news of the new superconductors was electrifying the scientific community while breakthroughs were being reported at a staggering rate. Initially, I redesigned a cryostat to measure the superconducting transitions of small YBCO superconductors being grown at Yale by Dr. Stanley Mroczkowski as well as by our collaborators at Olin Metals Research Laboratories (1). This cryostat became the one eventually used to measure YBCO thin films later grown here. The small-sample measurement technique is described in Appendix A. The cryostat used for all our work on high temperature superconductivity is detailed in Appendix B.

Many of the applications and much of the understanding of the high temperature superconductors stem from growth of high quality thin films and fabrication of devices from these films. However, thin film growth has been and continues to be very challenging. Device fabrication by traditional methods of film growth and patterning has proven to be an even greater challenge. Since 1988, it has been my intention to grow high quality thin films of YBCO, fabricate superconducting devices from them, and study the electrical characteristics of these devices.

The rest of this chapter serves to introduce and motivate the work covered. After describing the format of the thesis, a brief history of high temperature (also referred to as high T_c) superconductivity is given. Then, real, emerging, and potential applications of superconductors are described. Finally, the goals of our work in high temperature superconducting film growth and characterization are given.

A brief overview of superconductivity is given in Chapter II. Basic properties of superconductivity are described, especially those related to this

thesis. How the behavior of the new superconductors differs from the behavior of traditional superconductors is introduced.

In Chapter III, those properties of the new ceramic high temperature superconductors, particularly YBCO, which are relevant to the work presented are given. The unique crystalline, normal state electrical, and superconducting properties are described. The conditions necessary for growing thin films and the different growth methods used here as well as elsewhere are considered.

Chapter IV details our work on thin films grown by simultaneously sputtering from three metal targets (cosputtering). First, the deposition system used is described in detail. Next, films grown by ambient temperature deposition followed by an oxygen anneal are described. Finally, films grown *in situ* are described. By *in situ*, I mean they are grown at high temperature in the presence of oxygen so that the desired phase of YBCO grows as deposited. The results of *in situ* metal cosputered YBCO films presented in this thesis has not been reported anywhere else at the time of this writing.

Chapter V details our work on thin film growth by sputtering from a single target of YBCO. Two such methods are described. In the first, a high strength magnet is used in the sputter gun instead of the conventional strength magnet. For this method, the sputter gun is pointed at the substrate on which the film is growing. In the second method, a conventional strength magnet is used, but the sputter gun is pointed away from the substrate. We had far more success with the second method.

Superconducting devices are described in Chapter VI. Conventional superconducting weak links are described first. Next, an overview of the experimental work done in fabricating and measuring YBCO weak links by

other groups in the field is given. Although we have not succeeded in making a YBCO weak link here, the details of our progress towards this and the work that remains are given.

Finally, a summary and conclusion of the work described in this thesis is given in Chapter 7. Also given is a current status of the high T_c effort.

B. High Temperature Superconductivity

Ever since its discovery, there has been a quest to find superconductors at higher temperatures. The reason for this is that to take practical advantage of the fantastic properties of superconductors, it would be more attractive if the problem of cooling the material were not as great. Many scientists have searched for materials with ever higher critical transition temperatures with the hope that the field would move past just the research laboratory and into the marketplace. Specific applications, both realized and potential, are given in the next section.

Unfortunately, the field of high temperature superconductivity has been plagued by unsubstantiated claims. In 1946, superconductivity was reported at 185 K in rapidly cooled dilute solutions of alkali metals in liquid ammonia [Ogg (1946)]. In 1978, there was a Russian report of superconductivity in CuCl near 140 K [Brandt *et al.* (1978)]. This time, precedent was set when the validity and importance of the finding was debated in the New York Times. In 1983, there was a report from Japan of superconductivity at 200 K in a Nb layer grown on Si [Ogushi *et al.* (1983)]. These are just of few of the many reports of superconductivity that have not been substantiated.

For this reason, Bednorz and Mueller were cautious when they reported "Possible High T_c Superconductivity in the Ba-La-Cu-O System" above 30 K in 1986. Their results were soon reproduced. In 1987, they were awarded the Nobel Prize in Physics for their work. Superconductivity was soon discovered and reproduced above the boiling point of nitrogen (77 K) in another layered copper-oxide system, Y-Ba-Cu-O [Wu et al. (1987)]. Next, superconductivity was found in the Bi-Ca-Sr-Cu-O system above 100 K [Maeda *et al.* (1988)]. Then, superconductivity was found in the Tl-Ca-Ba-Cu-O system at about 120 K [Sheng and Hermann (1988)]. These four systems are similar because of the presence of Cu-O planes, which will be described in Chapter III.

Currently there are other systems which show evidence of high temperature superconductivity. These include K doped C_{60} (fullerenes) [Hebard *et al.* (1991)], $Ba_{1-x}K_xBiO_4$ (bismuthates) [Matheiss *et al.* (1988)], and organic superconductors [Uemura *et al.* (1991)]. These interesting systems are still being researched but are not covered in this thesis. Finally, there is a recent report by Malik *et al.* (1992) (Quaid-i-Azam University, Pakistan) of superconductivity over 300 K in $Y_{0.3}Ba_{0.7-x}Na_xCuO_{3-y}$. Time will tell if this finding is accurate and can be reproduced.

C. Applications of Superconductivity

With their unique electrical behavior, superconductors have properties which can be exploited in practical applications. These generally fall into two classes: those based on bulk superconductors such as wires, and those based on devices and other patterns fabricated from thin films. Some have been

For this reason, Bednorz and Mueller were cautious when they reported "Possible High T_c Superconductivity in the Ba-La-Cu-O System" above 30 K in 1986. Their results were soon reproduced. In 1987, they were awarded the Nobel Prize in Physics for their work. Superconductivity was soon discovered and reproduced above the boiling point of nitrogen (77 K) in another layered copper-oxide system, Y-Ba-Cu-O [Wu et al. (1987)]. Next, superconductivity was found in the Bi-Ca-Sr-Cu-O system above 100 K [Maeda *et al.* (1988)]. Then, superconductivity was found in the Tl-Ca-Ba-Cu-O system at about 120 K [Sheng and Hermann (1988)]. These four systems are similar because of the presence of Cu-O planes, which will be described in Chapter III.

Currently there are other systems which show evidence of high temperature superconductivity. These include K doped C_{60} (fullerenes) [Hebard *et al.* (1991)], $Ba_{1-x}K_xBiO_4$ (bismuthates) [Matheiss *et al.* (1988)], and organic superconductors [Uemura *et al.* (1991)]. These interesting systems are still being researched but are not covered in this thesis. Finally, there is a recent report by Malik *et al.* (1992) (Quaid-i-Azam University, Pakistan) of superconductivity over 300 K in $Y_{0.3}Ba_{0.7-x}Na_xCuO_{3-y}$. Time will tell if this finding is accurate and can be reproduced.

C. Applications of Superconductivity

With their unique electrical behavior, superconductors have properties which can be exploited in practical applications. These generally fall into two classes: those based on bulk superconductors such as wires, and those based on devices and other patterns fabricated from thin films. Some have been

realized, some appear near ready for market, and others are possible in the future. While most of the products currently on the market that include superconductors contain conventional low T_c materials, some products containing high T_c materials are emerging.

By far the most prevalent application of superconductors today is its use as wire. In particular, because superconductors can carry large currents without dissipation, superconducting wire is used in creating high-strength magnetic fields. For example, medical magnetic resonance imaging machines are becoming invaluable diagnostic tools. They require large (more than 1 Tesla), uniform (part per million) magnetic fields over a body size that only a superconducting magnet could provide. Superconducting magnets are also currently used in scientific research and for a prototype magnetically levitated train in Japan.

Today's magnets use conventional superconductor (pre-1986) wire technology. Wires of high T_c superconductors are potentially even more attractive because of their much higher operating temperature and potential large current carrying capacity, even in strong magnetic fields. J_c (the amount of current per unit area that a superconductor can carry) near 10^5 A/cm^2 at 77 K with slow fall off in magnetic field up to 4 T in bulk material has been reported [Zhou *et al.* (1991)]. Unfortunately, fabrication into wire is very difficult. As will be discussed in the next section, these materials are ceramic, anisotropic, and need high temperature processing. Despite these difficulties, progress has been made and short wires have been produced.

Many realized and potential applications of superconductivity stem from microelectronics. Here, the superconductor is deposited as a thin film which

can then be patterned into useful devices or interconnects. Devices whose unique properties are only found in superconductors include tunnel junctions described in Chapters II and VI, and SQUID's discussed briefly below. Furthermore, characterization of these films and of devices fabricated from them is important in understanding the properties of these superconductors. This understanding is in turn important in the advancement of bulk applications.

Superconducting QUantum Interference Devices (SQUID's) are the most sensitive detectors of magnetic fields. A SQUID is a ring of superconductor with one or more weak links. It works because of the phase coherence of the superconducting electrons and the effect of the weak links on this phase. Applications include biomedical and geophysical uses. A prototype high T_c SQUID magnetometer with all components working at 77 K has been demonstrated [Oh et al. (1991)].

The unique current-voltage relationship of superconducting tunnel junctions (or other weakly linked superconductors) allow for many potential applications. These include high frequency radiation detection, high speed - low power dissipation digital logic and memory device technology, and voltage standards. Hypres, Inc. of Elmsford, N.Y. has developed a high speed oscilloscope based on Nb (low T_c) tunnel junctions. However, progress in fabricating YBCO tunnel junctions has been slow and is discussed in Chapter VI.

Superconductors have zero resistance only for dc current. For ac current, the inertia of the electrons causes an electrical inductance. Therefore, for an ac signal, the normal electrons are also accelerated, causing dissipation. Nevertheless, the low loss as well as the low dispersion properties of

superconductors in the microwave frequency range can be exploited in delay lines, filters, oscillators, and strip lines. Progress has been made with high T_c thin films for these applications [Simon (1991), Gergis *et al.* (1992)].

Several high T_c superconducting products have recently entered the market in small niche applications. Lake Shore Crytronics in Westerville, Ohio sells a cryogenic liquid level sensor based on high T_c superconductivity. Superconductor Technologies Inc. of Santa Barbara, California offers a microwave resonator based on high T_c thin films. High T_c magnetic shielding is close to being ready for the market. And of course there is the ubiquitous high temperature superconductivity educational kit complete with neodymium magnet.

There are other potential applications of superconducting technology that have received renewed attention with the discovery of superconductors at higher temperatures. Using superconducting wire, these include power transmission lines, magnetic energy storage coils, generators, and motors. Because superconductors repel magnetic fields, high performance bearings are possible. With integrated circuit technology, computers with superconducting interconnects, devices, or as yet uninvented superconductor-semiconductor hybrids are being considered. Many materials and economic issues need to be addressed before any of these reach the market.

D. Research Goals

An immense amount of research has been done studying YBCO, both before we set out to join the effort and since. We chose initially to fabricate thin

films of YBCO because there was much interesting work to be done here, our group had experience with deposition and characterization of superconducting thin films, and we had an opportunity to purchase a custom designed deposition system. We decided on film growth because it is an interesting, complex, and important problem. Characterization of the films and of devices which can only be fabricated from them are an important way to study the properties of YBCO. Furthermore, the first large scale applications of high temperature superconductivity are likely to stem from thin film technology.

II. SUPERCONDUCTIVITY

The purpose of this chapter is to give a brief overview of superconductivity. Many of the physical properties of superconductors and the theoretical models that describe their behavior are fascinating and can be applied in a useful way. This chapter is obviously not intended to be a complete review of this well studied and broad field. It is instead intended to discuss some of the basic properties and terminology of superconductivity, particularly as it relates to the work presented. Three of the comprehensive books on this topic from which much of this chapter (and the rest of this thesis) has been drawn are those by Tinkham (1975), Parks (1969), and Van Duzer and Turner (1981).

Upon cooling metals such as mercury, lead, and tin below some low critical temperature characteristic of each metal (T_c), H. Kamerlingh Onnes, who was the first to experiment with such low temperatures, observed that the electrical resistance dropped dramatically, apparently to zero [Onnes (1911)]. Subsequent experiments have been unable to detect any resistance. This behavior is the most notable hallmark of superconductivity and the reason for its name. Between 1911 and 1986, many elements, alloys, and compounds were found to be superconducting below some material dependent temperature T_c, but never above the roughly 23 K critical temperature of Nb_3Ge [Gavaler (1973)].

Meissner and Ochsenfeld (1933) later discovered a second independent hallmark of superconductors. They found that bulk superconductors behaved

as perfect diamagnets. By Lenz's law, an object of zero resistance is expected to exclude magnetic flux from its interior when it is put into a magnetic field. Not only does a superconductor exhibit this behavior, but when an object first becomes superconducting in a magnetic field, contrary to Lenz's law, the magnetic flux is spontaneously expelled from its interior. This is called the Meissner effect. For what are called type I superconductors (in contrast to type II superconductors described below), below some critical field H_c, the magnetic field is excluded except near the surface. At the surface, it penetrates over a characteristic length scale λ, called the penetration depth of that superconductor. For pure elements well below T_c, λ is typically several hundred Å. Above H_c, the material no longer superconducts. Similarly, a superconductor can transport a current only up to a certain value I_c for that material and shape superconductor before it will no longer superconduct. This is called the critical current.

The understanding of superconductors made great strides during the 1950's. Ginzburg and Landau (1950) introduced a pseudo-wave function $\psi(\mathbf{r})$ as an order parameter such that $|\psi|^2$ equals the concentration of superconducting electrons. It turns out that the theory of Ginzburg and Landau (GL) in limiting circumstances can be derived from the landmark BCS theory described below [Gor'kov (1959)]. GL developed an expansion of the free energy in terms of ψ:

$$f = f_{n0} + \alpha|\psi|^2 + (\beta/2)|\psi|^4 + (1/2m^*)|[(\hbar/i)\nabla - (e^*/c)A]\psi|^2 + h^2/8\pi \qquad (2.1)$$

where α and β are parameters to be determined. Minimization of the free energy leads to differential equations for ψ. Solving these, for instance, introduces a characteristic length ξ, where:

$$\xi^2(T) = \frac{\hbar^2}{2m^*|\alpha|} \tag{2.2}$$

$\xi(T)$ is usually called the coherence length and is a characteristic length for variation of the concentration of superconducting electrons. For pure elements well below T_c, ξ is usually of the order of thousands of Å. The GL theory is an important tool in the description of superconductivity.

The theory that revolutionized the understanding of superconductivity was proposed by Bardeen, Cooper, and Schrieffer (BCS) (1957). They describe a weak electron-electron attraction mediated by an electron-phonon interaction. Evidence of the role of the phonons in conventional superconductivity is the existence of the isotope effect. Here, when an element of a superconductor is replaced with one of its isotopes, T_c changes in a predictable way. (BCS theory predicts that T_c is proportional to $m^{-1/2}$ where m is isotopic mass.) The electron-electron attraction results in electron pairs of equal but opposite momentum and spin. These are the superconducting electrons. A minimum energy denoted $E_g = 2\Delta$ is needed to break up the electron pair into single, non-superconducting electrons. This energy is referred to as the energy gap of the superconductor. The BCS theory predicts that E_g is related to T_c by the expression:

$$E_g = 3.5\, k_B T_c \tag{2.3}$$

Experimentally, E_g usually falls in the range 3.0 to 4.5 $k_B T_c$.

For type I superconductors, $\xi > \lambda$. Consider a superconductor in a magnetic field. Since the the superconducting electrons are in a lower energy state than the normal electrons, they have a negative contribution to the free energy density. Where magnetic field is expelled from the superconductor, there is a positive contribution. The density of superconducting electrons can vary over a distance no less than ξ. The magnetic field can vary over a distance no less than λ. Therefore, at the boundary between a normal and a superconducting region, there is a positive surface energy for a type I superconductor.

It turns out that when $\lambda > (0.7)\xi$, the surface energy is negative and the material is called a type II superconductor. This can be qualitatively understood using the same logic just used to describe positive surface energy. A negative surface energy allows for the coexistence of normal and superconducting domains within a material. For type II superconductors, a class to which YBCO belongs, the behavior is the same as type I superconductors up to a critical magnetic field called H_{c1}. Between H_{c1} and a higher critical field denoted H_{c2}, the magnetic field penetrates the superconductor in the form of a regular array of vortices. In this state, the superconductor can still carry a resistanceless current, but only if the vortices are pinned to specific locations. (The vortices experience a Lorentz force when there is a current in the material.) If the magnetic vortices move, the resulting changing magnetic field induces an EMF which accelerates the normal electrons causing dissipation. In certain materials the pinning can be strong enough to allow large current densities with no dissipation, even in the presence of large magnetic fields.

When two superconductors are separated by a thin insulating barrier, there is a finite possibility that electrons can tunnel through the barrier. The current-voltage relationship of single electron tunneling can give detailed information about the properties of the superconductor, such as its energy gap and density of states of single electrons when the material is in the superconducting state. This work was originally done by Giaever (1960). Soon after, Josephson (1962) correctly predicted that superconducting pairs of electrons could tunnel between superconductors at zero voltage. He also correctly predicted that when there is a voltage maintained across the barrier, there will be an alternating current. These are manifestations of the fact that the wave function ψ, where $|\psi|^2$ is the concentration of superconducting electrons, has a given phase. Tunnel junctions, as well as other systems where two superconductors are weakly coupled, have a profound impact on the understanding of superconductors and on their application. Junctions and other weakly coupled superconductors will be discussed more in Chapter VI.

In 1986, Bednorz and Mueller observed a drop in the resistivity of Ba-La-Cu oxide. This marked the discovery of the present class of high temperature superconductors. The hallmarks of superconductivity, zero resistance and the Meissner effect below some critical temperature, have been observed. These materials are extreme type II superconductors with very anisotropic behavior (Chapter III).

Cu-O superconductors differ from those studied in the past. Their properties and how they compare to the properties of conventional superconductors described in this chapter will be discussed further in the next chapter. Briefly, the superconducting transition temperature is much larger than

that found in any other system and larger than many ever expected. The observed isotope effect is too small to be explained by the BCS theory. Measurements of the energy gap, although still uncertain, are usually larger than predicted by BCS theory. The mechanism for superconductivity, while not yet understood, is not likely to stem from a phonon mediated electron-electron attraction [Freeman *et al.* (1989)]. Many, but not all, considered descriptions of the mechanism of high T_c superconductivity that are based on the interaction of the magnetic moments of the Cu atoms [Micnas *et al.* (1990), Hirsch (1989)]. The properties of YBCO are described in the next chapter.

III. $YBa_2Cu_3O_{7-\delta}$

In this chapter, properties of $YBa_2Cu_3O_{7-\delta}$ will be considered. In particular, its crystal structure, synthesis, normal state properties, superconducting properties, thin film growth, and the interrelation of these properties are covered. Implications for characterization and eventual applications of YBCO films and devices fabricated from them are also considered. While the properties of the different high temperature superconductors vary, YBCO is typical of those with two-dimensional Cu-O planes.

A. Properties of $YBa_2Cu_3O_{7-\delta}$

1. Crystal Structure

In 1987, superconductivity was discovered in the Y-Ba-Cu-O system [Wu *et al.* (1987)]. The superconducting phase was identified as $YBa_2Cu_3O_{7-\delta}$ (YBCO) where $\delta \approx 0.1$. The crystal structure was determined to be orthorhombic with lattice parameters a = 3.8 Å, b = 3.9 Å, and c = 11.7 Å [Cava *et al.* (1987)]. The crystal structure is shown in Figures 3.1 and 3.2. This can be related to the basic perovskite structure ABO_3 shown in Figure 3.3. The YBCO unit cell is an oxygen deficient perovskite structure with a tripling of one of the dimensions of the unit cell caused by the Ba-Y-Ba ordering at the A site. Cu represents the B cation. There is an orthorhombic distortion due to the ordering of the oxygens between adjacent Ba-O planes which creates Cu-O chains, as indicated in

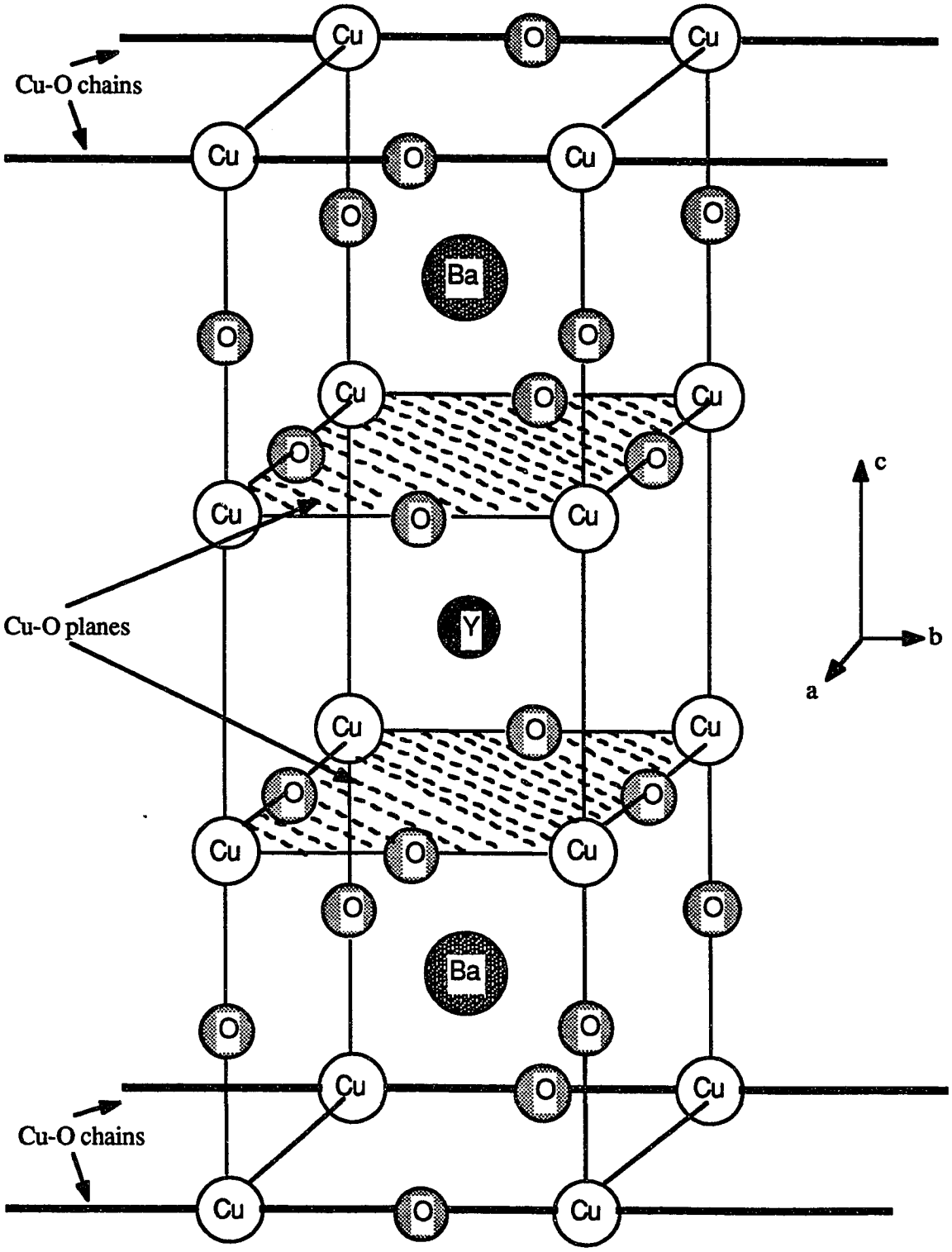

Figure 3.1: Unit Cell of YBCO showing the Cu-O planes and the Cu-O chains.

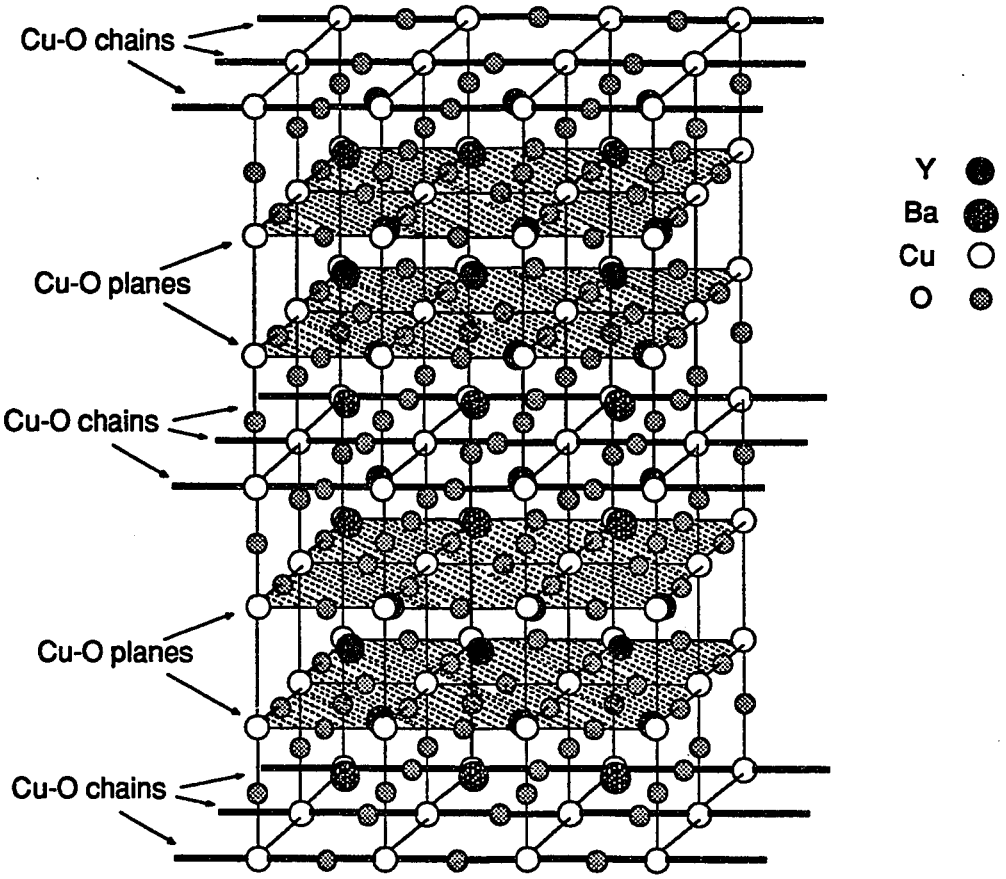

Figure 3.2: Crystal Structure of YBCO showing several unit cells.

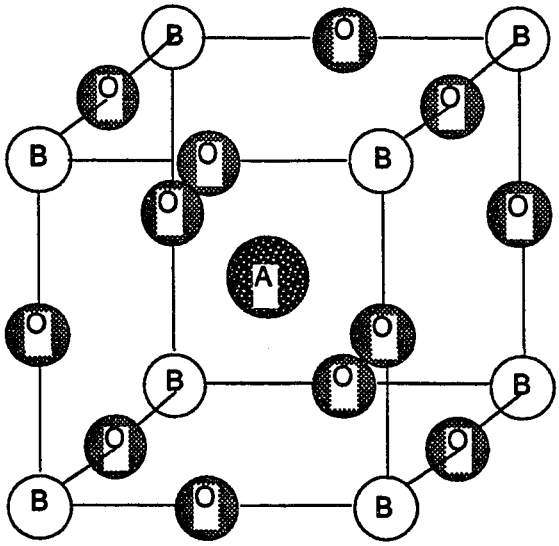

Figure 3.3: Unit cell of the perovskite crystal structure ABO_3.

Figures 3.1 and 3.2. Also noteworthy about the crystal structure are the planes of Cu-O identified in these figures. This is the origin of the very anisotropic properties which will be described in the following sections. Further details of the structure such as buckling of the Cu-O planes (not shown in Figures 3.1 and 3.2) and bond lengths and angles are well documented [for example, see Beyers and Shaw (1989) and the references therein].

2. Bulk Synthesis

The high temperature superconducting phase of YBCO is fabricated as follows. The metallic constituents in the proper stoichiometric ratio (1.0Y:2.0Ba:3.0Cu) are combined. This is usually done by mixing either the metals, oxides, or the carbonates of these elements. The mixture is then sintered at a high temperature ($\approx$ 800 °C) to form the right crystalline phase. This is then cooled slowly in oxygen in order to fully oxygenate the structure. Some groups have found increased success by annealing the material for a period of time at an intermediate temperature ($\approx$ 500 °C) to facilitate oxygenation. Above roughly 500 °C, YBCO is not fully oxygenated, there are no Cu-O chains, and the crystal is tetragonal. Below this temperature, YBCO is fully oxygenated and the crystal is the orthorhombic structure shown in Figures 3.1 and 3.2. Other groups have had improved results by regrinding the material after it is cool and then repeating the process. The keys to optimal results are having the correct stoichiometric ratio of cations, crystalizing at high temperature, and fully oxygenating while cooling. A recent review of bulk synthesis is given by Sleight (1991).

If the wrong stoichiometric ratio of cations is used, other phases of the Y-Ba-Cu-O system will form, usually degrading the superconducting properties of the material. Wu *et al.* (1987), who first discovered superconductivity in this system, actually had fabricated primarily Y_2BaCuO_5, which is a green semiconducting phase [Cava *et al.* (1987)]. $YBa_2Cu_3O_{7-\delta}$, which is the superconducting phase, is black.

The role of oxygen is extremely important in fabricating YBCO and understanding its superconducting properties. Above about 550 °C the a and b axes are equal and $YBa_2Cu_3O_x$ is tetragonal [Specht *et al.* (1988)]. Much below this temperature, oxygen does not easily move in and out of the crystal; well above this temperature it does. The variation in oxygen content, both at high temperature and room temperature, occurs mostly in the Cu-O chains, which are between the barium layers (as shown in Figures 3.1 and 3.2) [Jorgenson *et al.* (1987)]. This accounts for the orthorhombic - tetragonal phase transition. The room temperature oxygen content can be varied by changing the annealing procedure during cooling from high temperatures. For $\delta \approx 0.1$, $YBa_2Cu_3O_{7-\delta}$ (YBCO) is superconducting near 90 K. T_c decreases for increasing δ, becoming 0 when $\delta \approx 0.6$ [Beyers and Shaw (1989)].

Superconducting YBCO has been formed into pellets [Cava *et al.* (1987)], tapes [Kozlowski *et al.* (1991)], wires [Neal and Pathare (1991)], single crystals [Liu *et al.* (1987)], bearings [Weinberger *et al.* (1991)], thick films [Neiser *et al.* (1988)], and thin films (which will be described in depth in later sections). Ease in fabrication, which is important for many applications, is difficult because of the complicated processing described above and because YBCO is a

ceramic, and hence difficult to shape once formed. The greatest success in synthesis has been with thin films and single crystals.

3. Electronic and Magnetic Structure

In each unit cell of YBCO, there is one Y atom in the Y^{+3} state, two Ba atoms in the Ba^{+2} state, three Cu atoms in the Cu^{+2} state, and roughly seven O atoms in the O^{-2} state. Formal balancing of charges implies that there are positive charge carriers since the oxygen atoms are able to accept more electrons than the cations are able to donate [Bednorz and Mueller (1988)]. This is why the three Cu atoms of a unit cell of YBCO (2 in the Cu-O planes and one in the Cu-O chain) are in the Cu^{+2} state instead of the Cu^{+1} state. The carriers, and hence the conduction, reside in the Cu-O planes of Figures 3.1 and 3.2 [Anderson and Zou (1988), Hass (1989)]. For oxygen deficient YBCO, there will be fewer charge carriers and lower T_c. If deficient enough the material will no longer superconduct (see Figure 3.4).

To understand the planar electronic structure, consider $YBa_2Cu_3O_{7-\delta}$, where $\delta \approx 0.5$. Here the charge formally balances, leaving no charge carriers. (δ is actually slightly larger than 0.5 since some of the Cu ions of the Cu-O chains go into the Cu^{1+} state as δ increases [Hass (1989)].) The outer shell of the Cu^{2+} has 9 electrons in the 3d level. The outer shell of O^{2-} has 6 electrons in the 2p level. The Cu 3d and the O 2p levels are close in energy and are strongly hybridized with each other [Fujimori (1989)]. The unoccupied orbital of the Cu^{2+} ion has $x^2 - y^2$ symmetry, that is it points towards the O atoms within the Cu-O plane. Therefore, the oxygen ions in the plane see an orbital that is half empty; the ions that are out of the plane see full Cu^{2+} orbitals. This,

combined with the fact that the Cu 3d and the O 2p levels are strongly hybridized, is the key to the planar electronic structure [Anderson (1988), Pickett (1989)].

Figure 3.4 shows the phase diagram of YBCO as oxygen content and temperature are varied [Hass (1989)]. This diagram is based on a compilation of experimental results. For low oxygen content, there are few charge carriers and the material is an antiferromagnetic insulator [Tranquada et al. (1988)]. Cu atoms within the Cu-O planes couple antiferromagnetically, with the spin directions pointing within the plane. As the oxygen content increases, there is a transition to a metal that exhibits superconductivity. The crystal structure undergoes a phase transition from tetragonal to orthorhombic as the ordering of the oxygen within the Cu-O chains occurs. As the oxygen concentration increases, the number of charge carriers increases and the superconducting transition temperature increases to as high as 93 K when the crystal is fully oxygenated ($\delta \approx 0.1$).

4. Normal State Resistivity

The anisotropy in magnitude and temperature dependence of the resistivity of a single crystal of YBCO was first measured by Tozer *et al.* (1987) and the results are shown in Figure 3.5. The ρ_{ab} temperature dependence is in agreement with what has since been observed in epitaxial thin films. Consistent with the planar electronic structure just described, the magnitude of the resistivity in the Cu-O planes (ρ_{ab}) is much lower than the resistivity perpendicular to the Cu-O planes (ρ_c). No anisotropy was observed within the Cu-O planes. Just above T_c, $\rho_{ab} \approx 0.18$ mΩ-cm and $\rho_c \approx 17$ mΩ-cm. Anderson

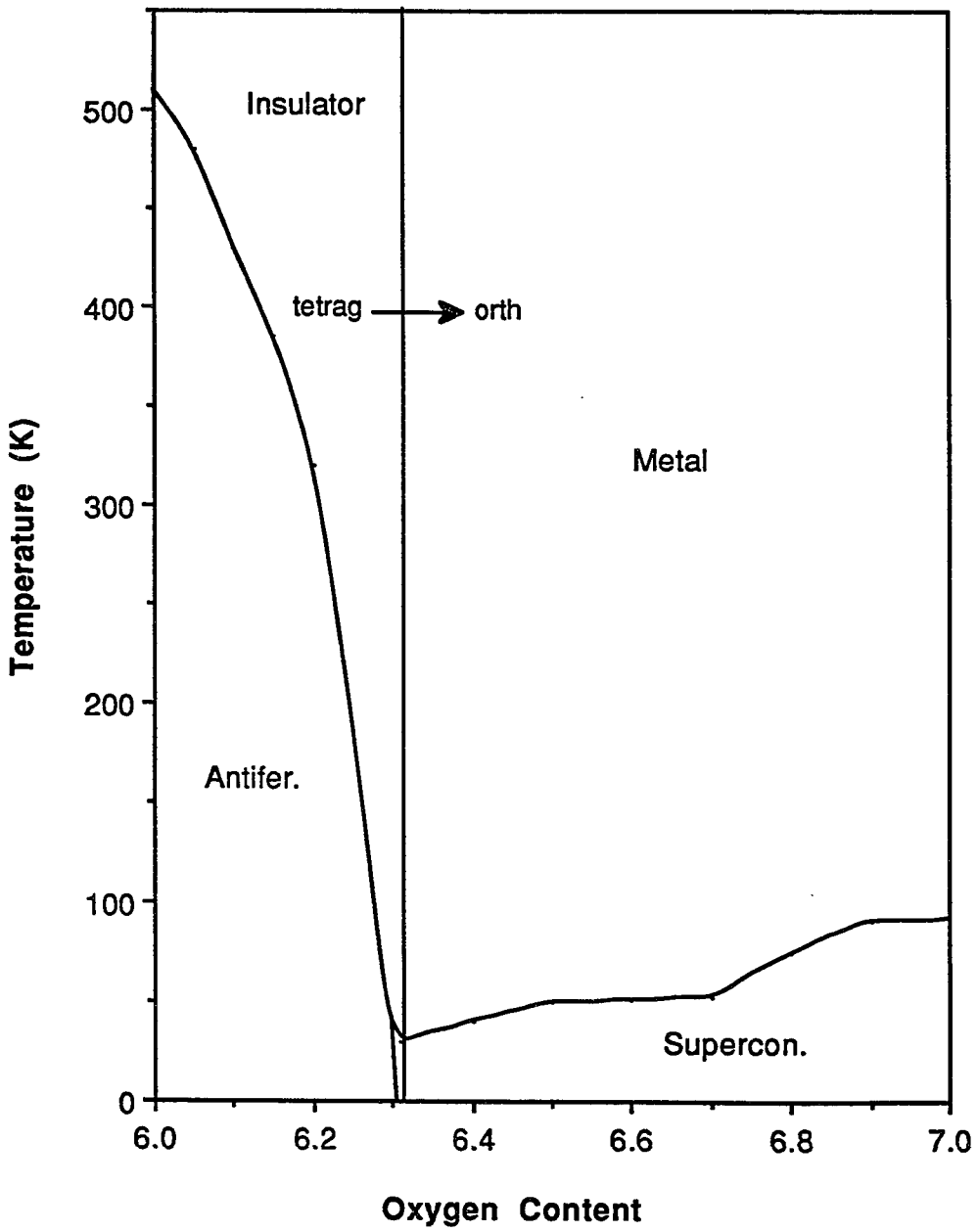

Figure 3.4: Phase diagram for YBCO [from Hass (1989)].

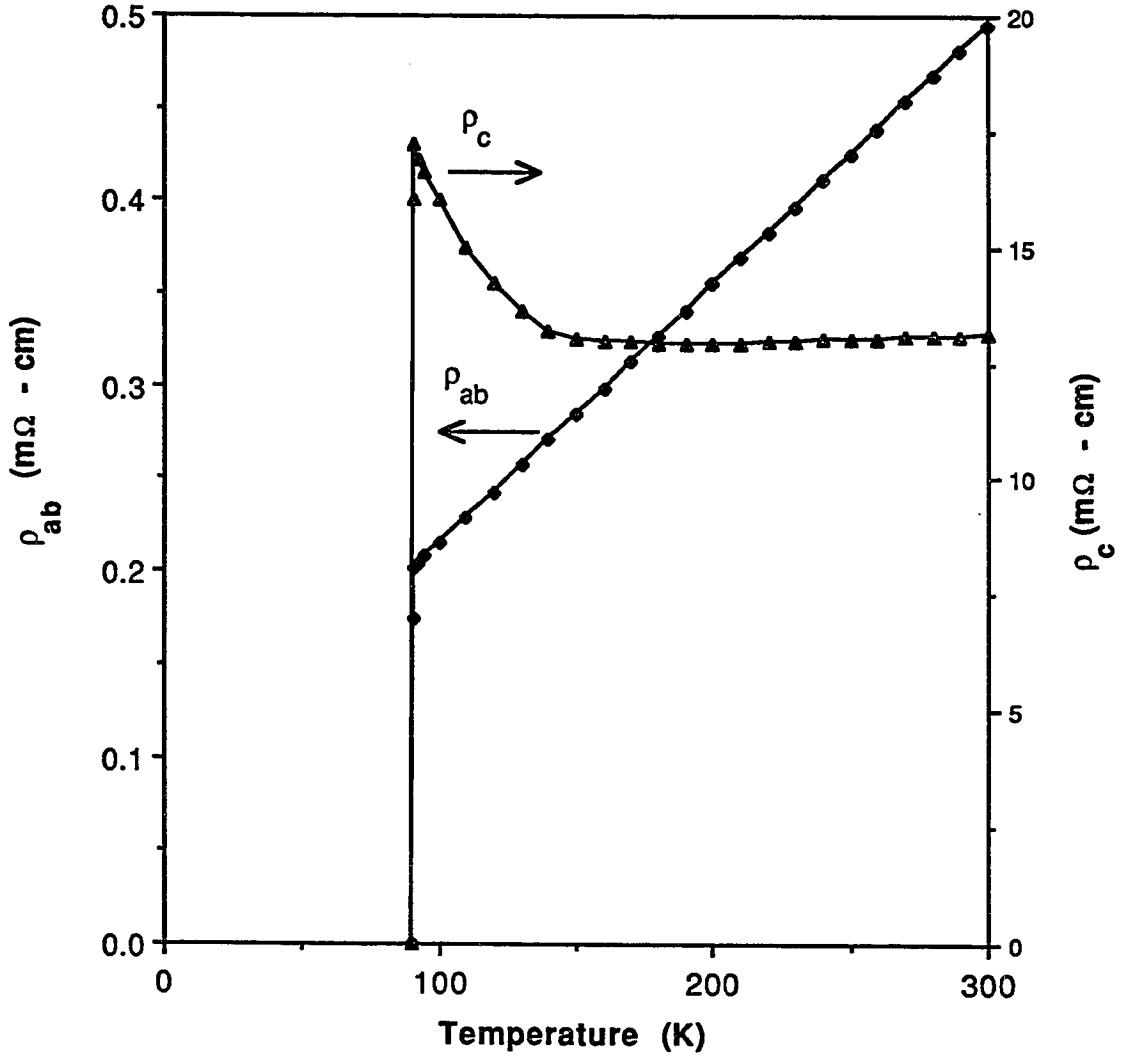

Figure 3.5: Resistivity within the Cu-O planes (the ab crystal direction) and perpendicular to them (the c crystal direction) [from Tozer et al. (1987)].

and Zou (1988) noted that assuming a sample misalignment of as little as 1/4° in these experimental results, the resistivity within the planes could be expressed:

$$\rho_{ab} = 1.4 \times 10^{-6} T \ \Omega\text{-cm} \qquad (3.1)$$

and the resistivity between the planes could be expressed:

$$\rho_{ab} = 1.35/T \ \Omega\text{-cm} \qquad (3.2)$$

where T is the temperature in K. They therefore describe YBCO as being a metal in the Cu-O planes and a "semiconductor" for conduction between planes. They attribute this to the charge carriers residing in the planes and the need for thermal excitation for charge transfer between planes.

5. Superconducting Properties

The superconducting properties of the cuprate superconductors, including YBCO, are different than those of traditional superconductors. Most notably, the transition temperature is much higher than what was expected from conventional theory of the electron-electron attraction via phonons. The electron-phonon interaction is too weak to expect transition temperatures much over 30 K [Freeman *et al.* (1989)].

The superconducting properties of YBCO are also very anisotropic, consistent with the crystal and electronic structure just described. It is essential

to account for this anisotropy in any description or potential application of YBCO. Much of this anisotropy can be described with the GL theory introduced in Chapter II with the mass scalar of equation (2.1) replaced with an effective mass tensor. Because of the electronic structure of YBCO, the elements of the tensor corresponding to the a and b crystallographic directions are roughly equal and considerably smaller than the element corresponding to the c direction. From this, an extreme anisotropy can be expected in the penetration depth λ, the coherence length ξ, the critical current J_c, and the critical magnetic fields H_{c1} and H_{c2}. These anisotropies have been observed experimentally and are shown in Table 3.1. For example, the anisotropy determined for ξ is consistent with equation (2.2) and the effective mass tensor components described above.

For comparison purposes, the superconducting parameters of Al and Nb_3Sn are also given in Table 3.1. In addition to the anisotropy and high transition temperature of YBCO, several other features are worth noting. YBCO is an extreme type II superconductor with an extremely short coherence length. In the c direction, $\xi \approx 5$ Å. This is comparable to the distance between the Cu-O planes, indicating that YBCO should exhibit 2-dimensional behavior. Also, although results vary widely, the normalized energy gap Δ/kT_c is much larger for YBCO than for conventional superconductors.

6. Substitutions and Defects

Soon after the discovery of these high temperature superconductors, substitution of the different elements led to discovery of new superconductors and an improved understanding of their properties. YBCO was first found [Wu

Table 3.1: Approximate values of the superconducting parameters for a type I superconductor (Al), an old high T_c type II superconductor (Nb_3Sn), and for YBCO. All values are for $T<<T_c$.

	Al	Nb_3Sn	YBCO (ab plane) (c direction)
T_c (K)	1.2	18	93
λ (Å)	160	1700	(1400)[a] (7000)
ξ (Å)	16000	70	(15) (5)
J_c (A/cm^2)	----	----	(10^7) (5×10^5)
H_c (T)	0.011	----	----
H_{c1} (T)	----	.003	(0.08)[b] (0.8)
H_{c2} (T)	----	26	(500) (100)
2Δ (meV)	0.34	7	18 - 79
$2\Delta/k_BT_c$	3.3	4.2	2.3 - 10

(a) Batlogg (1991)
(b) Dinger *et al.* (1987)

et al. (1987)] by attempting to substitute Y for La in $La_{2-x}Ba_xCuO_4$ [Bednorz and Mueller (1986)]. The resulting multi-phase material included the superconducting phase of YBCO, which is structurally different from $La_{2-x}Ba_xCuO_4$.

Substitution for Y in YBCO by many of the rare earth ions, which like Y also have a +3 valence state, results in little change in the superconducting properties [Tarascon *et al.* (1987)]. One notable exception is Pr. Partial substitution of Y with Pr results in a monotonic decrease in T_c until $T_c = 0$ when about half the Y has been replaced [Dalichaouch *et al.* (1988)]. This can be explained by the fact that Pr also has a +4 valence state. Formal balancing of charge of $Y_xPr_{1-x}Ba_2Cu_3O_{7-\delta}$ gives a decreasing number of charges with increasing x.

Further addition of rare earth ions results in partial substitution of the Ba site [Zhang *et al.* (1987)]. $RE_{1+x}Ba_{2-x}Cu_3O_{7-\delta}$ (where RE = La, Nd, Sm, Eu, Gd, or Dy) has decreasing T_c with increasing x.

Substitution for Cu also results in a decrease in T_c. For example, the effects of substituting Cu with Fe is shown in Figure 3.6 [Fueki *et al.* (1987)]. For Fe, a few elemental percent substitution results in a considerable degradation of the superconducting transition. However, when doped with only 1% Fe, they observed little degradation in the transition. Ni, Cr, Co, and Zn also substitute for Cu in YBCO and degrade its properties [Oseroff *et al.* (1987)].

Oxygen substitutions with other elements such as fluorine and nitrogen have not reproducibly enhanced the superconducting properties of YBCO. Many studies of ^{18}O substitution for ^{16}O have been conducted to determine if the isotope effect is the same as in conventional phonon mediated superconductors [Batlogg *et al.* (1987), Bourne *et al.* (1987)]. The small or

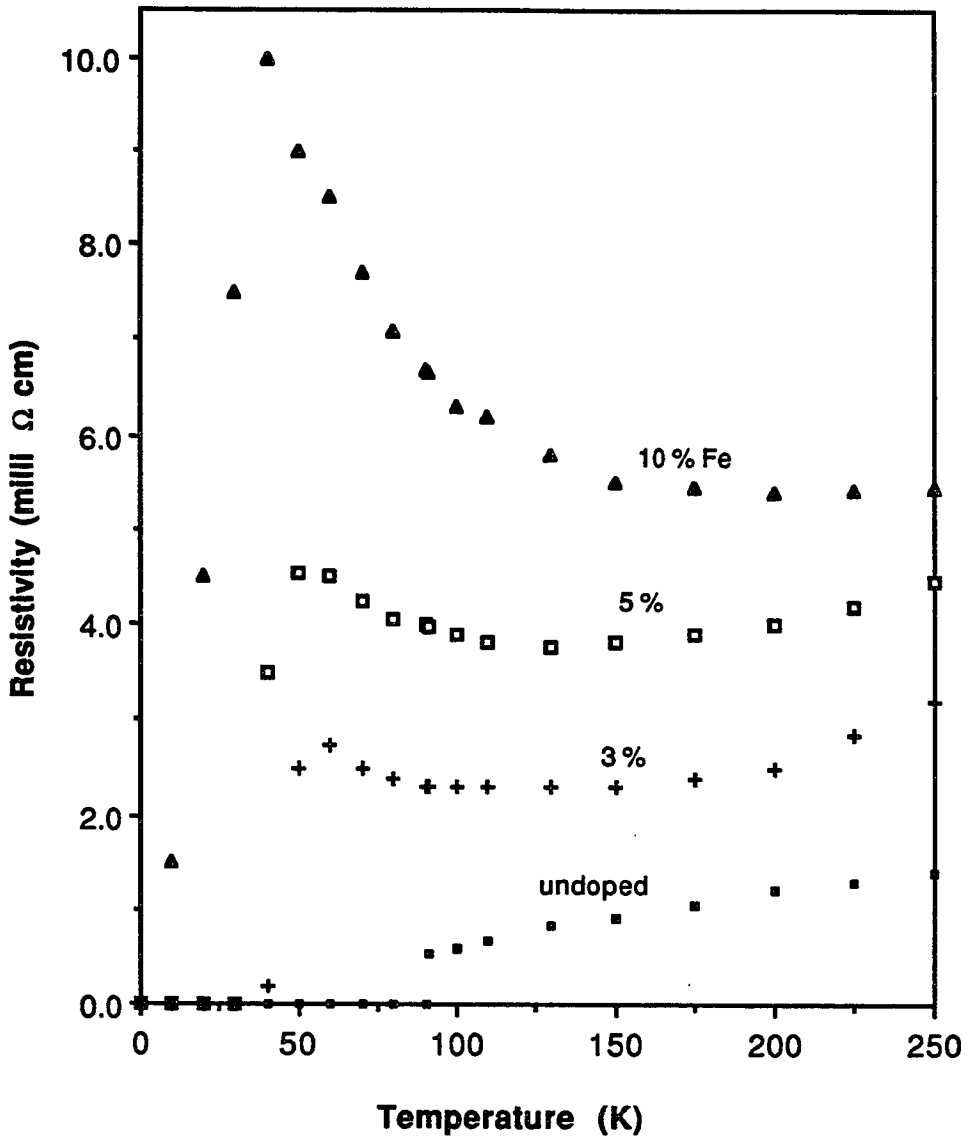

Figure 3.6: Resistivity vs. Temperature for Fe doped YBCO [from Fueki et al. (1987)].

negligible shift in T_c, in addition to the very high transition temperature, suggests that the superconducting mechanism is unconventional. Recent more thorough experiments agree with these early results [Ozhogin (1992)].

The most prevalent crystal defects in the crystal structure of YBCO (especially in epitaxial thin films) are twin boundaries in the ab plane. One model of such twinning consistent with high-resolution TEM is shown in Figure 3.7 [Hewat *et al.* (1987)]. Here the twin boundary is represented by the dotted line and the direction of the crystal axes on either side of the boundary is shown. The solid lines represent the Cu-O chains.

For polycrystalline YBCO, the superconducting properties are degraded. The critical current between grains is considerably less than the critical current within a grain [Dimos *et al.* (1988)]. Furthermore, because of the strong anisotropy of YBCO's properties, when there is a polycrystalline material, the favorable transport properties in the Cu-O planes can not be exploited and interpretation of results becomes more difficult.

B. Synthesis of YBCO Thin Films

1. Implications of YBCO Properties

Historically, the use of superconductors in microelectronics, both for applications and research, was preceded by the necessary development of a reliable, high quality thin film deposition process [Simon (1989)]. Lead alloy superconducting films require simple evaporation in moderate vacuum systems. Niobium films needed more advanced deposition techniques such as sputtering and better vacuum. For niobium nitride, reactive sputtering and heated

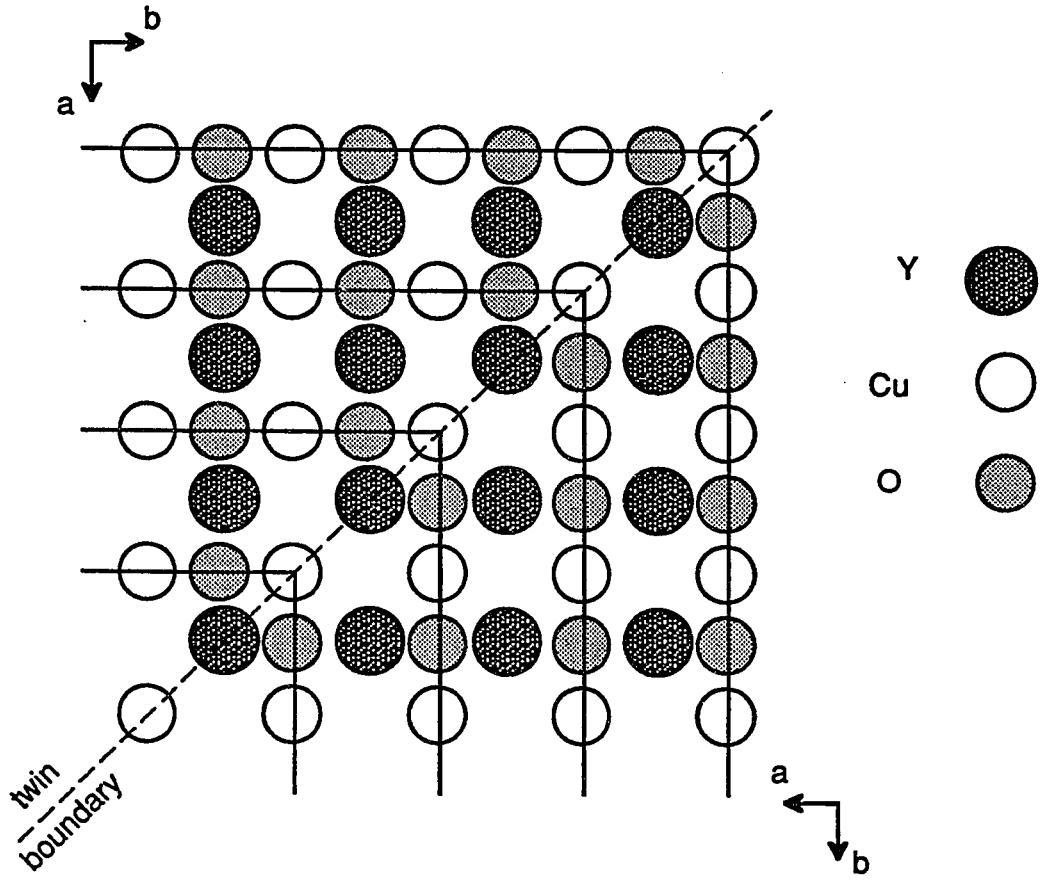

Figure 3.7: Schematic of twinning in ab plane. The dotted line represents the twin boundary. The solid lines represent the Cu-O chains.

substrates have been employed. As now described, deposition of YBCO films is proving to be an even greater challenge.

The properties of YBCO outlined above have implications for the growth, characterization, and practical exploitation of thin films. A recent review of high temperature superconductor thin films is given by Phillips (1992). As with synthesis of bulk YBCO, the three metallic constituents must be intimately combined in the correct stoichiometric ratio, crystalized at a high temperature, and oxygenated during cooling. Uniform, stoichiometric mixing of several elements can be very difficult in many conventional thin film deposition techniques. The necessity of a high temperature step means there is a potential for interdiffusion between the film and the substrate as well as between layers during multi-layer processing. All these issues need to be addressed in order to grow quality YBCO films.

If the film is polycrystalline, its properties are degraded. As described earlier, the transport between grains can dominate that within a grain. Also, as described earlier, the anisotropy of the properties of YBCO makes it desirable to have the crystal oriented to take advantage of the favorable conduction in the Cu-O planes. Finally, the surface is no longer as smooth when the film is polycrystalline. These considerations all point to the need for epitaxial growth. Epitaxial growth requires a lattice matched substrate. This, in addition to the potential for detrimental substrate-film interdiffusion at the high processing temperatures, limits the choice of substrates.

The most common choices of substrates for epitaxial growth of YBCO are currently $LaAlO_3$ and $SrTiO_3$ although others substrates, as well as buffer layers, are being explored. For example, despite a large lattice mismatch

(Table 3.2), quality YBCO films have been grown on MgO by us, as well as by others [Li *et al.* (1989)]. Table 3.2 lists a summary of the crystal properties of YBCO, $LaAlO_3$, MgO, and $SrTiO_3$. For a further review of the properties of the substrates used for YBCO growth see Phillips (1992).

Table 3.2: Crystal properties of YBCO compared to the substrates used here.

Crystal	Structure	Lattice Constants (Å)	Lattice Mismatch (%)	Expansion at 700 °C (%)
YBCO	Ortho	a = 3.82 b = 3.89 c/3 = 3.89	----	a, b - 0.77 c - 1.75
$LaAlO_3$	cubic (perovskite)	a = 3.79	a - 0.8 b - 2.6	?
MgO	cubic (NaCl)	a = 4.21	9.4	0.94
$SrTiO_3$	cubic (perovskite)	a = 3.91	a - 2.3 b - 0.2	0.75

The growth mechanism of epitaxial YBCO with the c-axis normal to the substrate has been reported by Hawley *et al.* (1991). Using Scanning Tunnelling Microscopy, they have observed that YBCO nucleates as islands which grow by adding material to the edge of a spirally rising step. Details of the properties of epitaxial YBCO films are given by Xi *et al.* (1991).

The magnitude and anisotropy of the coherence length are important in the design of superconducting devices fabricated from thin films. Since the coherence length is a measure of any spatial changes in the superconducting

wave function, the crystal should be uniform to within a coherence length of the interface of the superconductor in layered devices. Since ξ is of the order of the lattice spacing for YBCO, this is a significant materials science challenge. Such near perfect interfaces have been achieved with $PrBa_2Cu_3O_{7-\delta}$ [Inam *et al.* (1990)] and with MgO (despite not being a good lattice match) [Tanaka *et al.* (1990)]. Finally, ξ is much smaller perpendicular to the Cu-O planes ($\xi \approx 5$ Å) than it is within the planes ($\xi \approx 15$ Å). Therefore, the orientation of YBCO growth should take advantage of the longer coherence length within the Cu-O planes. Which orientation is desired would depend on the specific device design. Superconducting device designs are described in Chapter VI.

2. Synthesis Techniques

YBCO films are either deposited and then post-annealed in oxygen or are grown *in situ*. For post-annealed films, Y, Ba, and Cu are mixed at a temperature below crystallization (usually ambient temperature) and the combination is then crystallized and oxygenated at high temperature after growth. For films grown *in situ*, deposition takes place at high temperature in the presence of oxygen (so it is crystalline as grown) and is then slow cooled in oxygen (so that it is fully oxygenated and hence superconducting). Films grown *in situ* tend to be better crystallographically matched to the substrate and do not need as high a processing temperature [Beasley (1989)]. However, *in situ* growth is more difficult. The presence of high temperatures and oxygen complicates the already difficult process of stoichiometrically combining three elements on select substrates. These issues will be addressed in more detail in a later chapter.

The deposition of YBCO films can be from one source or from several. Each approach has its advantages. One advantage of codeposition from multiple sources is a much higher deposition rate if metal sources are used. Our deposition rate for metal cosputtering is about 100 Å/min, which is more than an order of magnitude higher than we obtain with sputtering from a single composite target. A second advantage of codeposition is its flexibility. Codeposition readily allows for controlling film stoichiometry by adjusting the relative rates of each element. Also, any of the elements can be easily substituted. These changes can be made without interrupting film growth; one can either change individual rates or use several shuttered sources. The main advantage of deposition from a single source is that it is less complex. For example, it is difficult to achieve the high pressure of oxygen at the growing film needed for *in situ* growth in several codeposition techniques. For one of our techniques, metal cosputtering, a higher oxygen pressure leads to undesirable target oxidation. For e-beam coevaporation, the electron beam guns usually do not operate well at a high pressure of oxygen. Another disadvantage of codeposition, and in particular of metal cosputtering, is the strong interdependence of many variables, as will be discussed later. This makes reproducibility difficult.

Coevaporation from several sources followed by a post-deposition anneal was one of the first techniques that resulted in superconducting YBCO films [Chaudhari *et al.* (1987), Oh *et al.* (1987)]. Here, Y, Ba, and Cu are evaporated at the same time either with an electron beam or by heating a vessel. The composition is controlled by varying the individual rates. The film is deposited at ambient temperature or some low temperature (<400 °C). It is

amorphous as deposited and does not superconduct. A high temperature post-deposition anneal (near 900 °C) is needed to form the superconducting phase. After the anneal, films may superconduct at a high temperature (90 K), but they are often not epitaxial and not as high a quality as films grown *in situ*.

Cosputtering from several sources followed by post-annealling was soon used. In one study [Char *et al.* (1987)], Y, Ba, and Cu metal targets were simultaneously sputtered. A post-deposition anneal up to 850 °C was needed to make the films superconducting. These films had zero resistance as high as 88 K but were not epitaxial. In another study [Scheuermann *et al.* (1987)], YCu and BaCu alloy targets were simultaneously sputtered. Here a post-deposition anneal of 900 °C was necessary. Zero resistance was as high as 86 K, but again the films were not epitaxial.

In situ superconducting films have been grown by coevaporation in low pressures of oxygen [Lathrop *et al.* (1987), Silver *et al.* (1988), Terashima *et al.* (1988), Missert *et al.* (1989)]. Here, during growth, the epitaxial substrate is heated typically to 650 - 700 °C, in less than 10 mT of oxygen. Epitaxial growth of high quality films is possible, but results are usually not as good or as reproducible as composite target techniques, discussed below. Higher pressures of oxygen are technologically difficult.

One more recent and very successful technique of growing YBCO films *in situ* is by laser deposition from a single composite source [Chang *et al.* (1988), Witanachchi *et al.* (1988)]. With laser deposition, a YBCO target is vaporized by a laser beam and deposited on a substrate. During growth, the substrate is heated, typically to 600 - 700 °C, in the presence of oxygen, typically 100 mT. This technique works very well. Transition temperatures are over 90 K and are

narrow. The films are smooth and epitaxial. Reproducibility, critical currents, and normal state resistivities are also good.

A second very attractive approach to growing superconducting YBCO films *in situ* is sputtering from a stoichiometric target of YBCO in an off-axis geometry [Li *et al.* (1988), Eom *et al.* (1989)]. Here, the face of the target points away from the substrate. The reason for this is to avoid bombardment of the growing film with negative oxygen ions [Rossnagel and Cuomo (1988)]. This is an inherent difficulty of sputtering in oxygen and will be discussed thoroughly in Chapter IV. As before, during growth, the films are heated to 600 - 700 °C. In addition to the sputtering gas (usually Ar), there is typically 50 mT partial pressure of oxygen in the chamber. Film quality is comparable to that of films grown by laser deposition. Our results of off-axis composite target sputtering are described in Chapter V.

An approach to growing films *in situ* from several sources is simultaneously sputtering from three oxide targets onto a heated substrate in the presence of oxygen. In one study [Akutsu *et al.* (1990)], Y_2O_3, BaO_2, and CuO targets were used. The deposition temperature was about 700 °C and the oxygen partial pressure was of order 10 mT. Depositions with the targets facing the substrate and facing away were tried. As-grown films had zero resistance temperature as high as 84 K. In another study [Kuroda *et al.* (1989)], $Y_{1.5}Ba_2Cu_3O_x$, $Y_1Ba_3Cu_3O_x$, and $Y_1Ba_2Cu_{4.5}O_x$ targets were used. The deposition temperature was 620 °C and the sputtering gas was 300 mT of pure oxygen. The highest zero resistance temperature achieved was 81 K. Sagoi *et al.* (1989) have cosputtered Y, Ba_2CuO_3, and Cu onto a heated substrate in the presence of oxygen with as grown films having T_c as high as 70 K.

We have grown films *in situ* by simultaneously sputtering from three metal targets in a differentially pumped chamber [Steinberg *et al.* (1991)]. This is discussed in detail in the next chapter. Others have had much improved success with this technique since our work with it [Anderson (1991)].

Other novel approaches to high temperature superconductor thin film growth include MOCVD [Kirlin (1991)], molecular beam epitaxy [Kwo *et al.* (1988)], screen printing [Fardnanesh *et al.* (1991)], spin-on pyrolysis [Rice *et al.* (1987)], and spraying [Numata *et al.* (1991)].

IV. FILMS GROWN BY COSPUTTERING

Late in 1987, an approach to deposition of YBCO films and a vendor were sought. Metal cosputtering was decided upon for several reasons. Codeposition allows the flexibility that seemed especially important at that time. As described earlier, film stoichiometry could be varied by adjusting the relative rates of each element. Also, any of the elements could be easily substituted. Metal targets were chosen because metal sputtering is easier than sputtering from an oxide. It is easier to ignite and maintain a stable plasma and the rate is higher and more stable. It was decided that the oxygen needed for *in situ* growth would be introduced at the substrate and the chamber would be differentially pumped in order to prevent target oxidation during sputtering. This will be described in detail in this chapter. Another advantage of this approach was that sputtering was a technique with which the group had had much experience. Finally, the success of composite target sputtering had not yet been fully established.

By the end of 1988, after much consideration about the system design and possible vendors, Kurt J. Lesker Co. (2) was selected. They had had experience with similar system designs and were also willing to meet our specifications. Furthermore, we felt that their customer service department was impressive. This proved to be true. After considerable delay in assembly, testing, and shipment, by September, 1989, the system was installed in the Yale microelectronics clean room facility.

This chapter describes the details of the deposition system and the results of the work growing films *in situ* by metal cosputtering.

A. Deposition System Design

Figures 4.1 and 4.2 show the side and top views of the configuration of the deposition system soon after its arrival. The main chamber is 28-inches in diameter and the inside of the load lock is about 15-inches across. After substrates were mounted on a two-inch pallet, they were put in the loadlock which was then evacuated. Substrates were then transfered to the main chamber and drawn up into the base of the radiant heater. The support stage of the pallet was free to rotate to improve the uniformity of deposition and temperature across the pallet. If need be, the pallet could then be transferred down to a second transfer arm which could rotate over any of three other different stations *in situ*. Originally, as labelled in Figure 4.2, there was one blank station (available for future use), two sputter stations, and one station with an ion gun. Attached to the second transfer arm were two crystal monitors which were also free to rotate over any of the stations and were important in the initial calibrations of the Y, Ba, and Cu rates. Oxygen was introduced directly at the substrate and Ar, the sputter gas, was introduced directly into the sputter guns. A stainless tube rested on the oxygen inlet ring in order to increase the local pressure of oxygen at the growing film. To have better control of the partial pressures and net flows of the two gases used during growth, a flow restrictor was installed between the deposition region and the main chamber vacuum valve. For the same reason, soon after original installation, flow restrictors were

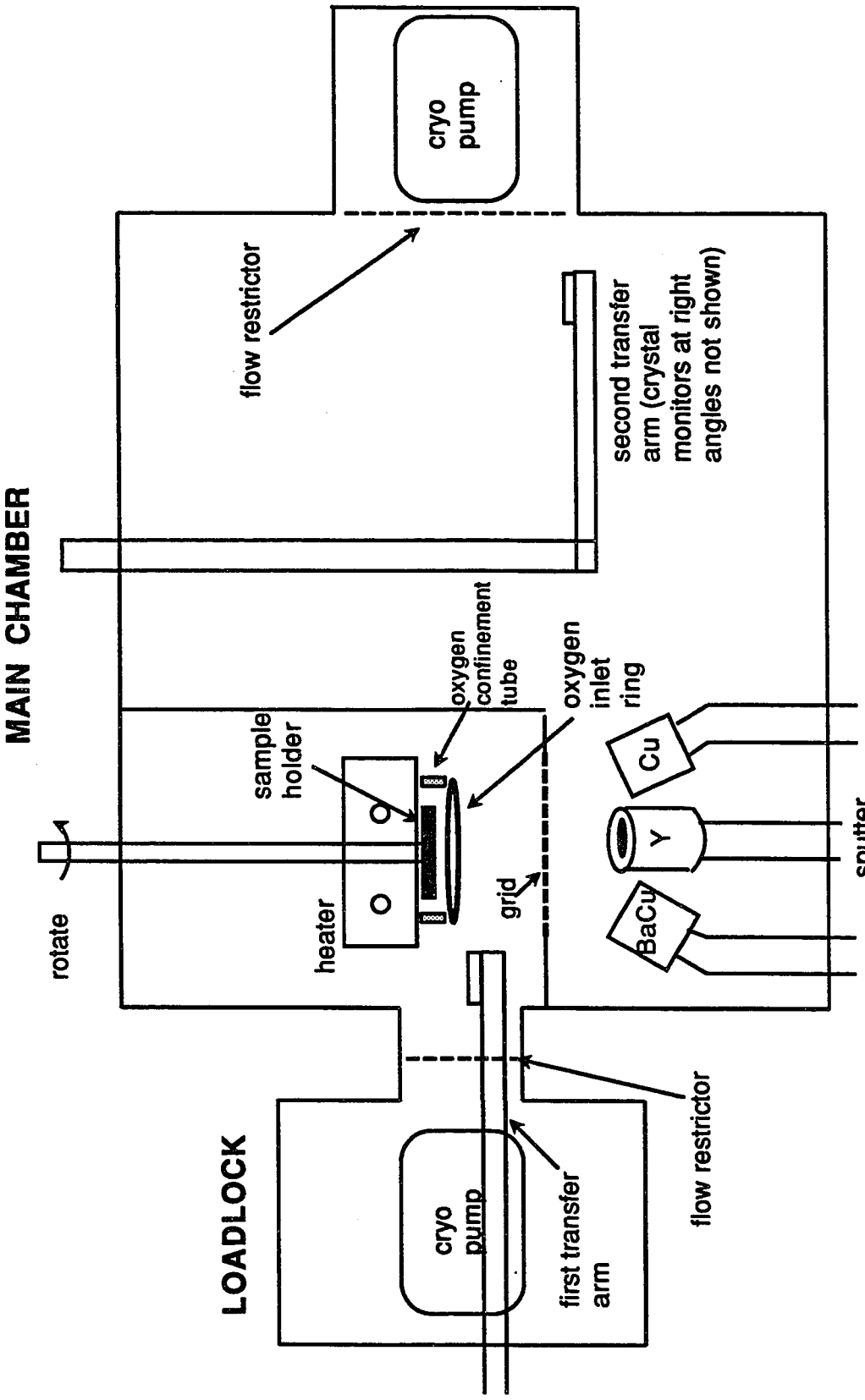

Figure 4.1: Schematic of the front view of deposition system.

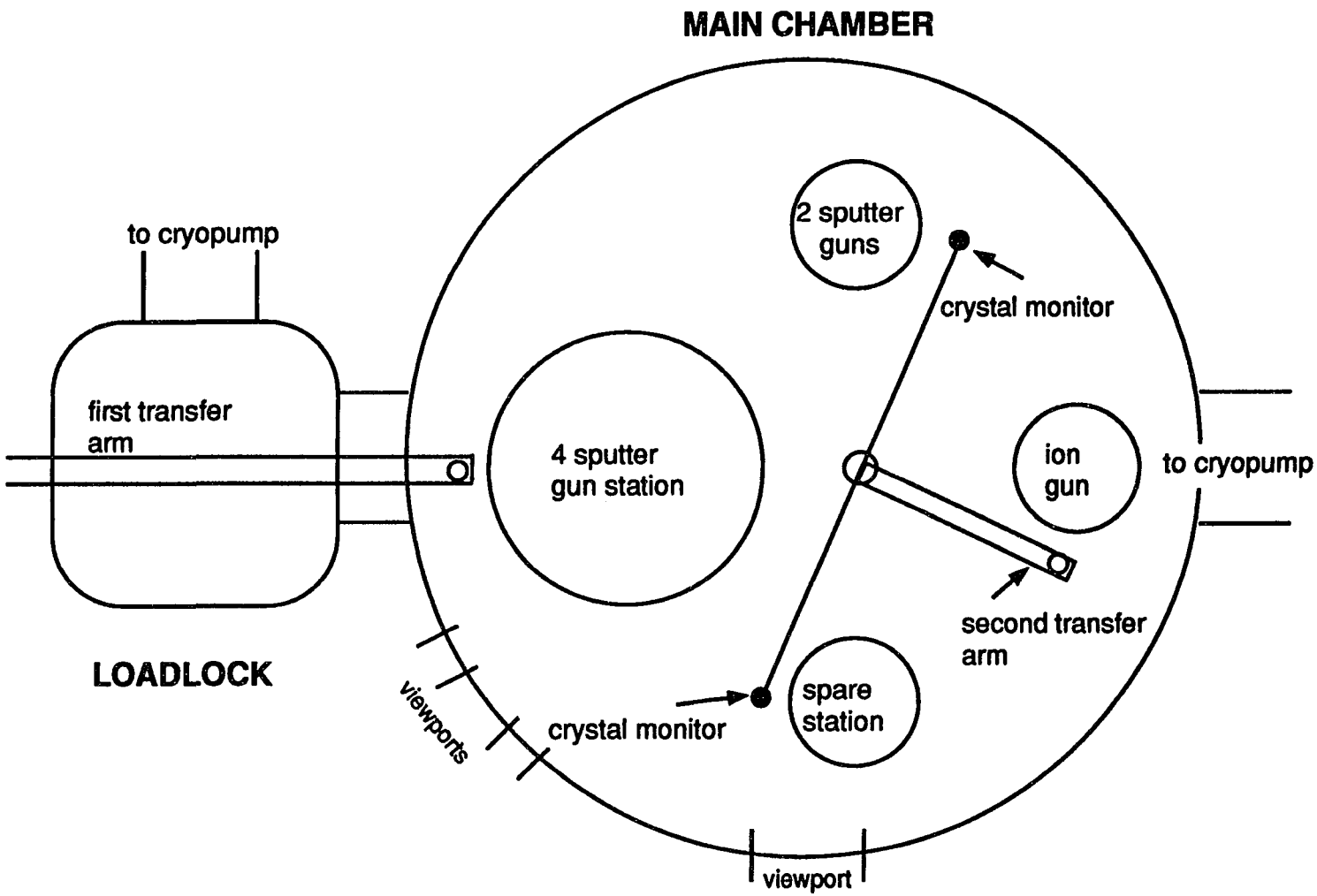

Figure 4.2: Schematic of top view of the deposition system.

added between the deposition region and the loadlock high vacuum valve as well as between the sputter gun and the substrate regions. Deposition was through this second restrictor, or grid, but the reduction of the deposition rate was not significant.

The cluster of four sputter guns located under the heater was originally arranged as follows. The Torus 2C sputter guns (2) were mounted on a 13-inch stainless steel conflat flange. The power supplies available to drive the guns were two 1000 Watt dc and two 600 Watt rf power supplies from Advanced Energy Industries (3). Into each gun was plumbed an Ar gas line. In front of each was a stainless shutter which operated individually. There was also a fifth shutter which could block deposition from all the guns. Three of the guns were pointed at the center of the substrate pallet. One contained an Y metal target, another a Cu metal target, and the third a BaCu alloy target. The BaCu alloy was used instead of pure Ba because it oxidizes less easily than pure Ba [Scheuermann *et al.* (1987)]. This was important for *in situ* film growth because oxygen was present during deposition, during cool down in oxygen, and when the system was open. The fourth gun faced straight up (not at the pallet). This was not used during the film growth but instead allowed extra flexibility for other potential processing. Computer calculations of deposition rate and of stoichiometry uniformity based on gun specifications and gun-pallet geometry were performed before final system design. This was important in determining the geometry of the guns and the pallet location. The final design had the sputter gun targets located 5-inches below the substrate pallet and 2.5-inches off the center axis, with the guns aimed at the pallet center. This yielded a prediction of better than 2 percent uniformity in deposition from each gun across

the two inches of the pallet. Measured variations in stoichiometry were usually less than 5 percent.

The substrate heater was designed, built, and installed at Kurt J. Lesker Co. It was a radiant heater with two 1500 Watt quartz lamps encased in layers of stainless steel and Haynes Alloy #214 (4). Haynes Alloy does not oxidize easily at high temperatures. Two of the walls were water cooled. The pallet rested in a hole in the bottom. The pallet was supported by a rotating shaft which came through a hole in the top of the heater. Temperature was measured with several thermocouples. Two were free standing in the heater box. Two others were thermally anchored to the bottom of the rotating shaft not far from the pallet. These two were fed through the top plate of the chamber through a set of thermocouple slip rings. All thermocouples were occasionally calibrated against several thermocouples which were screwed directly to the pallet and fed out the chamber through the loadlock door. This arrangement allowed testing without opening the main chamber. According to these measurements, uniformity was about 15 °C within one-inch of the center. Temperature reproducibility was more important than knowledge of absolute temperature. Reproducibility was probably also good to about 15 °C. Absolute accuracy of our temperature readings was probably reasonable, given that our optimal deposition temperature setting was not very different from that reported by other groups.

Each chamber was evacuated with a CTI Cryo-Torr 8 cryopump (5). Both chambers were rough pumped with the same Leybold-Heraeus D-90 mechanical pump (6) with Fomblin fluid. Base pressure of the main chamber

with both high-vacuum valves open was typically 5 x 10^{-7} Torr. This remained fairly consistent with time with standard chamber cleaning.

B. Post-annealed films

Initially films were grown at ambient temperature, in argon only, onto MgO substrates. A summary of these runs is given in Appendix C. Sputter gun powers were set according to deposition rates determined with the crystal monitors. The films were then post-annealed in flowing oxygen up to 850 °C.

It was not long before superconducting films were grown. The resistance vs. temperature curve of a post-annealed film is shown in Figure 4.3. The cryostat used for all the measurements, which was redesigned from the cryostat used for the high T_c work covered in Appendix A, is described in Appendix B. However, since the ultimate goal was to grow high quality films, we next concentrated on *in situ* film growth.

For improved control of film stoichiometry, it was eventually our objective to adjust gun powers based on measured stoichiometry of the previous run. Therefore, it was necessary to find a technique to measure composition which was reliable and accurate, and which could be done with a small turn-around time. Eventually, we determined that the inductively coupled plasma atomic emission spectroscopy (ICP) technique at Olin Metals Research Laboratories (1) was the best composition measurement technique available to us.

Other important issues were also necessarily addressed when we grew both post-annealed films and *in situ* films (see Section C below and Appendix D). Substrates were eventually cleaned with sequential two-minute rinses in

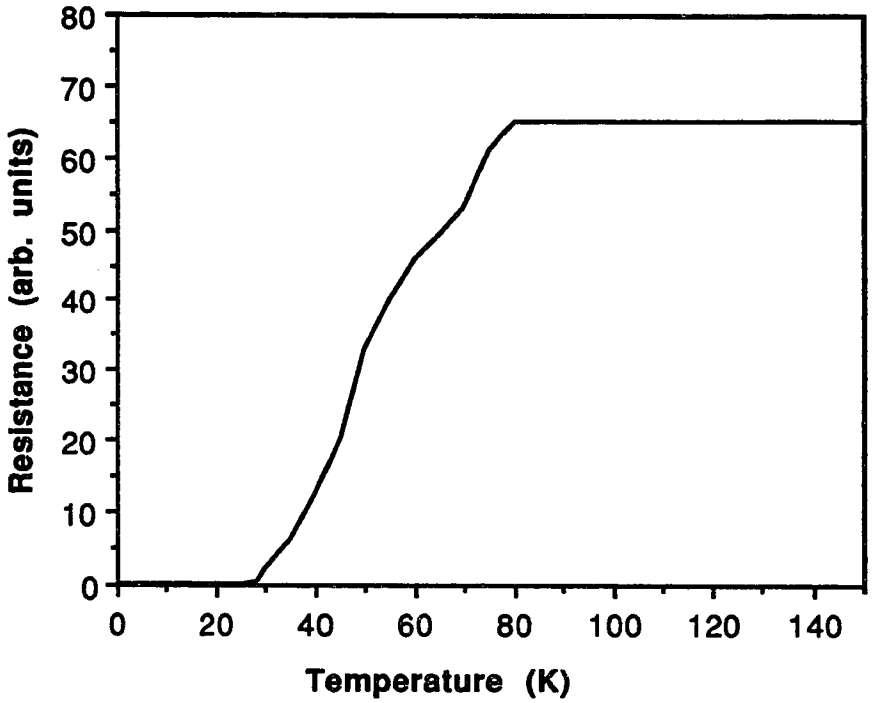

Figure 4.3: Resistance vs. temperature for a post-annealed film (sample 3-1). This was our first film that superconducted.

trichlorethane, acetone, and methanol. Films grown on $SrTiO_3$ had slightly higher transition temperatures than films grown on MgO. We were unable to grow superconducting films on sapphire or Si. We inadvertently discovered that when the power to the sputter gun containing BaCu was too high, the target melted. We therefore sputtered at lower gun powers. Described in the next section is how we eventually thermally and mechanically anchored our substrates to a deposition pallet. Also described in the next section is how we made electrical contact to our films in order to measure their resistive transitions.

C. *In situ* films

1. Sputtering and Resputtering

When sputtering in oxygen, it is important to account for the effects of oxygen ion bombardment of the growing film. For YBCO sputtering, these effects have been reported by others [Rossnagel and Cuomo (1988)] and have been observed by us.

The description of conventional sputter deposition is the following. The geometry for on-axis sputtering is shown in Figure 4.4. On-axis refers to the fact that the face of the target points to the growing film. The voltage between the target and ground creates an electric field which accelerates positive particles (such as Ar^+) toward the target. Upon hitting the target, energy of the particle goes into heat, the emission of secondary electrons, and the sputtering of the target (removal of atoms from the lattice). The secondary electrons collide with the neutral Ar atoms, ionizing them. The reason for the magnetic field is to

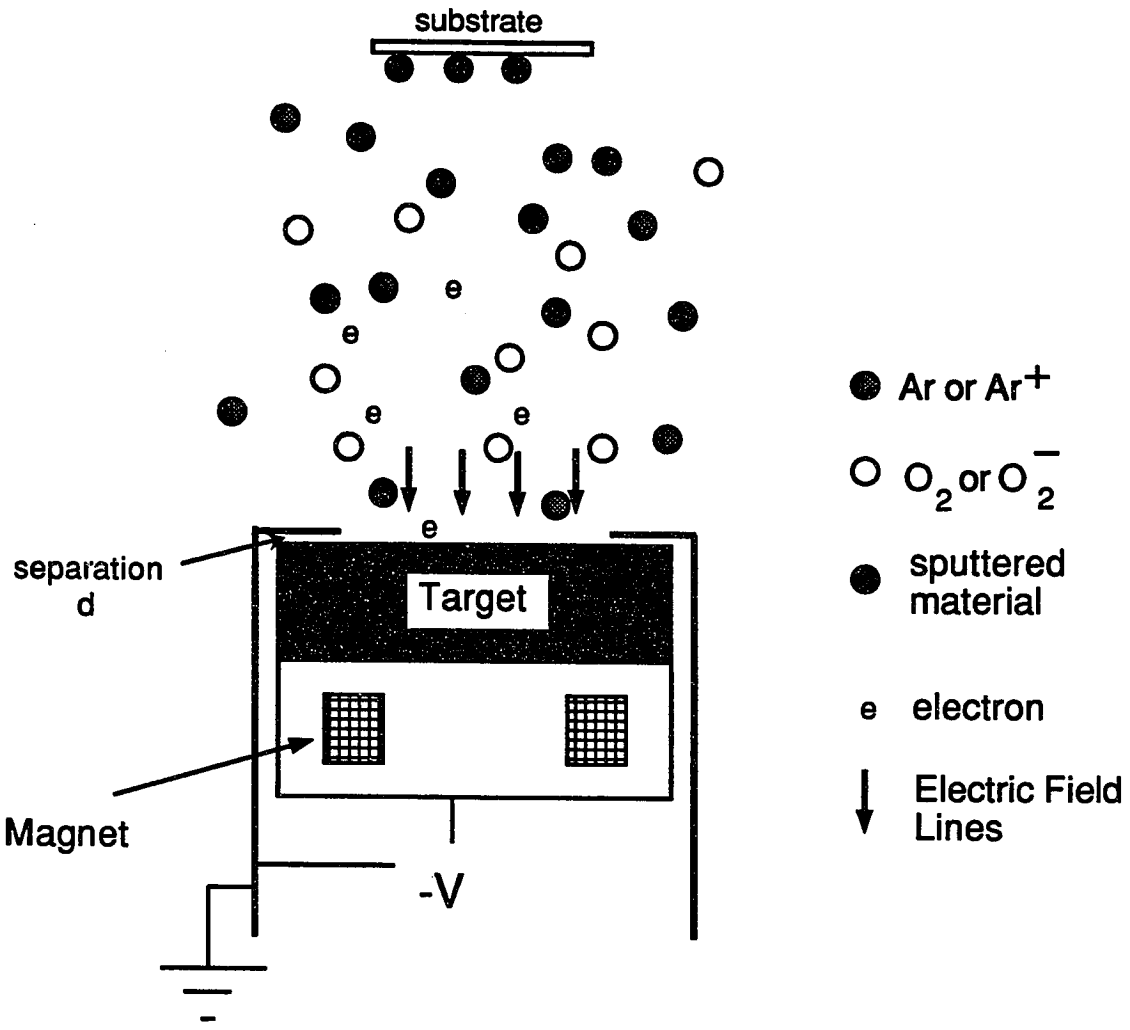

Figure 4.4: Schematic of on-axis reactive magnetron sputtering. The separation d between the grounded can and the high voltage target was 40 mils during our metallic sputtering but was decreased when sputtering YBCO (Chapter V).

increase the path length of the electrons and hence the ionization and sputtering efficiency. The sputtered atoms eventually condense on all surfaces including the substrate. For reactive sputtering, a reactive gas is included in the deposition chamber.

Either a dc or a rf voltage can be used. Although rf sputtering is more difficult, it is necessary at times, such as when the surface of the target is an insulator (as is the oxide of the BaCu target). A rf voltage makes it possible to capacitively couple to the target when the surface of the target is insulating. Furthermore, electrons oscillating in the plasma acquire enough energy to cause ionizing collisions, reducing the dependence of the discharge on secondary electrons [Vossen and Cuomo (1978)].

The reason there is oxygen ion bombardment of the growing film (resputtering) is that oxygen can form negative ions. Both positive and negative ions exist in the plasma [Enami *et al.* (1990)], but it is the negative ions that accelerate towards the growing film (in the on-axis geometry) [Rossnagel and Cuomo (1988)]. This negative oxygen ion bombardment sputter etches the film to some extent. Since the Ba etches in this way at the highest rate of the three elements, the film grown is Ba deficient degrading its superconducting properties. As will be shown later, other damage is also possible.

2. Deposition Conditions

A summary of the *in situ* cosputtered depositions is given in Appendix D. Bare substrates were mounted on a two-inch Haynes alloy pallet. Substrates were usually 1/4-inch squares. Thermal anchoring was done either with a screw and a washer or with Ag paste (and no screw or washer). When using a

screw and a washer, part of the film was masked and S from the screw lubricant (MoS_2) contaminated the films. We found greatest success by mounting the substrates as follows. A small amount of Ag paste was applied to the back of the substrate such that it was just enough to cover most of the substrate when pressed against the pallet. A small pressure was then applied to the perimeter of the substrate during a ten-minute bake at 100 °C on a hot plate. The pallet was then left at room temperature for at least several hours to finish drying. The mounted pallet was then transferred to the sputter station.

Prior to each run, all sputter guns were turned on, the targets were presputtered, and the heater was turned on. The chamber was brought to a total pressure between 6 and 8 mT of argon and oxygen. Argon was fed into the sputter gun region at a rate of 40 - 90 sccm and oxygen was introduced at the substrate at a rate of 1 - 3 percent of the Ar flow. Targets were presputtered for about 20 minutes to stabilize conditions and to sputter through the oxide. We judged whether we had sputtered through the oxides by waiting for the gun voltages to stabilize for a fixed power and for the plasmas to turn the appropriate colors. In particular, the BaCu gun had a purple plasma when the target surface was oxidized and a bright green plasma when the oxide was properly cleaned off. BaCu oxidizes the most easily of the three targets. To stabilize substrate temperature, the heater was turned on at the beginning of each presputter. The substrate temperature was set to the desired deposition temperature of roughly 700 °C. To improve thermal and compositional uniformity, the substrate pallet was rotated at about 10 rpm for the presputter and the run. A typical run was 30 minutes for a 3000 Å film.

We found that if a metal target oxidized while sputtering, its rate, and hence the film stoichiometry, became more difficult to control. For this reason, the chamber was differentially pumped; the substrate region was pumped separately from the sputter gun region. Deposition was through a grid with roughly 2 square inches of total open area. With the above conditions, the color of the BaCu gun plasma remained green during the deposition, indicating that this target was essentially not oxidized.

The partial pressure of O_2 in the substrate region was considerably higher than in the sputter gun region. During a run, the total pressure was measured to be roughly 3 mT in the substrate region when the sputter gun region pressure was set to 7 mT. Based on these pressures and typical flow rates of 70 sccm argon and 1.5 sccm oxygen, the partial pressures of oxygen in each region were estimated.

Figure 4.5 (a) shows a schematic of the gas flow in the deposition system. The flow resistances were due to the constrictions described earlier. This arrangement is modelled in a convenient way in Figure 4.5 (b). V1 and V2 represent the total pressures in the substrate and sputter gun regions respectively. IO and IAr represent the flow of oxygen and of argon respectively. R1, R2 and R3 represent flow resistances. The gas flow/electrical flow analogy is summarized in Table 4.1. Experimentally, we determined that R1 ≈ (1.5) R2. Using IAr >> IO (that is, the flow of Ar >> the flow of O_2), the resistances were estimated from the experimental values measured: R1≈ 0.19, R2 ≈ 0.13, and R3 ≈ 0.26 mT/sccm. Using these values of resistances, the partial pressure of oxygen in each chamber region was estimated. Using the experimental values given above and the correspondences defined in Table 4.1, the simple circuit

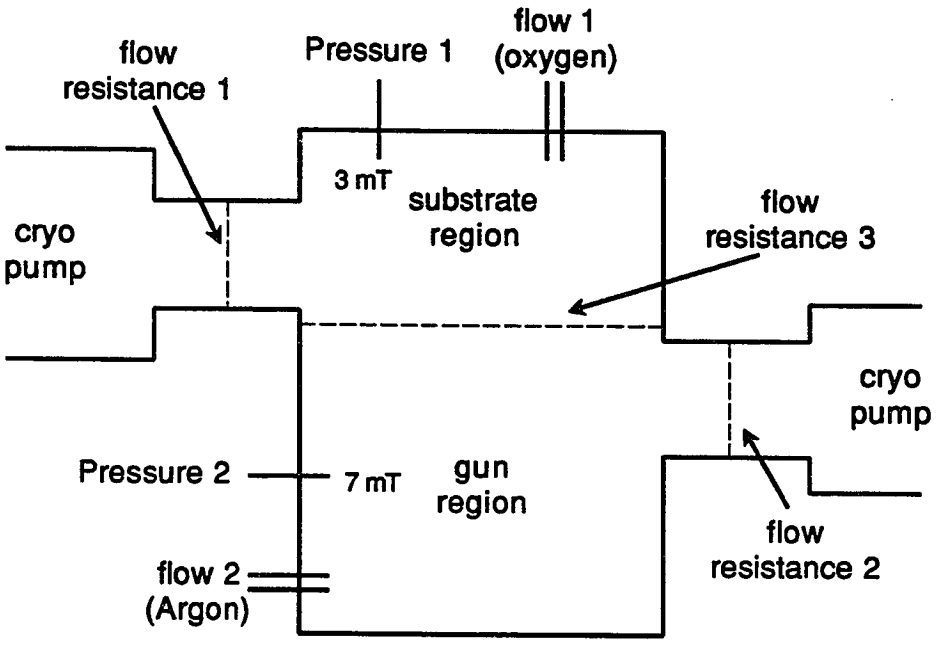

(a)

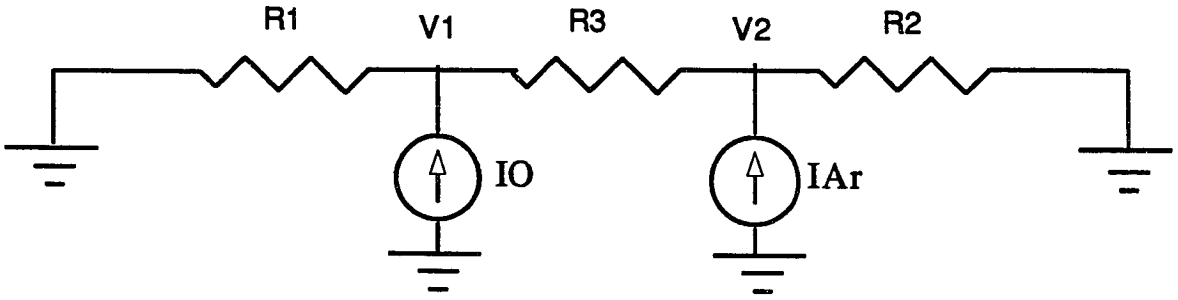

(b)

Figure 4.5: (a) Schematic of gas flow in the deposition system showing where gas is fed in and where the pressure is measured. (b) Model used to calculate flow resistances and partial pressures (also see Table 4.1).

diagram in Figure 4.5 (b) was then solved (neglecting IAr to give the oxygen partial pressure). In the substrate region, $P(O_2) \approx 0.2$ mT. This is a low estimate though because the oxygen inlet was directed at the substrate and the region between this inlet ring and the heater box was surrounded by a 4-inch diameter, 1-inch tall confinement tube, as shown in Figure 4.1. In the sputter gun region, $P(O_2) \approx 0.06$ mT.

Table 4.1: Definition of variables in gas flow/electrical analogy.

Gas Flow	oxygen flow	argon flow	substrate pressure	gun region pressure	flow resist 1	flow resist 2	flow resist 3
Electrical	IO	IAr	V1	V2	R1	R2	R3

It is worth noting that an oxygen partial pressure of 0.2 mT corresponds to enough oxygen bombarding the surface of the growing film to oxygenate of order of 200 monolayers per second. This is as compared to a growth rate of about 0.5 monolayers per second.

The powers of the sputter guns were set as follows. Initially, the gun rates were separately calibrated using the crystal monitors. Eventually, powers were adjusted based on results of the previous run. For the BaCu target a power range high enough to minimize target oxidation, yet low enough that the target did not melt was chosen; the gun power was kept between 125 and 150 W (rf). We did observe that the BaCu target melted at much higher powers. Since the targets are very expensive, care was taken to avoid this. As expected, based on plasma color, we observed that the BaCu target oxidized

during sputtering more easily at lower powers. The Y and the Cu were sputtered at powers between 30 and 75 W (dc). These two values were adjusted according to measurements of film stoichiometry in order to achieve the correct cation ratios. Film stoichiometries were measured by the ICP technique at Olin. Based on measurements of Y-Ba-Cu solutions of known composition, film composition measurements were accurate to better than 5 percent. Rutherford Backscattering Spectroscopy (RBS) performed at the University of Arizona produced results in reasonable agreement with ICP measurements. The ICP measurements were carefully calibrated and thus are quoted here.

After the deposition, the main shutter was closed and the sputter guns were turned off. Then, the high-vacuum valves were closed and the chamber was brought to of order 10 Torr of oxygen. The sample was then cooled slowly over several hours with a programmable heater controller. After cooling, the samples were transferred out of the system. Although the targets were exposed to oxygen during cooling, we found that it was relatively easy to sputter through this oxide layer before the next run.

Usually when the resistive transitions of the films were to be measured, four electrical contact pads were sputtered through a mechanical mask. It is well established that either Ag [Tzeng *et al.* (1988)] or Au [Ekin *et al.* (1988)] make low resistance non-destructive contact to YBCO. We found that contact resistance using our Pogo Contacts (Appendix B) without a metal pad was typically several hundred Ohms and unstable. With Ag or Au pads on a good film, the contact resistance was less than a few Ohms.

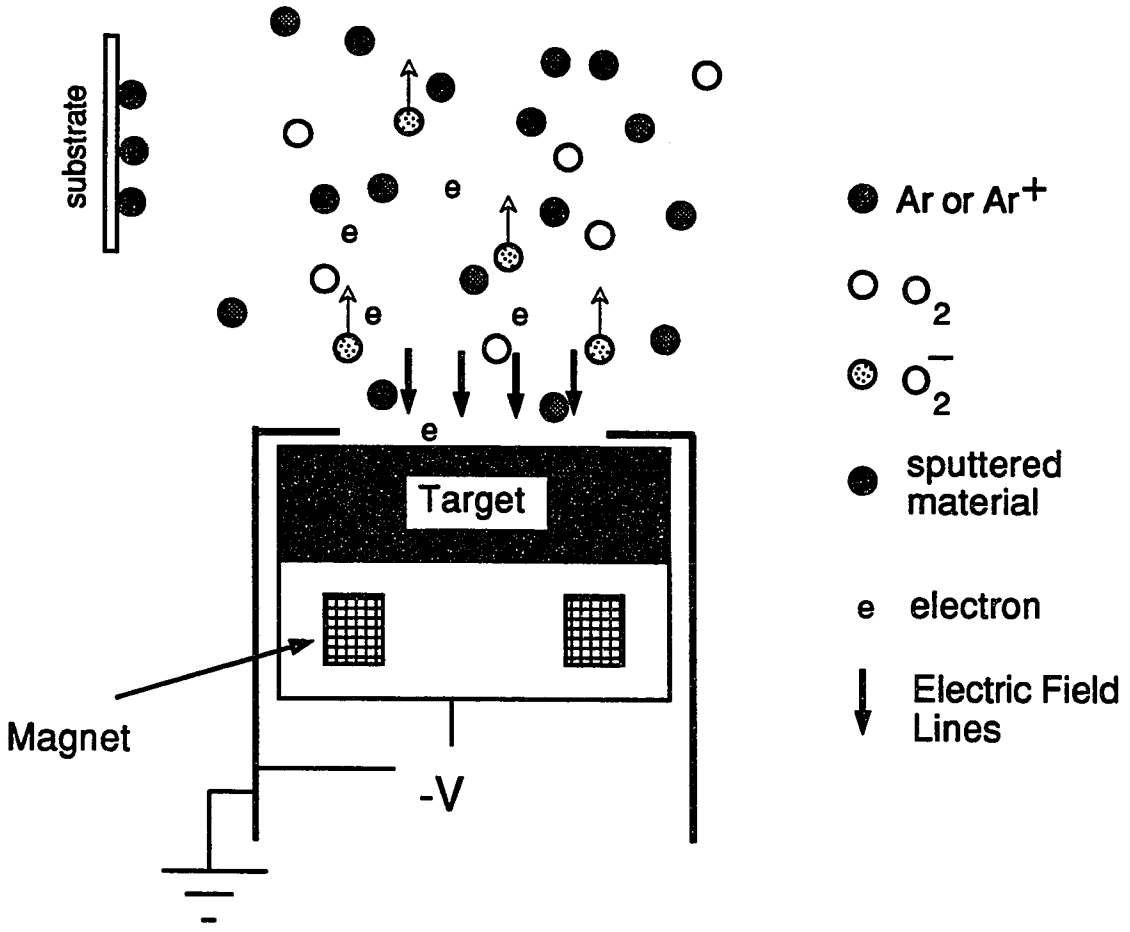

Figure 4.6: Schematic of off-axis sputtering. Oxygen ions are accelerated away from the target. In the on-axis geometry this damages the growing film. In geometry shown in this figure, the effect is minimized (with some loss in deposition rate).

In the on-axis geometry shown in Figure 4.1, transitions of films near the correct stoichiometry were broad and had low temperatures at which R = 0, near 60 K. Because of these poor results for T_c and our suspicion of film damage due to oxygen ion bombardment in this geometry, we switched to an off-axis geometry. This was achieved by rotating the guns such that they pointed several inches away from the substrate. The reason for this is that the electric field, and hence the oxygen ion bombardment, is highly directional. Sputter deposition is much less directional. Therefore, pointing the gun away from the substrate dramatically lessens the ion bombardment with far less effect on the deposition rate. We observe less than a factor of 2 decrease in rate after rotating the guns. Figure 4.6 schematically shows off-axis sputtering.

3. Results

Results for T_c were significantly better for films grown in the off-axis geometry. Figure 4.7 shows the resistance as a function of temperature for a good film grown in the off-axis geometry and for a good film grown in the on-axis geometry. These two films were grown in very similar deposition conditions (roughly 700 °C, 7 mT total pressure, 2.5% oxygen flow rate) and have similar Y:Ba:Cu ratios (1.00:1.90:3.26 for the film grown in the on-axis geometry and 1.00:1.82:3.28 for the film grown in the off-axis geometry). However, in switching to the off-axis geometry, zero resistance temperature improved from 57 K to 85 K, the resistivity ratio between room temperature and the temperature just above the transition improved from 1.0 to 1.8, and the normal state resistivity just above the transition was lower by a factor of 4.

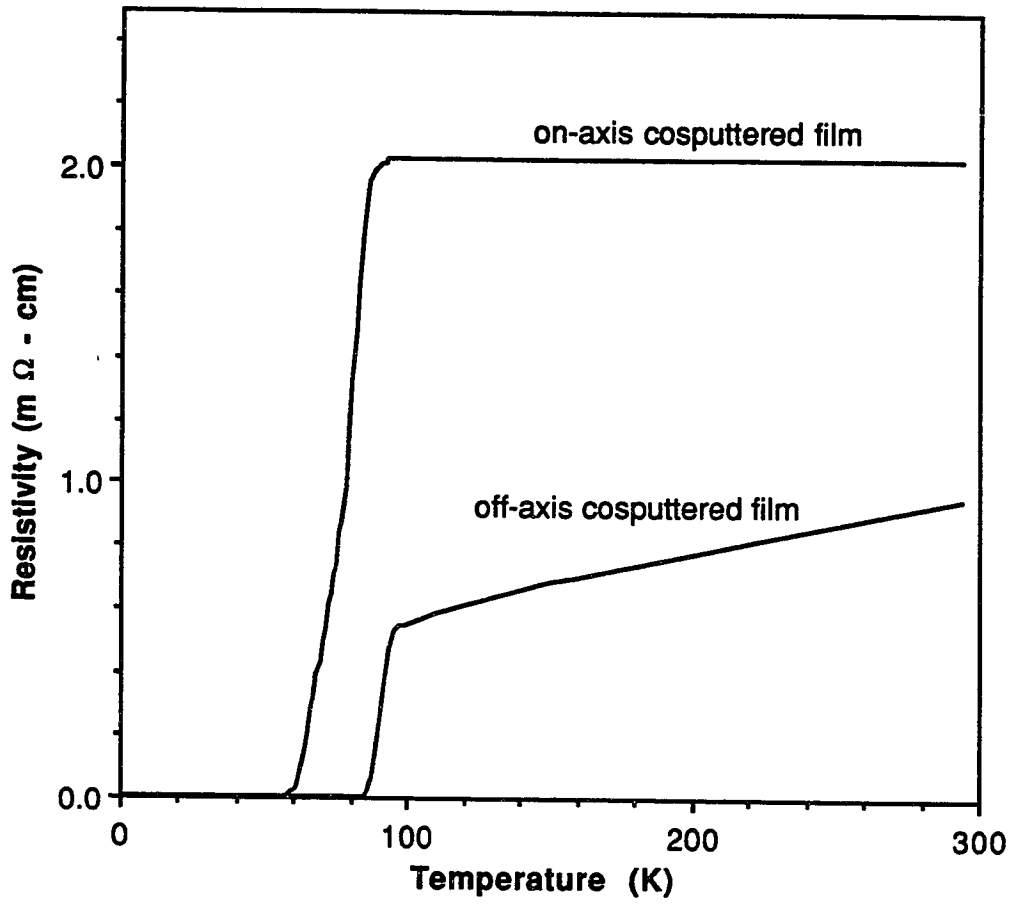

Figure 4.7: Resistivity vs Temperature for films grown in the on-axis (sample 42-3) and the off-axis (sample 55-2) geometries. Growth conditions and stoichiometries are nearly identical.

Unfortunately, reproducibility was a problem for the off-axis geometry as well as the on-axis geometry, as discussed below.

To determine the crystal structure of our films, x-ray diffraction patterns were measured at Olin. Figure 4.8 shows the results for a film grown on MgO in the on-axis geometry with cation ratio of 1.0:2.2:3.3. The measured peaks compare well with expected values of locations and relative intensities [Cava *et al.* (1987)] indicating we had grown YBCO. The peak at 43° is due to the substrate. From this curve we estimate that the lattice constants had the following values: $a = 3.83 \pm 0.01$ Å, $b = 3.85 \pm 0.02$ Å, and $c = 11.73 \pm 0.03$ Å.

4. Discussion

Our proposed explanation of why film properties improved in switching from the on-axis to the off-axis geometry is as follows. The effect of pointing the sputter guns away from the substrate is to lessen the effects of ion bombardment of the growing film. Normally this bombardment preferentially resputters the Ba, changing the stoichiometry of the film. We were able to compensate for this Ba resputtering by adjusting sputter gun powers, and could grow films of nearly identical stoichiometry in each geometry. We conclude that there was damage done to the film in the on-axis geometry other than Ba resputtering. Similar observations of damage to sputtered films have been reported by Akutsu *et al.* (1990) and by Enami *et al.* (1990) who postulate that it was due to lattice distortion, similar to the damage done by ion bombardment [Clark *et al.* (1987), Valles *et al.* (1989)].

Compared to other *in situ* techniques (see Chapter III) the oxygen partial pressure, $P(O_2)$, is small for our technique. Evidence of low $P(O_2)$ at the

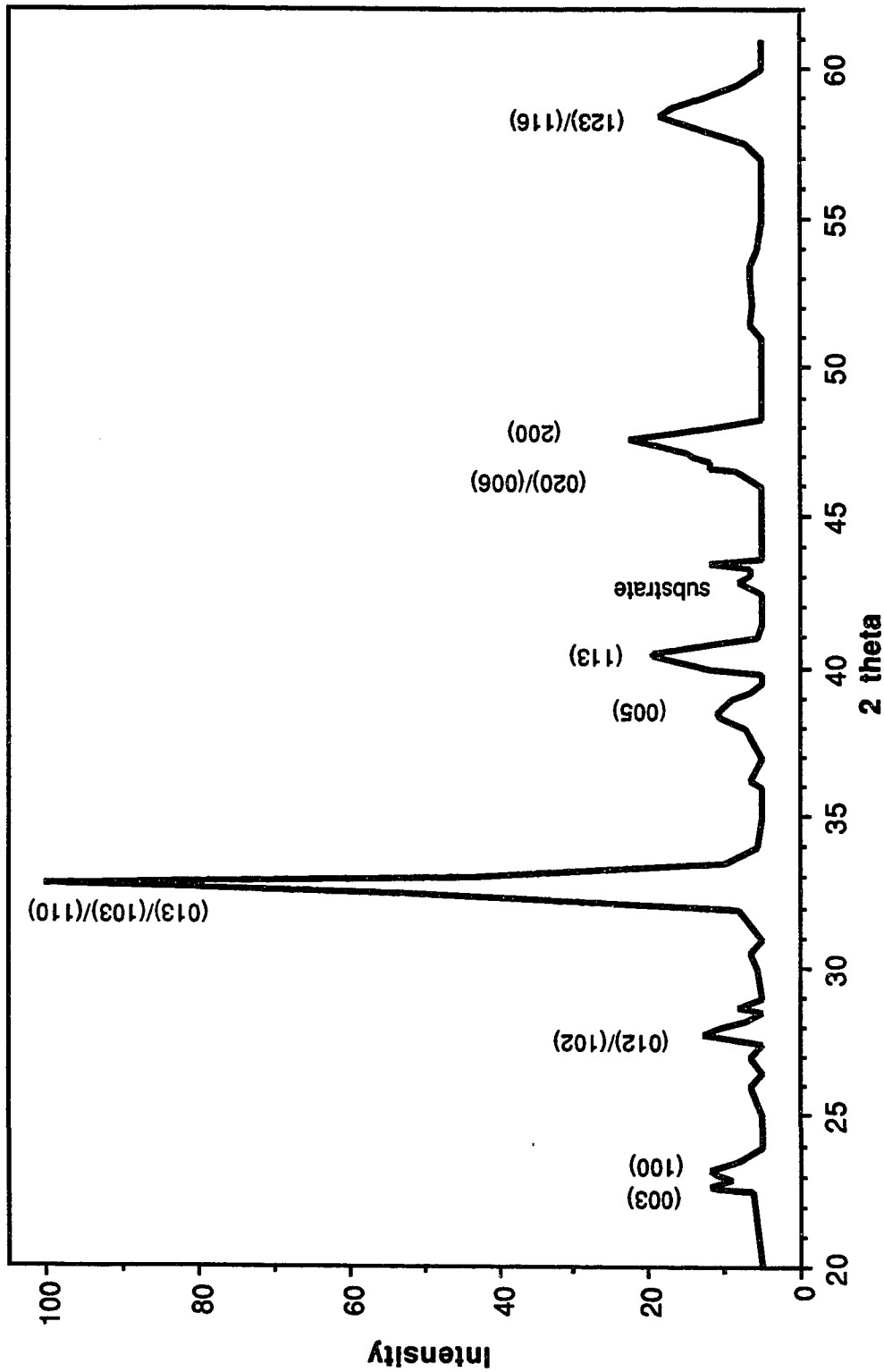

Figure 4.8: x-ray diffraction pattern of cosputtered film (sample 41-1).

substrate during deposition is the fact that we observed an improvement in T_c for Ba deficient films, as described below. Figure 4.9 shows R vs. T for a film with Y:Ba:Cu ratio of 1.00:1.05:3.21 grown in the on-axis geometry which has T_c = 77 K. This compares to T_c = 57 K for the film grown on-axis with the same deposition conditions but with cation ratio of 1.00:1.90:3.26 shown in Figure 4.7. A comprehensive study of coevaporated films at low oxygen pressures (0.2 - 10 mT) was reported by Matijasevic *et al.* (1991). In that study, they also found that stoichiometric films have reduced T_c values, and that Ba-deficient films have higher values of T_c. They attribute this effect to an oxygen-deficiency-induced cation disordering, described below. Recent results support these findings [Shinohara *et al.* (1992)]. We note that our films are deposited near T = 700 °C and probably less than 10 mT of oxygen, but are superconducting. These and other similarly deposited YBCO films are superconducting, despite being grown in a thermodynamically unstable region of $P(O_2)$ - T phase space (shown in Figure 4.10) [Bormann and Nolting (1989)]. Sputter deposition, however, is not an equilibrium process.

Oxygen-deficiency-induced cation disordering [Matijasevic *et al.* (1991)] means that at low oxygen pressures, Ba could substitute for Y in the lattice during growth. Consider less O (which tends to gain 2 electrons) in the Cu-O planes during crystallization. Ba (which tends to lose 2 electrons) substitution for Y (which tends to lose 3 electrons) is more favorable from the point of view of valence. Also, when there is less O in the lattice, there is more space for the larger Ba in the normally Y site. After cooling, Ba is "frozen in." Matijasevic *et al.* speculate that if Ba is in the Y site, during cool-down in oxygen, the lattice does not fully oxygenate and T_c is reduced. They claim that if the film is Ba

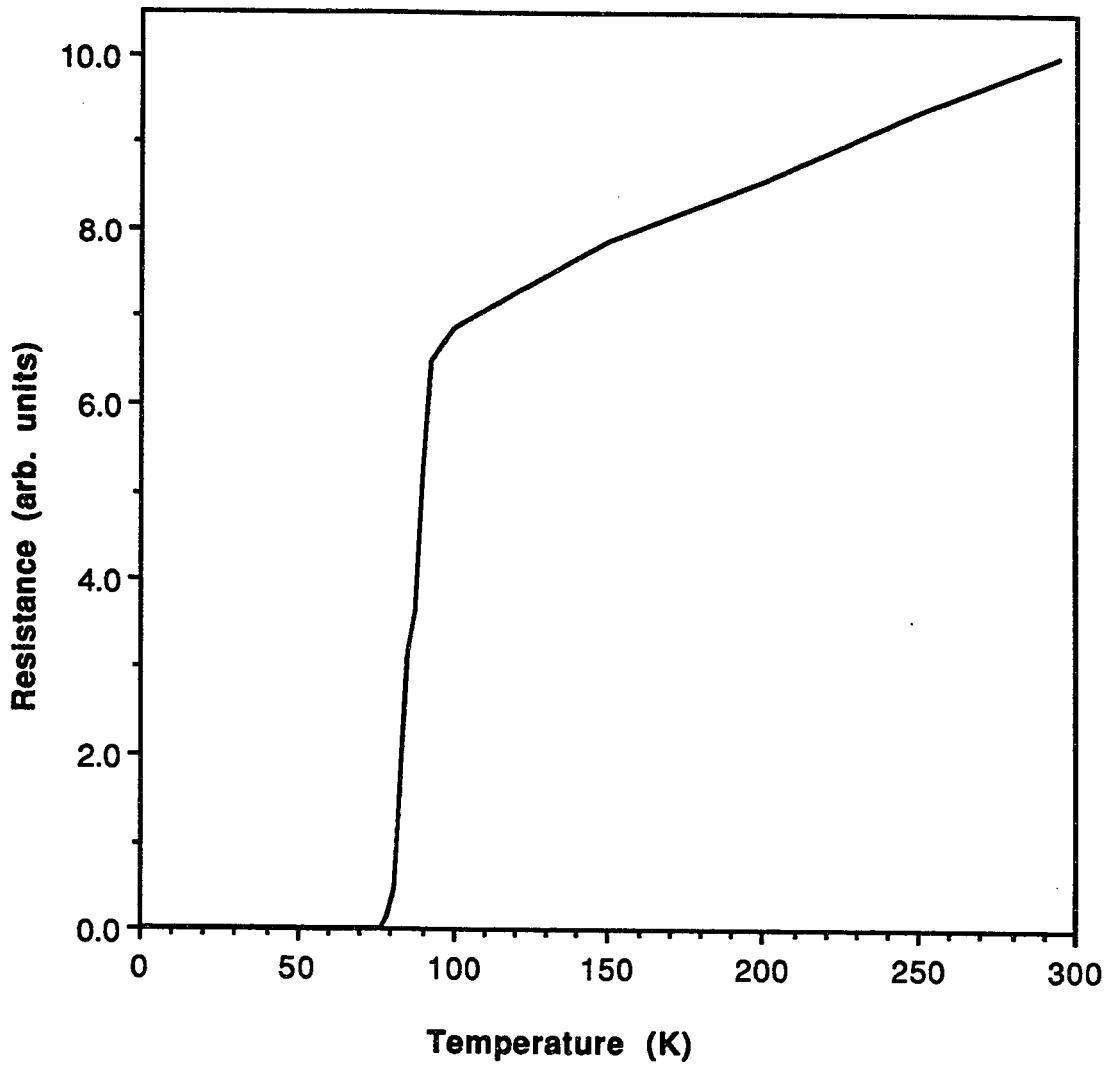

Figure 4.9: Resistance vs Temperature for a Ba deficient film (sample 47-1) grown in the on-axis geometry. The zero resistance temperature improved from 57 K for a stoichiometric film grown with the same deposition conditions, to 77 K for the Ba deficient film shown here.

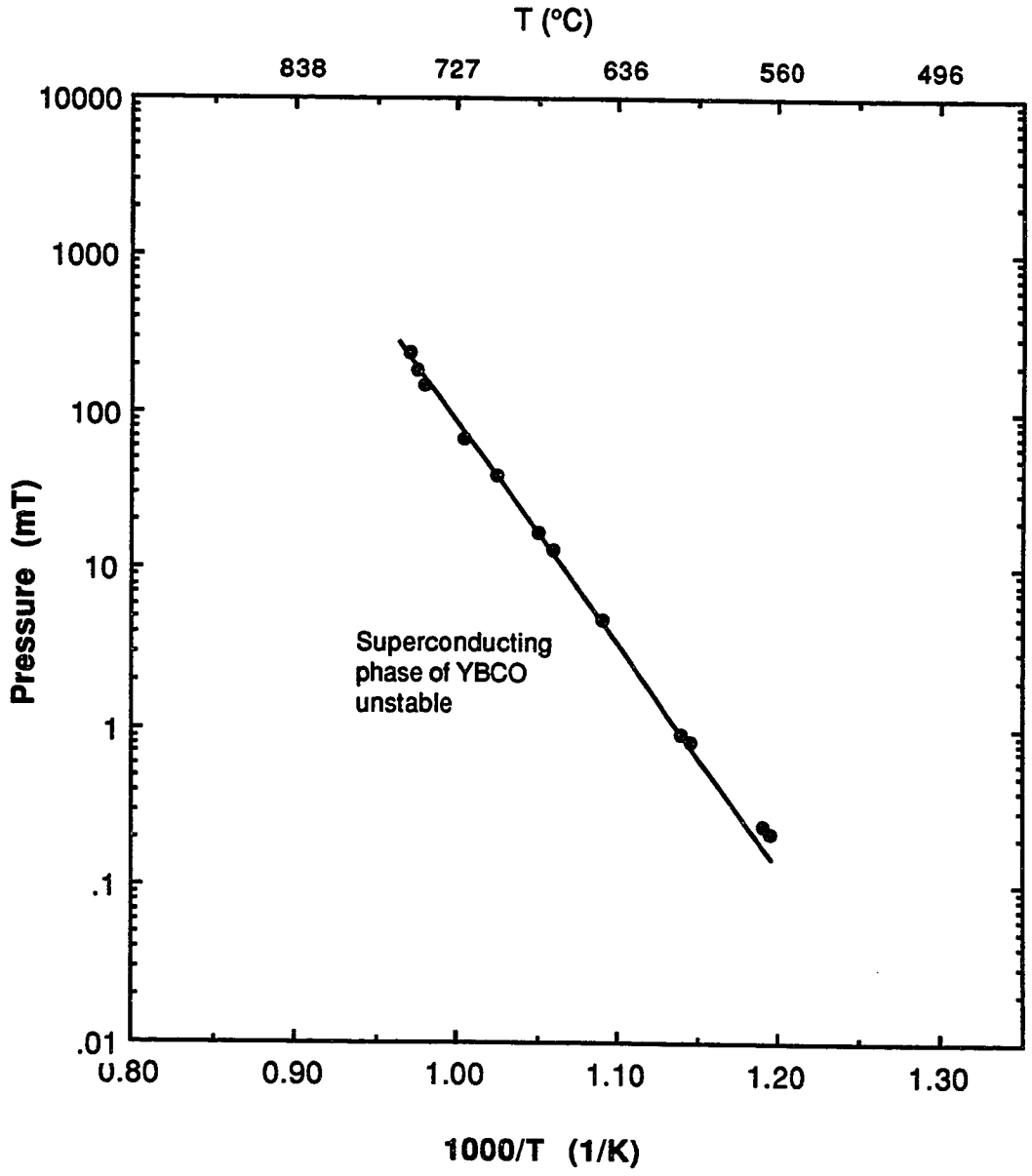

Figure 4.10: Critical oxygen partial pressure below which the superconducting phase of YBCO becomes thermodynamically unstable [from Bormann and Nolting (1989)]. Our films were grown in less than 10 mT at about 700 °C.

deficient, Y substitutes for Ba and this does not happen. This model is consistent with their experimental results.

Recently, introduction of ozone at the growing film during coevaporation has enabled high quality YBCO growth at very low pressures *in situ* [Kublinski *et al.* (1992)]. A partial pressure of oxygen of 10^{-5} Torr, about 1% of which was ozone, was in the chamber during growth. The deposition temperature was about 700 °C. Deposition rate was about 10 Å/min. Films had T_c = 90 K and $J_c = 2 \times 10^6$ A/cm^2 at 77 K. For higher concentrations of ozone, film quality did not improve. They also reported that the pressure of oxygen necessary for *in situ* YBCO growth scales linearly with deposition rate.

With our cosputtering technique, the film composition depended quite sensitively on deposition parameters, especially when compared to other techniques. To illustrate this, Figure 4.11 shows the measured Y:Ba composition ratio as a function of Y gun power for a fixed BaCu sputter gun power. (These results are from off-axis cosputtering but are indicative of both geometries.) Even though the deposition conditions were changed only slightly, the dependence of Y content on Y gun power changed dramatically. We also found that the appearance of the plasma over the BaCu source changed somewhat with changes in substrate temperature and in oxygen flow, probably due to the local partial pressure of oxygen at the BaCu target.

In conclusion, we have grown superconducting YBCO films by off-axis metal cosputtering. Results for T_c compare well with other codeposition techniques, but are not as good as those obtained with a composite target, discussed in the next chapter. In the on-axis geometry, we have observed film degradation caused by oxygen ion bombardment, even for stoichiometric films.

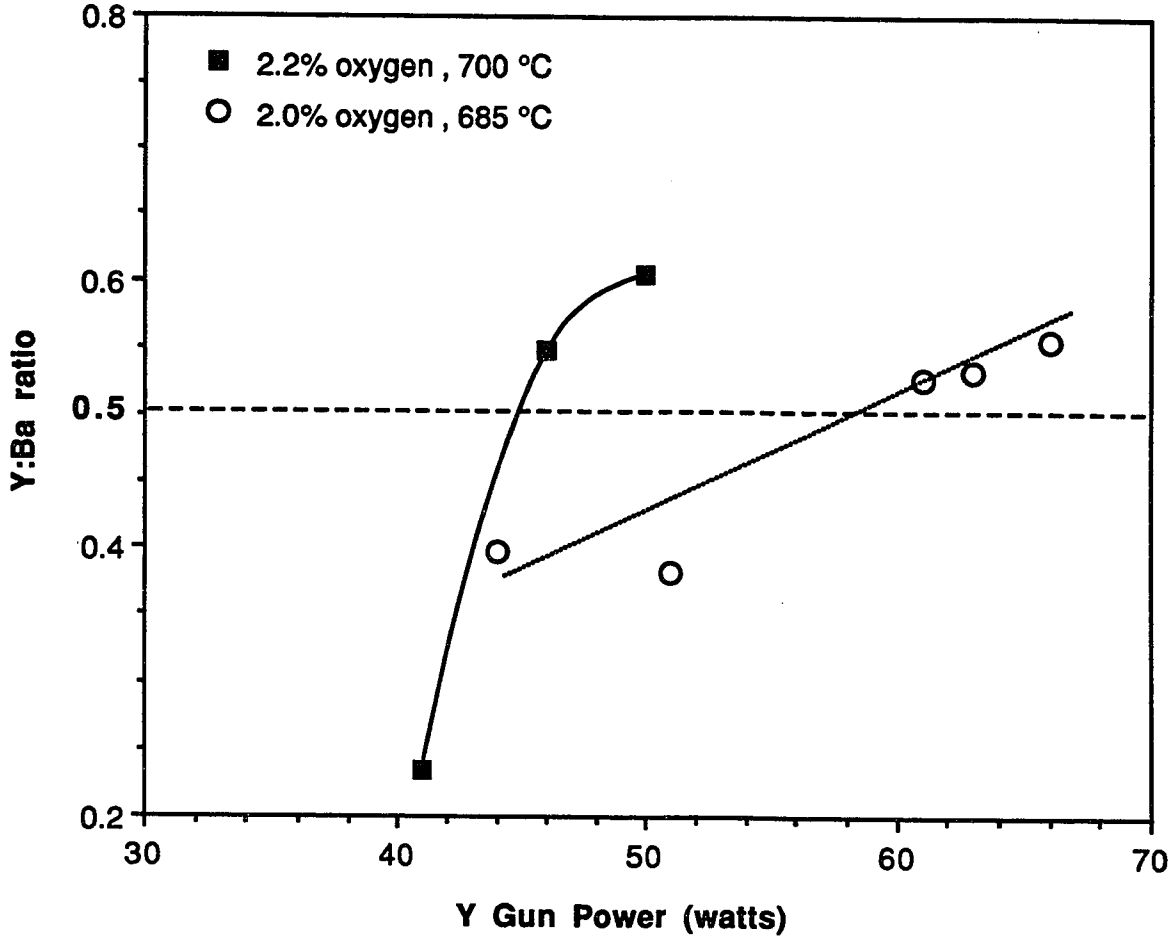

Figure 4.11: Y:Ba ratio as a function of Y sputter gun power for 2 different growth conditions. Power to the BaCu sputter gun was held fixed.

This was apparently eliminated by changing to an off-axis geometry. Further improvement in both film properties and reproducibility should be possible with improvements in the ability to differentially pump. This could be achieved with improved pumping and/or a system geometry that allows a smaller hole between the sputter guns and the growing film. This would allow a higher oxygen pressure at the substrate and a lower oxygen pressure at the sputter guns. These are the most comprehensive results reported for as grown YBCO thin films by metal cosputtering to date.

V. FILMS GROWN BY COMPOSITE TARGET SPUTTERING

YBCO films can also be grown using a single composite source, in contrast to the codeposition approach detailed in the previous chapter. A disadvantage of single source deposition is that it is less flexible. Adjusting stoichiometry or substituting for any of the constituents is less straightforward. However, for YBCO, it turns out that reproducibility and reliability improve and stoichiometry could be indirectly adjusted by varying deposition parameters.

As already described, the presence of resputtering makes *in situ* sputter deposition of superconducting YBCO films difficult. When sputtering from a single source, this is of particular concern because Ba is preferentially etched and there is no direct means to adjust the stoichiometry. In this chapter, I describe two single source sputtering techniques we have tried. One, sputtering with a high strength magnet, we found ineffective. The second however, sputtering in an off-axis geometry, we found very successful, as have other groups.

A. Sputtering with a High Strength Magnet

One attempt at alleviating the problem of resputtering and ion bombardment of the growing film was reported by Migliuolo *et al.* (1990). They reported that stoichiometric YBCO films can be deposited by on-axis, composite target sputtering if a high strength magnet is used in the magnetron sputter gun instead of the conventional strength magnet. They claimed that a stronger

magnet results in lower operating voltages at a given power level, and hence lower oxygen ion energies at a given deposition rate.

The standard magnet they used was SmCo which produced a field of 450 G at the target surface above the magnet. The two parts of the high strength magnet were NdB and NdFeB which produced a field of 1.05 kG above the target's magnetron racetrack. Films were grown at ambient temperature onto Si substrates. Deposition rate and film stoichiometry as a function of magnet strength and substrate position relative to the magnetic field were measured. Lower operating voltages for the high strength magnet were reported. As expected, films grown with the standard magnet were Ba deficient. However, films grown with the high strength magnet were reported not to be Ba deficient. Therefore, they concluded that using a high strength magnet resulted in "little or no resputtering." This effect was attributed to the lower operating voltages. In collaboration with Dr. Migliuolo, we deposited YBCO films at Yale using the same high strength magnet and compared results for films made with the same conventional magnet.

Our results differ from those of Migliuolo *et al.* We found little improvement in film composition when we used the stronger magnet. (Composition measurements were done with ICP.) Films were still Ba deficient. Furthermore, the presence of heat during *in situ* sputtering degraded the films even further. When the deposition was done at an elevated temperature (roughly 600° C), the Cu content was greatly reduced. Results are summarized in Table 5.1.

The Ba deficiency of films grown with this technique using a stoichiometric target is indicative of preferential Ba resputtering. As further

evidence of this resputtering, Figure 5.1 shows deposition rate vs. target-to-substrate distance for films we grew in 20 mT Ar using the high strength magnet. Also shown are rates for films of aluminum and copper reported in the Torus product information provided by Kurt J. Lesker Co. As described in Chapter IV, Section C2, high energy ion bombardment is more directional than sputter deposition. Therefore, oxygen resputtering becomes a more important effect at greater distances. To see this, consider the oxygen ion sputtering to have no angular spread. The removal rate would be independent of target-to-substrate distance. The arrival rate of Y, Ba, and Cu falls with increasing distance. For an ideal point source, rate falls off as $1/r^2$. Sputter deposition, not being from an isotropic point source, falls off at a slower rate. This is especially true for the distances of interest, as can be seen for the Al and Cu rates. The net deposition rate = arrival - removal. Figure 5.1 shows that for YBCO on-axis sputtering with the high strength magnet, the deposition rate fell off considerably faster than expected, indicative of resputtering. Finally, the magnitude of the Ba deficiency became greater with distance (see Table 5.1), again indicative of resputtering.

These results are not encouraging for the use of on-axis composite target sputtering of high temperature superconductors, particularly onto heated substrates.

B. Off-Axis Sputtering

1. System Modifications

It turns out that the most effective way to minimize the effects of

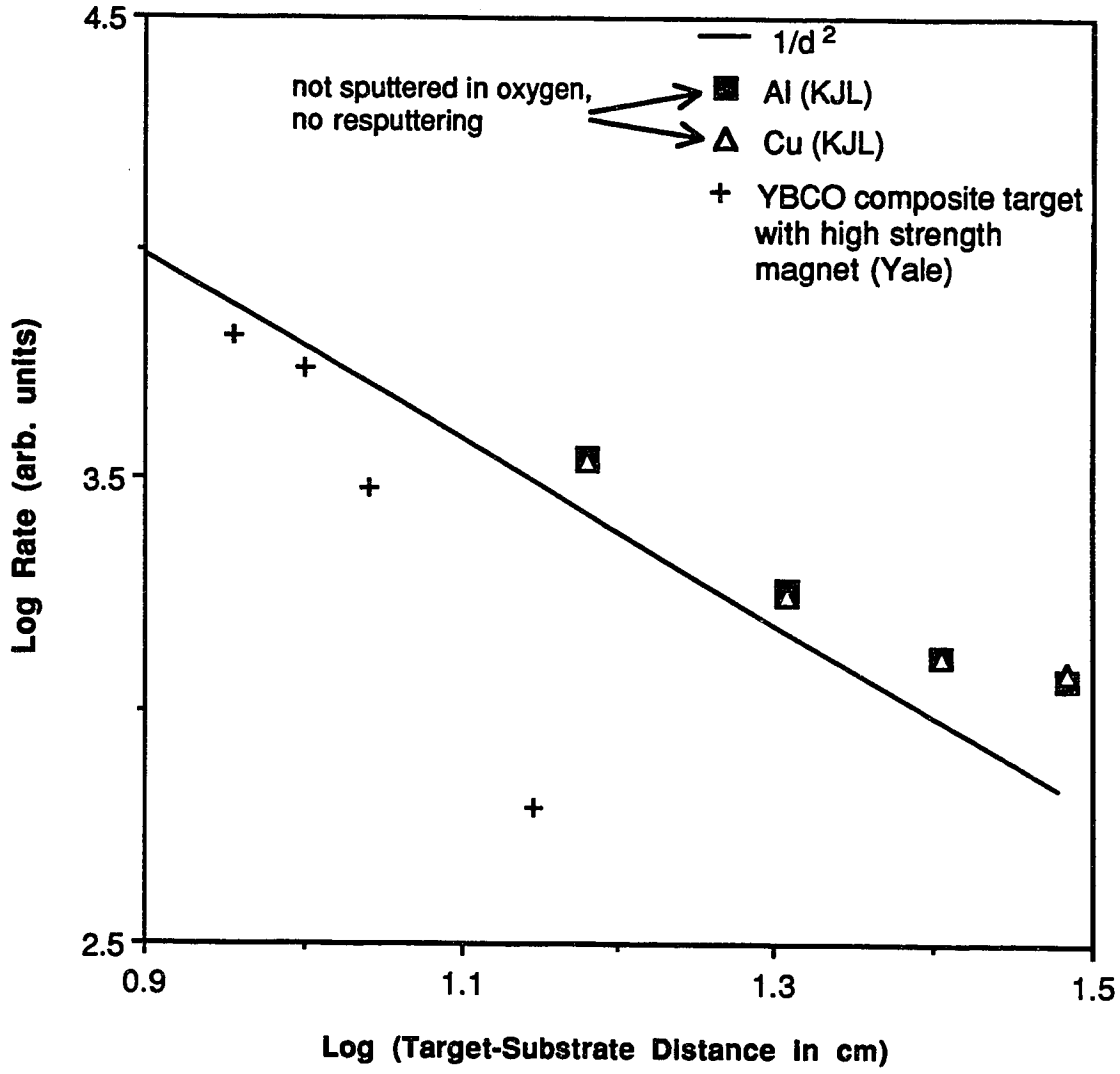

Figure 5.1: Rate vs. target-substrate distance (d) showing the effect of resputtering in oxygen.

resputtering when sputtering from a single source of YBCO is to simply point the gun away from the substrate [Li *et al.* (1988), Eom *et al.* (1989)]. This is the off-axis geometry described earlier. A summary of our deposition runs using a composite target in the off-axis geometry is given in Appendix E.

Initially, the gun was raised slightly and the the can dividing the substrate region from the sputter gun region (see Figure 4.1) was left in place. The YBCO films were not superconducting and eventually, the modifications to the system shown in Figure 5.2 were made. Most notably, the gun with the YBCO target was pointed away from the substrate by turning it so that it pointed several inches away from the growing film. This is similar to the change made in our off-axis cosputtering work. The gun was also raised in order to increase the deposition rate. Even with this rise, the rate was of order 100 Å/hour for composite target sputtering as compared to of order 6000 Å/hr (100 Å/min) for cosputtering.

Initially, we had the problem that after a few runs, the target would crack and craters would form on the target surface. The cracking problem was solved by switching to a target which came bonded to a Cu backing plate. This improved the thermal contact to the water cooled backing plate and added mechanical support to the target. The crater problem disappeared when we switched from sputtering with dc voltage to rf. This apparently decreased the dependence of the plasma on secondary electrons and hence prevented the formation of hot spots during sputtering.

As will be described shortly, for composite target sputtering, it is necessary to sputter at higher pressures (100 mT and higher). Several modifications were necessary to accommodate this. At these pressures the

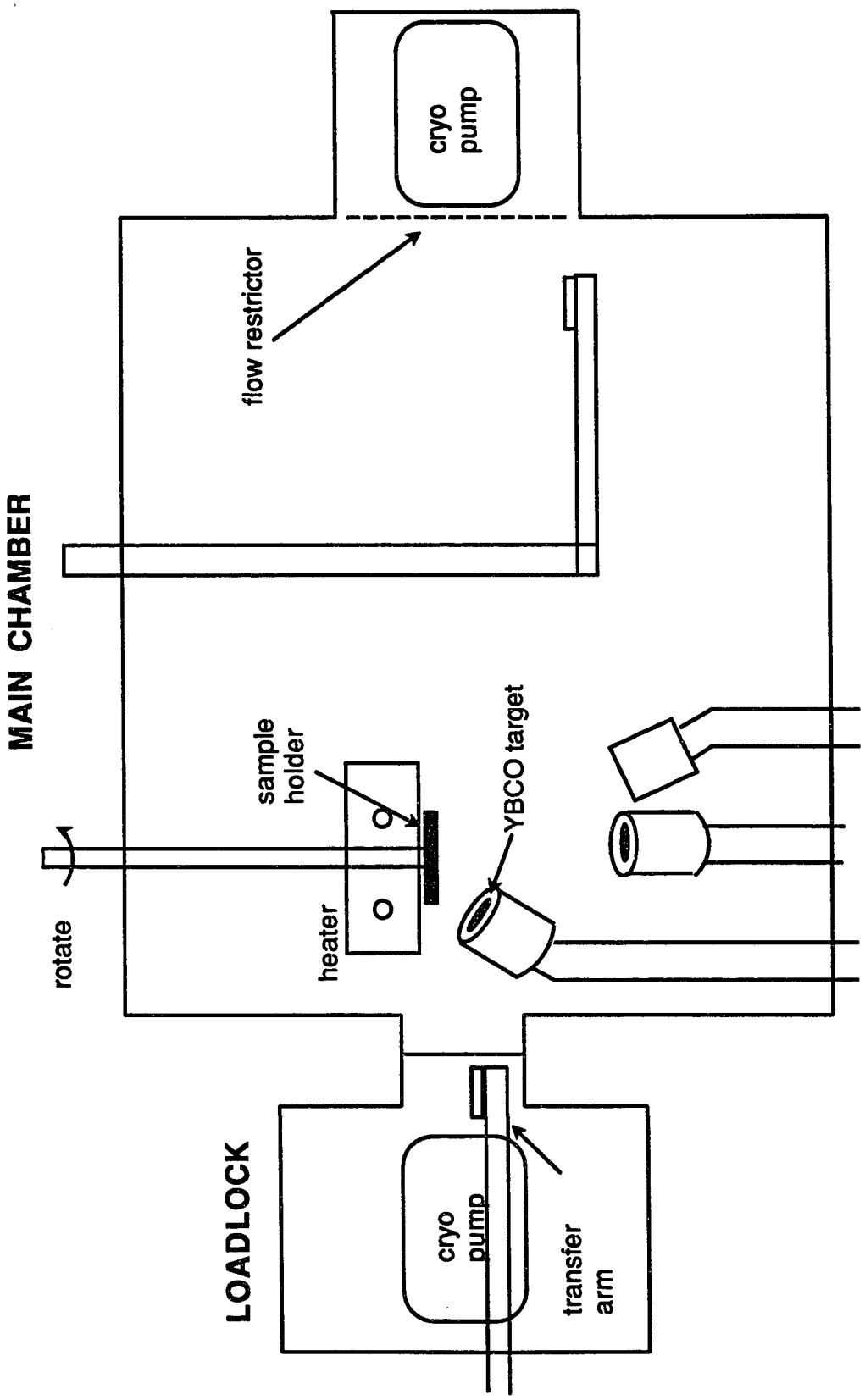

Figure 5.2: Schematic of deposition system after modifications were made for composite target sputtering.

mean free path is very short (of order 1 mm). Because there were many collisions before deposition, YBCO landed all over, even when there was no line of sight to the target. The quartz lamps became covered with YBCO (which is black). As the coating became thicker, more of the power which originated from the inside of the lamp coupled into the quartz envelopes of the lamps, making it hotter. The lamp exploded after just one or two runs. This problem was alleviated by putting a quartz sleeve over the lamp to block the deposition. This proved effective, extending the lamp lifetime usually to more than ten runs.

A second problem with sputtering at high pressures was that an unwanted plasma could occur between the grounded can and the high voltage target within the can (see Figure 4.4). This distance d shown in Figure 4.4 was initially set at 40 mils (about 1 mm). At higher pressures, the dark space distance of a plasma decreases. At the pressures used, the dark space distance was of the order of 1 mm creating the unwanted plasma within the can. This apparently etched the stainless steel ground can and/or the stainless steel target support causing impurities to deposit in the film. We saw Fe impurities in our films until we decreased the distance between the ground can and the target. Figure 5.3 shows the resistive transition of a YBCO film with 2.2% Fe impurities (by mass of the cations, as measured using ICP). This result is in agreement with the results shown in Figure 3.6. When the distance d of Figure 4.4 was decreased to about 25 mils, the Fe content in our films had dropped below the detectable level (about 0.6%).

Other changes were also made. Because there was no longer differential pumping or large pressure gradients, the oxygen confinement tube,

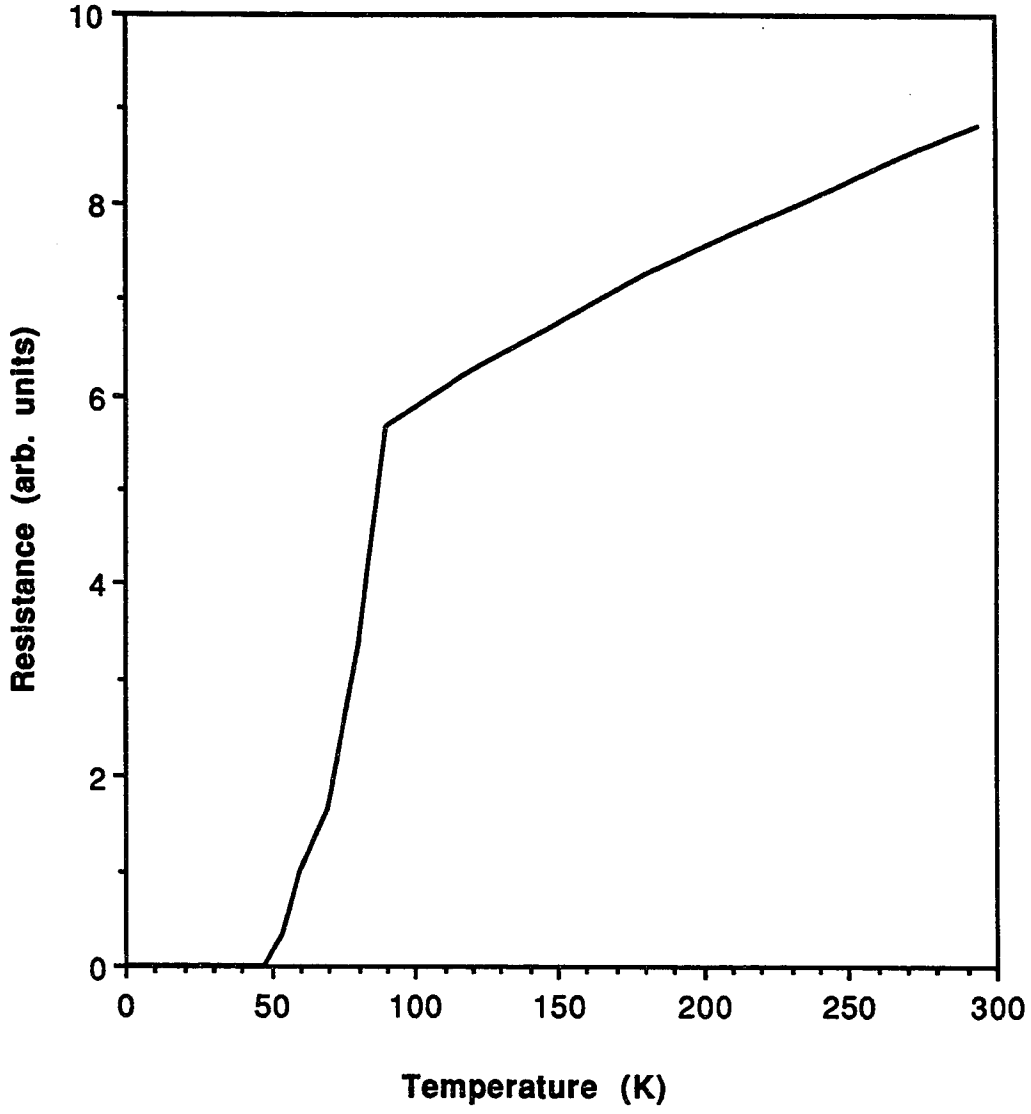

Figure 5.3: Resistance vs. Temperature of an Fe-contaminated film (sample B42-4) grown from a single target in the off-axis geometry.

the oxygen inlet ring, the can dividing the substrate region from the sputter gun region, and one of the flow restrictors were removed. Oxygen was fed in at the bottom of the chamber and only the main chamber cryopump was used during sputtering. The crystal monitors, which were no longer needed, were also removed. These changes are shown in Figure 5.2.

2. Deposition Conditions

When sputtering from a single composite target, the following parameters need to be optimized: cool down temperature and time, gun power, oxygen partial pressure, system geometry, temperature, and total pressure. It is worth noting that with one target, there are no separate gun rates which can be varied to adjust stoichiometry. In optimizing deposition conditions, the film properties initially of most interest are critical temperature, deposition rate, and film stoichiometry. Since runs are costly and time consuming, a method of efficiently spanning parameter space is desired. Orthogonal design is such a method [Yin and Jillie (1987)]. With orthogonal design, it is possible to vary several input parameters each over several settings simultaneously in such a way that the average effects of each parameter can be analyzed separately. This is done in a minimum number of total runs.

This is best illustrated by an example. Table 5.2 shows how each of 4 input parameters can be varied over three separate settings for each. Without the orthogonal design approach, $3^4 = 81$ runs would be necessary to span parameter space. With the orthogonal approach, the dependence of properties on each of the input parameters can be extracted after 9 runs. For example, the dependence of some property A on, for example input parameter 2 can be

Table 5.2: Orthogonal table with 4 inputs each varied over 3 settings (a,b,c).

Run Number	Input Parameter 1	Input Parameter 2	Input Parameter 3	Input Parameter 4
1	a	a	a	a
2	a	b	b	b
3	a	c	c	c
4	b	a	b	c
5	b	b	c	a
6	b	c	a	b
7	c	a	c	b
8	c	b	a	c
9	c	c	b	a

determined. For setting a of parameter 2, the value of property A is averaged over runs 1, 4, and 7; for setting b, property A is averaged over runs 2, 5, and 8; and for setting c, property A is averaged over runs 3, 6, and 9. For each of the 3 settings of parameter 2, the values of each of the other 3 input parameters are ideally averaged out, leaving only the dependence of parameter 2. The same can be said of the determination of any property at any setting of any input parameter, which is determined in a similar way. With this approach, parameter space is spanned most efficiently.

The most important deposition parameters to vary were chosen. The initial values of the parameters were chosen by considering our earlier work and typical settings found in the literature. An orthogonal table like that of Table 5.2 was constructed. The runs were performed and the film properties of interest were measured. The input parameters varied were total pressure, percent oxygen, substrate temperature, and gun angle. Gun angle refers to how much the gun was turned from its original position (see Figure 5.2). By increasing the gun angle, the target faced farther away from the substrate. $SrTiO_3$ substrates were used and they were mounted to the Haynes alloy pallet by the technique using Ag paste described in Chapter IV. The film properties measured for films of each run were resistive onset to superconductivity, zero resistance temperature, Ba:Y ratio, Cu:Y ratio, and deposition rate. Composition and rate were determined by the ICP technique described earlier.

3. Results

The results of the orthogonal approach are shown in Table 5.3. Several identical runs were performed (identical runs B19 and B22 are shown) and

Table 5.3: Orthogonal table used initially for off-axis sputtering.

Run #	Total Press. (mT)	Percent Oxygen	Deposition Temp (°C)	Gun Angle	Resist. Onset (K)	Zero Resist (K)	Ba : Y ratio	Cu : Y ratio	Rate Å/hour
							ideal=2	ideal=3	
B19	150	13	650	0	84	28	1.67	2.41	279
B22	150	13	650	0	84	19	1.67	2.50	242
B23	150	20	700	10	84	69	1.74	2.34	188
B27	150	5	725	20	84	81	1.93	2.40	164
B28	200	13	700	20	83	78	1.90	2.52	150
B20	200	20	725	0	86	74	1.73	2.47	215
B26	200	5	650	10	84	67	2.04	2.86	158
B25	250	13	725	10	?	14	1.92	2.63	153
B29	250	20	650	20	86	67	1.91	2.82	144
B21	250	5	700	0	85	65	2.19	2.88	247

results were found to be reproducible. Dependence of film properties on input parameters was determined by the method of orthogonal design. The dependences which gave useful information are now described.

The dependence of the Ba:Y ratio on total pressure is shown in Figure 5.4. The dots show all the data. The line is a simple fit to the average at each of the three values of pressure. The spread in Ba:Y ratio at each value of pressure is expected since the other parameters vary within these points. This is why the average is of interest. The graph indicates that the films were Ba deficient at lower pressures. This could be explained by resputtering (which is a greater effect at lower pressures where the mean free path is shorter). Furthermore, the results indicate only a weak dependence of deposition rate on pressure. Based on this information, a slightly higher total pressure (250 mT) was eventually used.

Figure 5.5 shows the results for zero resistance temperature vs. substrate temperature during film growth. Again, like all these results, the dots show all the data, the curve is a simple fit to the averages, and the spread in points is expected. This indicates that the optimal temperature was probably near the middle of the temperature range shown.

An interesting effect is observed when the Ba:Y ratio was plotted vs. gun angle (Figure 5.6). There was less of a spread in Ba:Y at a given angle as the angle was increased. The spread of points was due to the fact that the other input parameters were varied. The smaller spread at the higher gun angle indicates that there was less of a dependence of the Ba:Y ratio on other input parameters as gun angle was increased. Furthermore, Figure 5.7 indicates that there was some improvement in zero resistance temperature with increasing

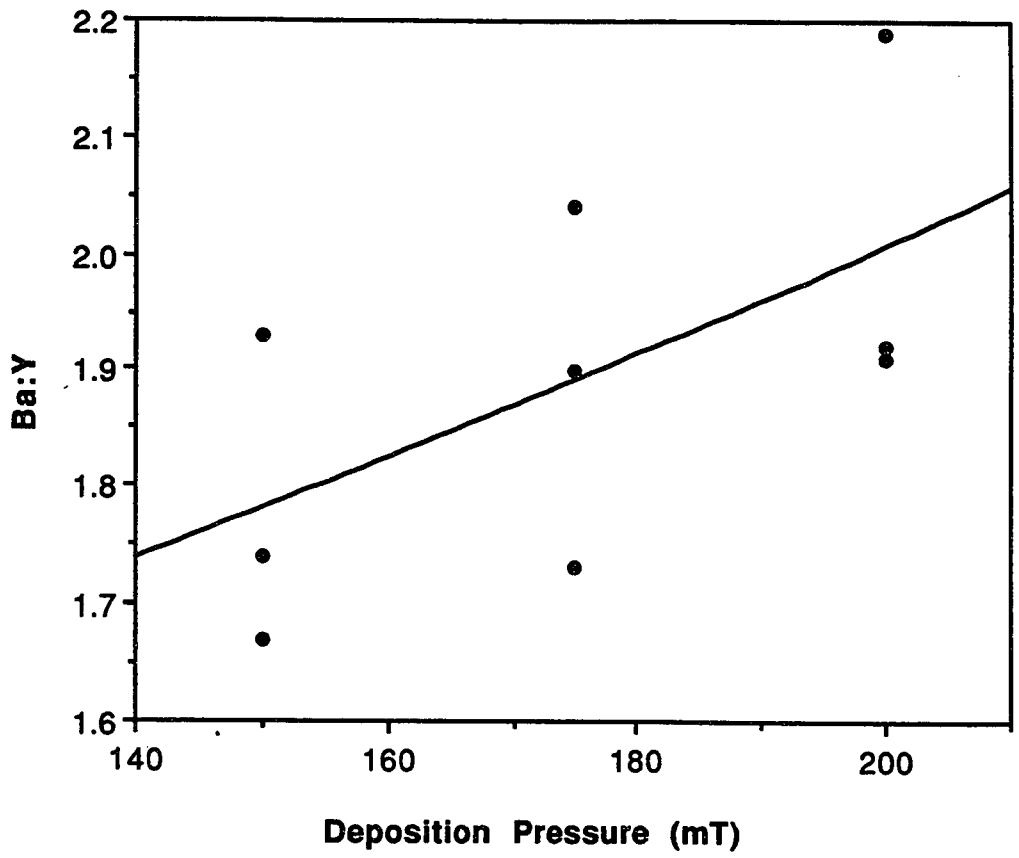

Figure 5.4: Dependence of Ba : Y ratio on total pressure.

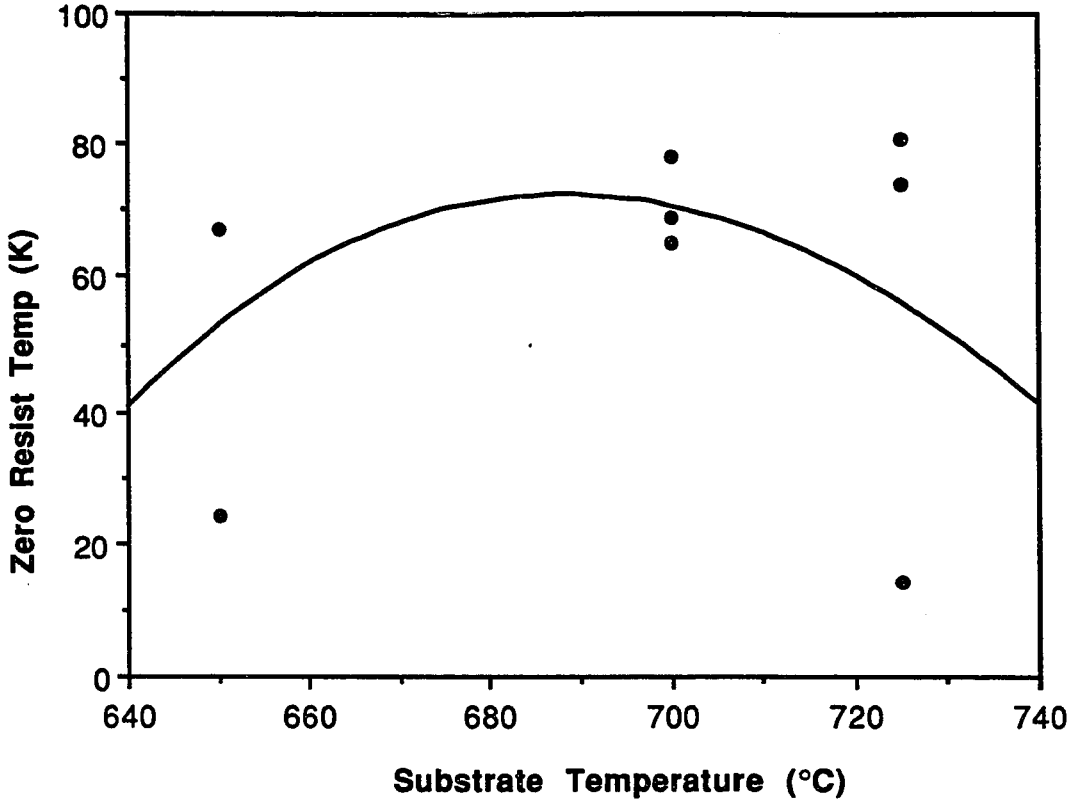

Figure 5.5: Zero resistance temperature as a function of deposition temperature.

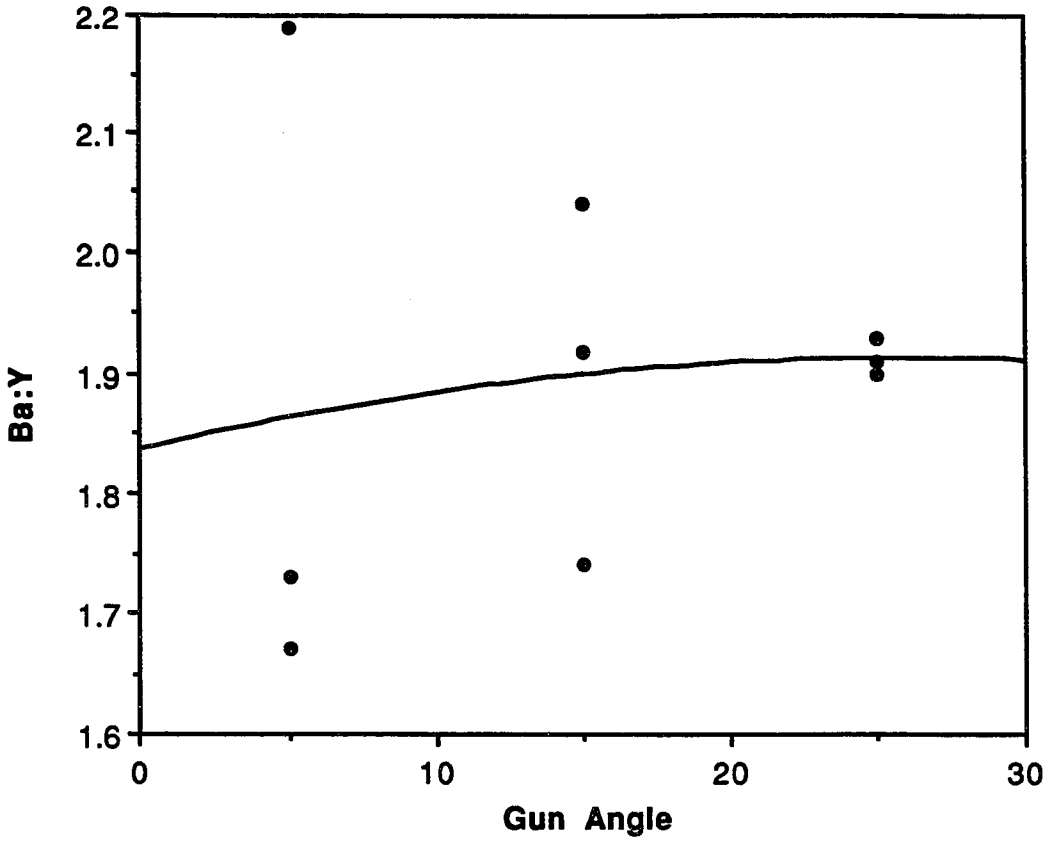

Figure 5.6: Dependence of Ba : Y ratio on the angle which the gun is twisted away from the growing film.

gun angle. However, not surprisingly, there was a decrease in deposition rate as the gun pointed farther away from the substrate (Figure 5.8). For these reasons, the gun angle was set at an angle of 35°.

After considering results from the orthogonal design, from the literature, and from our earlier work, the deposition conditions were set to the following: 250 mT total pressure, 38% oxygen (oxygen flow/total flow = 0.38), and $T_{dep} \approx$ 700 °C. Cool down conditions were typically a 6 hour ramp down to room temperature in 50 Torr of pure oxygen. The problem of Fe contamination was eliminated by decreasing the distance between the grounded can and the target, as described earlier. Films were eventually grown mostly on $LaAlO_3$. The film properties were very good. Figure 5.9 shows the resistive transition of a film grown with these deposition conditions. The onset to the superconducting state was at 92 K and the film had zero resistance just above 90 K. These temperatures are indicative of a high quality film.

Another way the superconducting transition was measured was with a mutual inductance technique. The film was placed between two coils (see Appendix B for a figure). Each coil was about 1/4-inch in diameter and 20 turns. Using a lock-in amplifier, an ac current was put through one coil and the induced voltage of the other coil was measured. The excitation current was typically 31 μA and the frequency was typically 50 kHz. The induced voltage was of order of 0.1 mV. This voltage was plotted vs. temperature. When the film became superconducting it excluded magnetic field, so the induced voltage decreased. This is a more critical test of superconductivity than a resistive measurement where a single superconducting path between the current leads shows up as zero resistance. Furthermore, this is a non-destructive, non-

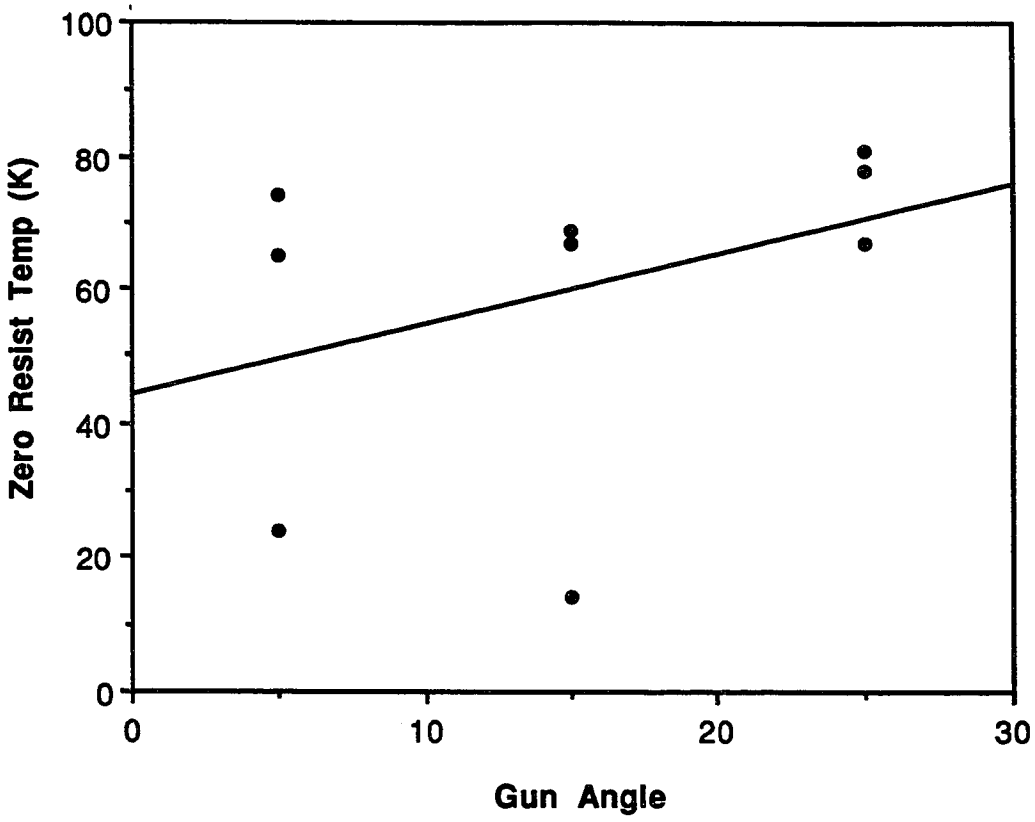

Figure 5.7: Zero resistance temperature as a function of gun angle.

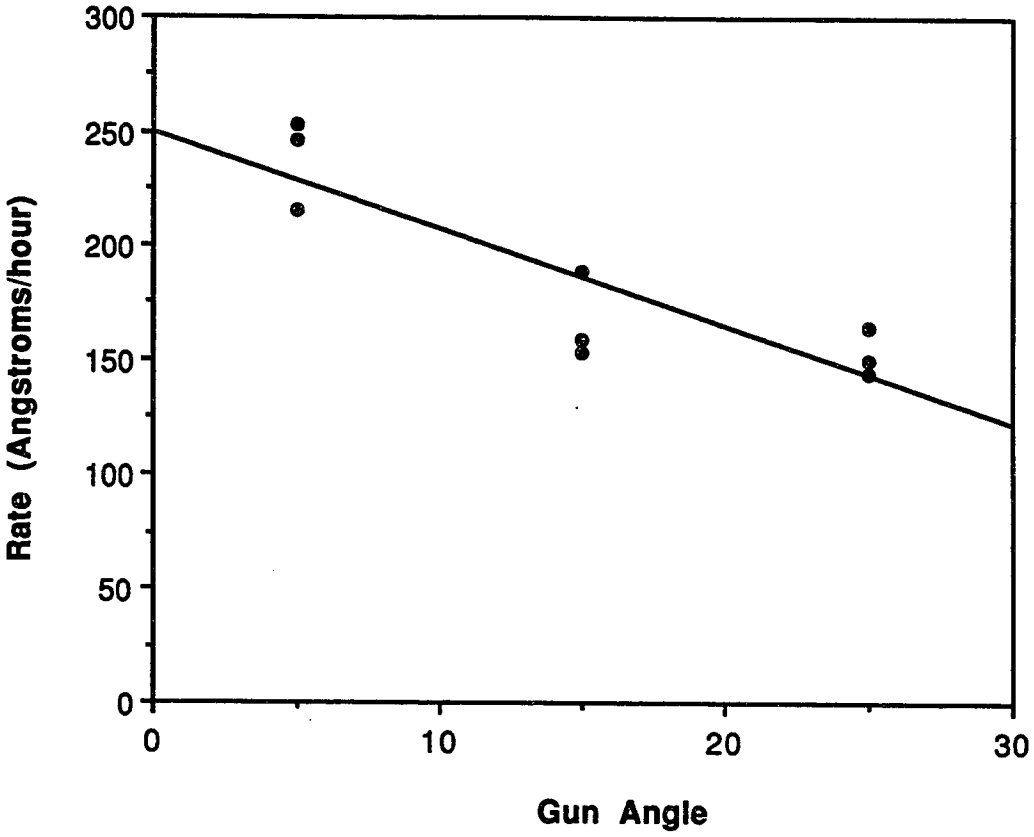

Figure 5.8: Dependence of deposition rate on gun angle.

contacting, easy way of measuring the superconducting transition. The inductive transition of the same film of Figure 5.9 is shown in Figure 5.10. Again this indicates a very good film. Finally, there was very little dependence of the inductive transition measurement on the magnitude and the frequency of the current through the coil.

For the reasons described in Chapter III, epitaxial growth was desired. Figure 5.11 shows x-ray diffraction results of a film grown by off-axis composite target sputtering. It is a θ - 2θ scan. There are only (00*x*) peaks which indicates that the film is epitaxial with the c-axis normal to the substrate.

Preliminary measurements of J_c of one of our films has been performed. The measurement technique is one developed by Scharen *et al.* (1991) based upon remnant magnetization measurements. In this technique, the sample is placed in an external magnetic field greater than a saturation field H^* (of order 200 Gauss) which is then reduced to zero. Because magnetic flux is trapped in the superconductor, the sample has a remnant magnetization. This magnetization can be related to the critical current density of the material by the Bean model. For initial external magnetic fields greater than H^*, the remnant magnetization remains the same. Scharen *et al.* show how a measurement of the magnetic field a known distance from the superconductor can be related to the critical current density using the Bean model [Bean (1964)]. For a square film, they show that:

$$H(z) \approx 5.66 J_c d/c \, [\ln(a/z) - 0.207] \qquad (5.1)$$

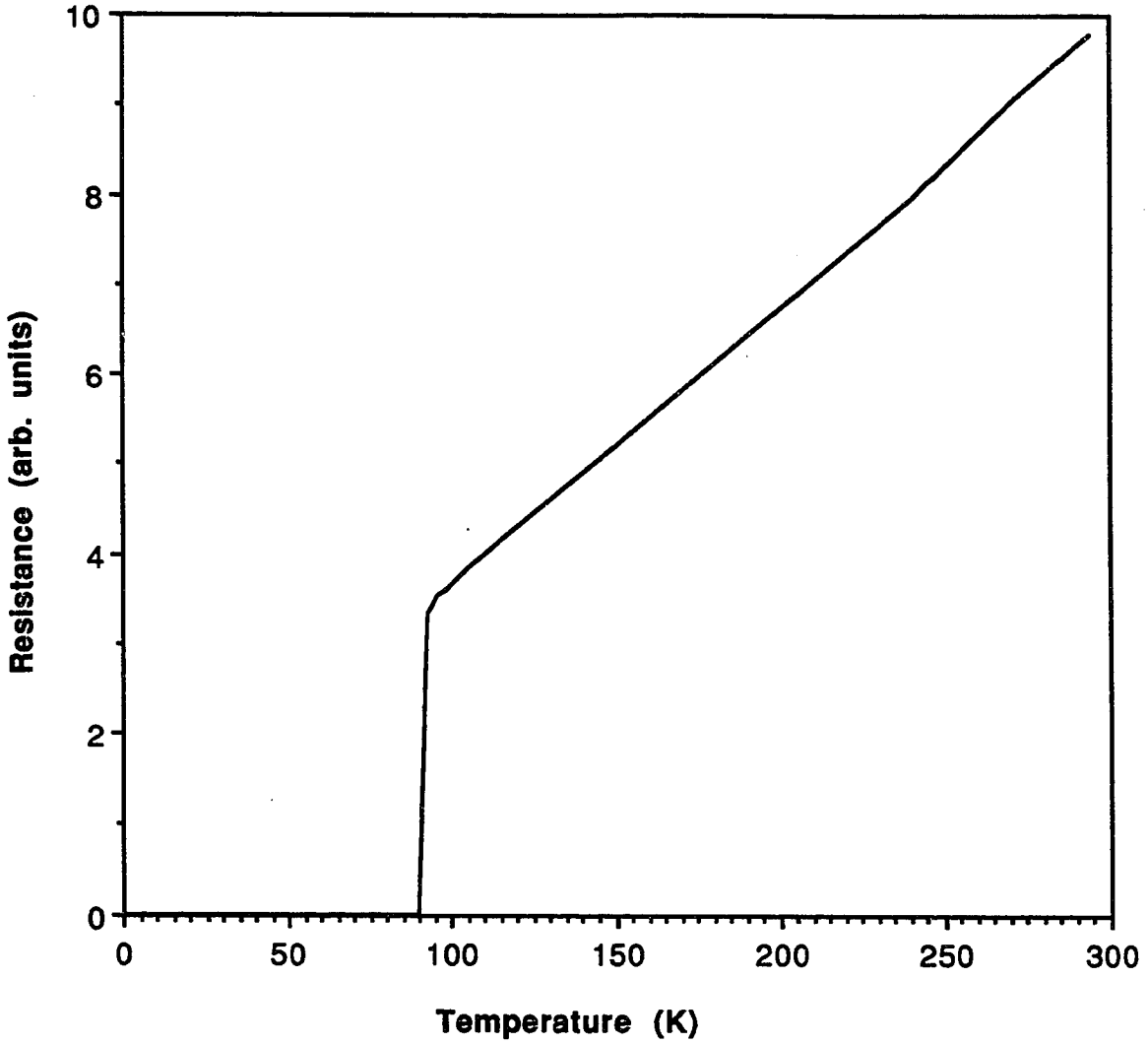

Figure 5.9: Resistance vs temperature for a film grown with a composite target in the off-axis geometry (sample B51-2). The film had zero resistance at 90 K.

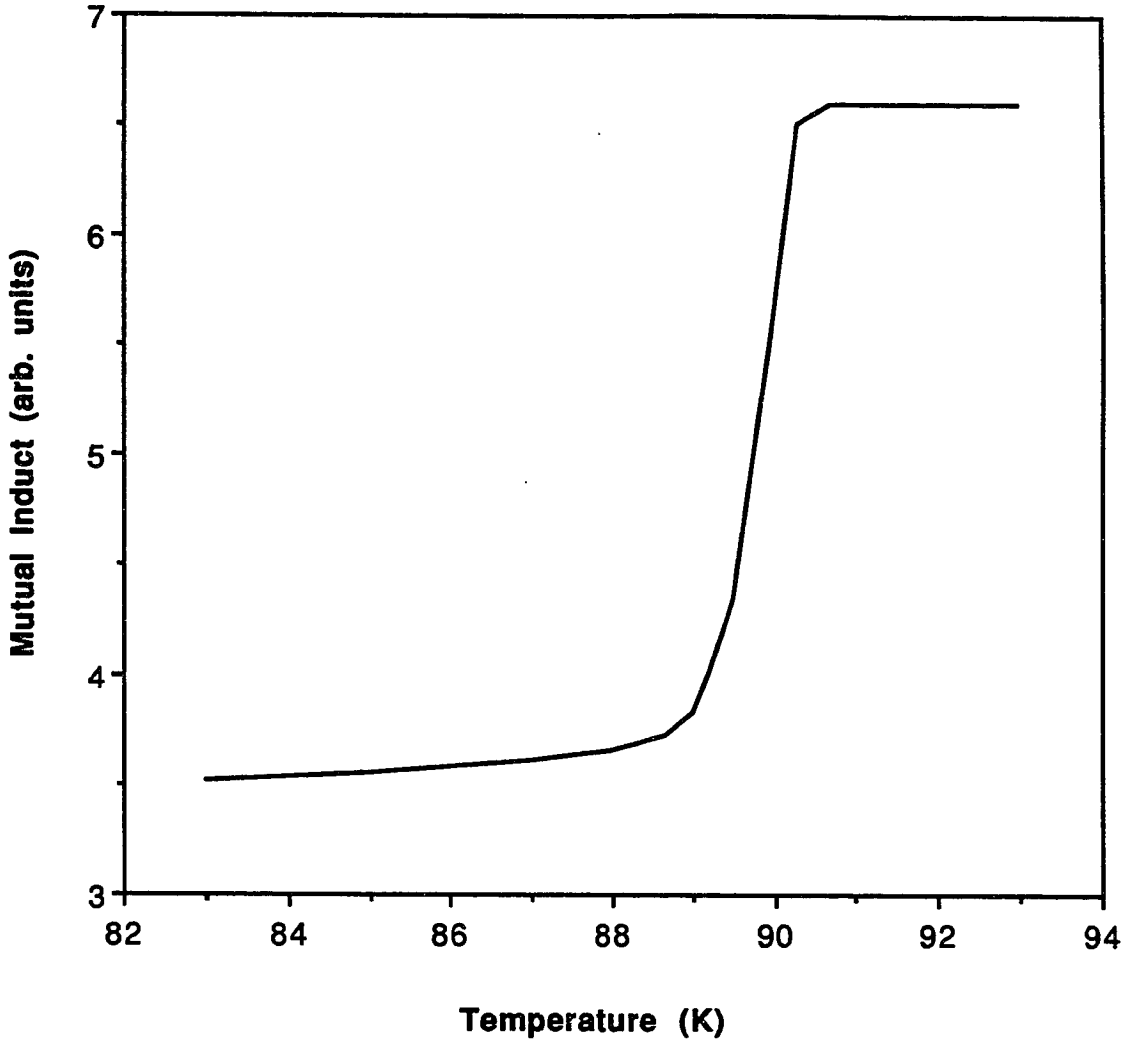

Figure 5.10: Mutual inductance between 2 coils vs. temperature for the same sample of Figure 5.9. The sample was between the 2 coils as it cooled and hence this curve shows the superconducting transition.

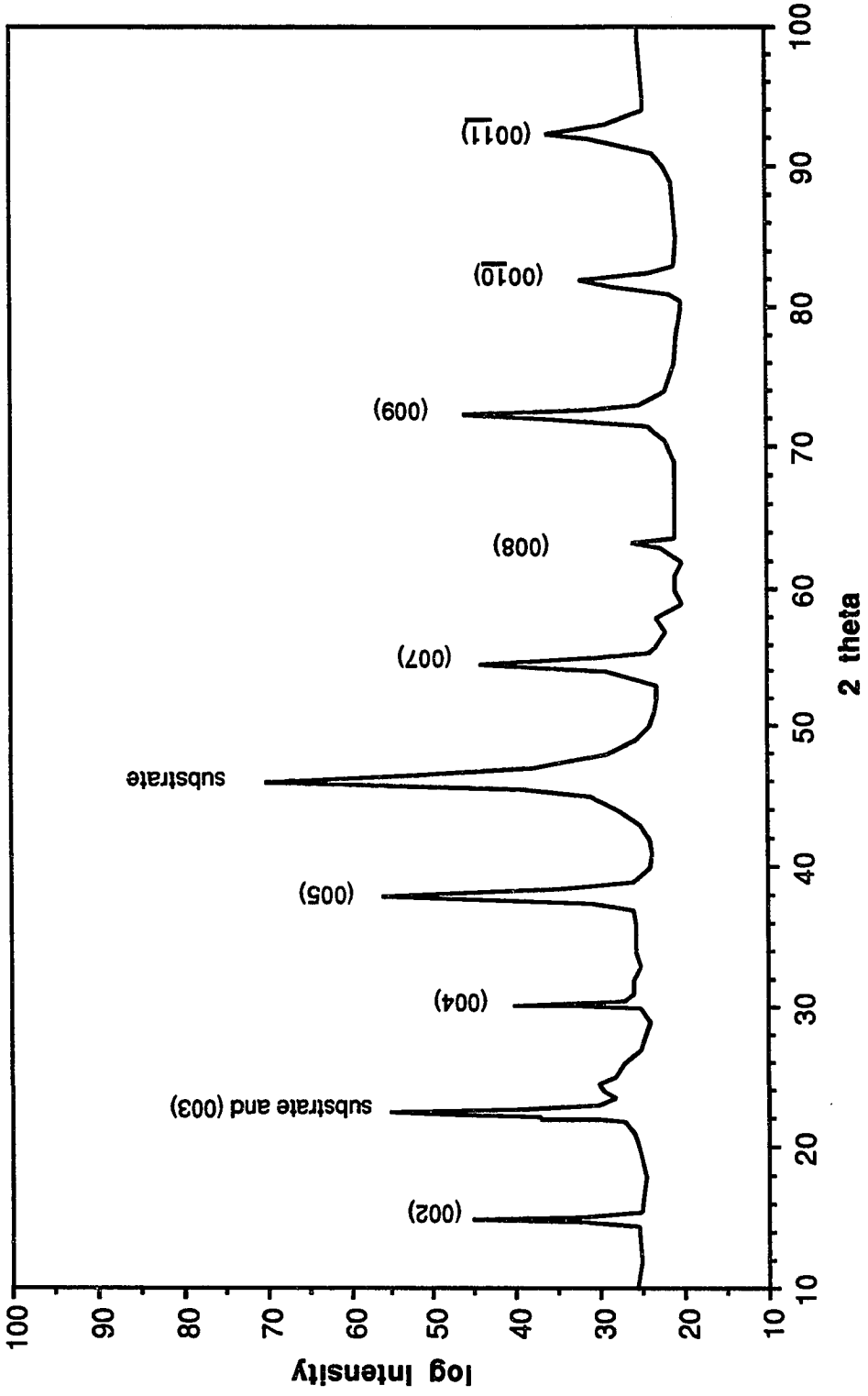

Figure 5.11: x-ray diffraction pattern of composite target sputtered film (sample B39-3).

where H is the magnetic field measured a distance z above the center of the film, d is the thickness of the film, c is the speed of light, and a is half length of the film edge.

A schematic of our measurement apparatus is shown in Figure 5.12. The Hall probe assembly was screwed to the bottom of the cryostat (see the figure in Appendix B). Magnetic field was measured with a GaAs Hall probe. For sample B55-1 we measured a remnant magnetic field of 37 Gauss at liquid helium temperature. Using equation (5.1) this corresponds to a critical current density of 8×10^6 A/cm^2. Based on calibration of this technique by Scharen *et al.*, on measurement of a sample with known J_c in our cryostat, and on considerations of uncertainties of parameters of equation (5.1), we estimate that this value of J_c is accurate to within about 40 percent. It would be necessary to perform further measurements to improve upon the accuracy of this measurement. However, this result does demonstrate that J_c is reasonably high in our films, especially since this was not one of our best films (T_c = 80 K).

4. Discussion

In conclusion, we have demonstrated that we can grow high quality epitaxial thin films of YBCO by off-axis composite target sputtering. Even further improvement should be possible with further optimization of parameters. One complication that arose was Ta contamination in our films resulting from work being conducted in a different part of the chamber. This will be discussed in the conclusion.

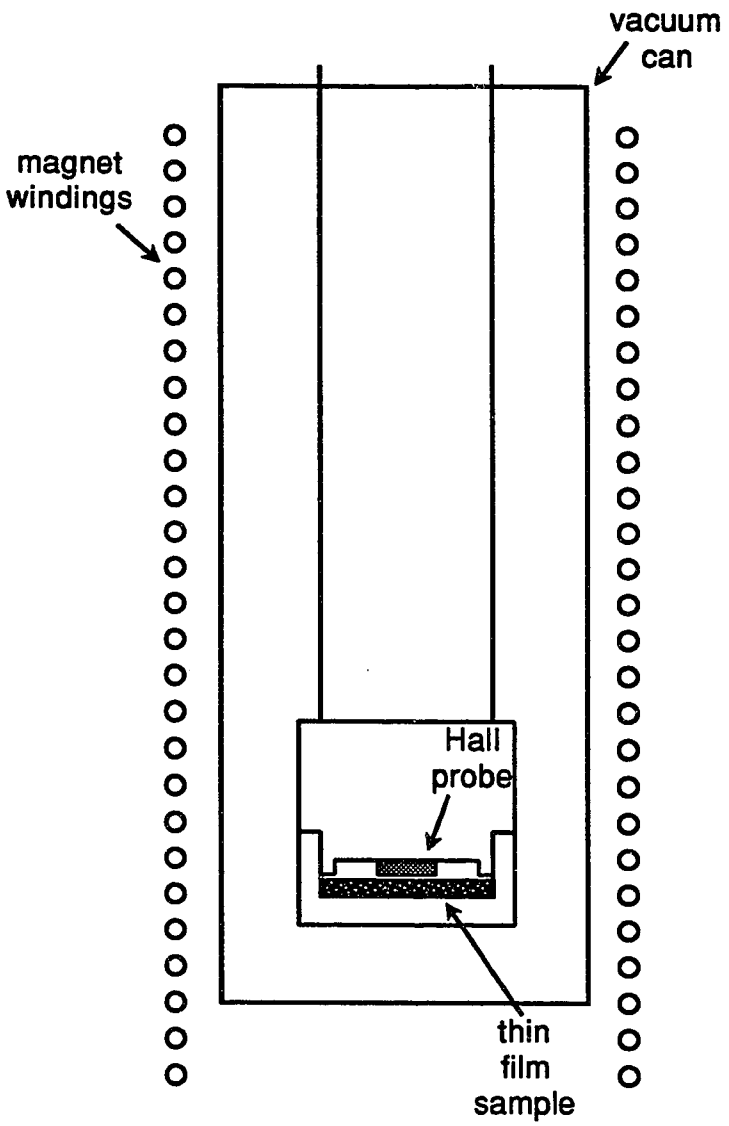

Figure 5.12: Experimental apparatus used for magnetic measurement of Jc.

VI. SUPERCONDUCTING DEVICES

Our goal in the field of high temperature superconductivity has been to fabricate superconducting devices and study their behavior to gain physical insight into these fascinating materials. To fabricate quality devices, it is necessary to grow quality films. Film growth here has been described in the previous two chapters. In this chapter, after further describing superconducting devices, both in general and for YBCO, our work towards fabricating a device is described. Progress towards a novel approach was made and is described.

A. Superconducting Weak Links

As described in Chapter II, devices where two superconductors are weakly coupled have a profound impact on the understanding and application of superconductors. Such devices are called weak links. Traditionally, a tunnel junction, that is a superconductor - insulator - superconductor (SIS) sandwich, has often been the structure chosen for such weak link devices. However, fabrication of such devices has been elusive for YBCO.

Consider two superconductors separated by a thin insulating barrier (a SIS junction). For low T_c superconductors, this barrier is often just the native oxide of the first material. If the barrier is sufficiently thin, electrons can quantum-mechanically tunnel through the barrier. Consider the current-voltage relationship of such a junction at low temperatures. For $V < 2\Delta/e$, there is insufficient energy to break up the superconducting electron pairs and there is

no current of single electrons. When $V \approx 2\Delta/e$, there is enough energy to break up the pairs and there is a sudden increase in current due to the tunneling of the resultant excited single electrons. Since the tunneling current depends on the density of available excited states, the density of states can be extracted from the I-V curve.

In addition to single electron tunneling of a junction, there is Josephson superconducting tunneling. The dc Josephson effect is tunneling of electron pairs. A current density up to some critical value which depends on the thickness of the barrier can tunnel through the junction. The magnitude of this supercurrent depends on the difference in the phase of the electron pair waves on either side of the barrier. More practically, the difference in phase is determined by the value of the current set.

If a dc voltage V is maintained across the junction, the phase difference changes with time and the supercurrent will oscillate with a frequency $\omega = 2eV/\hbar$. Inversely, if a junction is subjected to microwave radiation at a frequency ω, current steps in the I-V curve will occur at integral multiples of $V = \hbar\omega/2e$. This is the ac Josephson effect.

Superconductors can be weakly coupled in many ways in addition to the SIS sandwich. These include through a normal metal (a SNS junction), a mechanical constriction, a point contact, or a grain boundary. Fabrication of a SIS YBCO junction is very difficult. One reason is that the short coherence length of YBCO is problematic. Since the coherence length ξ is the minimum length for spatial variations in the superconducting wave function, the interfaces of a device should be near perfect on the scale of ξ. Since for YBCO ξ is not much larger than the lattice spacing, near perfect interfaces are necessary. By

contrast, for a superconductor-normal metal interface, superconducting electron pairs leak into the normal metal, and hence fabrication of a SNS device is more forgiving. For these reasons, most work on YBCO weak links are not of the SIS variety.

As introduced in Chapter II, a SQUID is formed when weak links are fabricated in parallel. Because of the phase coherence of the electron pairs and the effect of the weak links on the phase, the critical current of the SQUID is modulated by a magnetic field. Similarly, a current biased SQUID can show modulation of voltage in a magnetic field. This effect is another hallmark of superconducting weak links.

B. YBCO Weak Links

Many techniques have been used to fabricate YBCO superconducting weak links. The complexity of film growth, the need for high temperatures during processing, the lack of an insulating native oxide (YBCO is itself an oxide), the short coherence length, and the anisotropy of the crystal, all combine to make the fabrication and analysis of a weak link difficult. In this section I will describe some of the approaches that have been attempted. In particular, I will describe our choice of weak link, fabrication, and results.

One of the earliest successful reports of a high T_c weak link fabricated from an epitaxial thin film was by Rogers *et al.* (1989). Here, a four layer structure of YBCO - $PrBa_2Cu_3O_{7-\delta}$ -YBCO - Au was deposited *in situ* using laser deposition with a rotating target carousel. Figure 6.1 (a) shows a schematic of the device. As described earlier, $PrBa_2Cu_3O_{7-\delta}$ (PBCO) is not superconducting

but has a nearly identical crystal structure to YBCO and is therefore an excellent candidate for a weak link. Also, near perfect interfaces between YBCO and PBCO can be grown [Xi *et al.* (1991)]. Because the crystal structure of YBCO and PBCO are closely matched, the entire structure was epitaxial, in this case with the c-axis oriented perpendicular to the substrate. The Au layer served as a means of making electrical contact to the film. After deposition, using conventional photolithographic techniques, a roughly 10^{-6} cm^2 junction was made. Typical barrier thickness was 500 Å. The current - voltage relationship of this junction displayed SNS like behavior. There was a supercurrent which increased with device area. Resistances scaled with 1/area. These properties indicate that the results are not due to grain boundary junctions within an electrode. Finally, there was evidence of the ac Josephson effect when the junction was exposed to microwaves.

YBCO - Au - YBCO weak links have been fabricated by bridging narrow gaps in epitaxial YBCO films, as shown in Figure 6.1 (b) [Forrester *et al.* (1991)]. Here, an YBCO - Au bilayer was deposited *in situ* by off-axis composite target sputtering. The YBCO was epitaxial with its c-axis oriented perpendicular to the substrate. A roughly 0.1 μm wide slit was etched. Then, 10 μm wide junctions were isolated by photolithography and gold was again deposited to link the two superconducting banks. There was evidence of Josephson behavior in these junctions. However, the resistance of the junctions, almost 1 ohm, was much greater than the expected resistance of the gold (of order of m-ohms), which indicates that the Au - YBCO interface was playing an important role in the properties of the junctions.

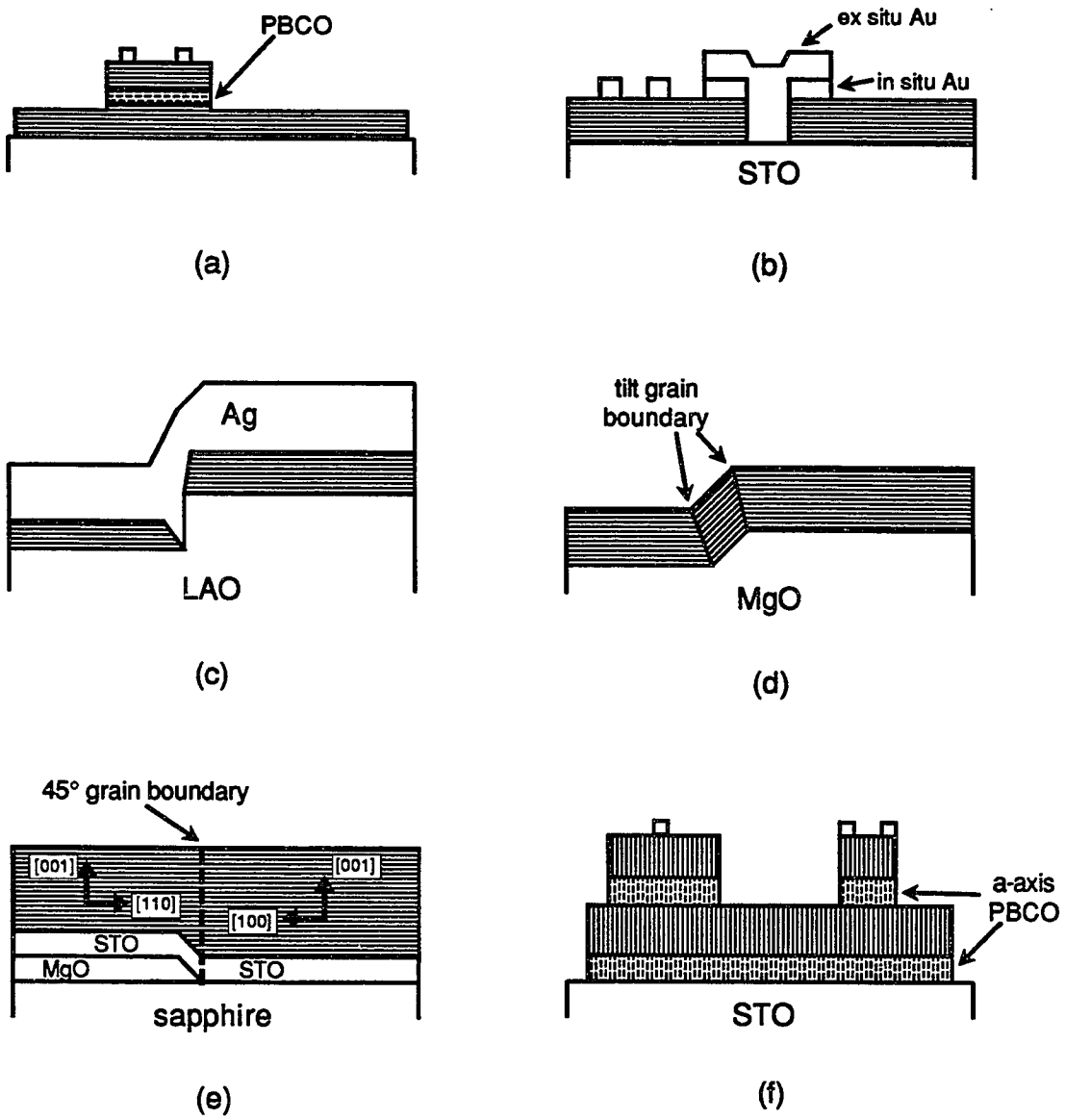

Figure 6.1: Different device geometries reffered to in the text. Striped regions represent YBCO with Cu-O planes oriented along the stripes. White regions represent Ag or Au either as normal metal in SNS structure or as contact pads. STO is SrTiO3, and LAO is LaAlO3.

YBCO - Ag - YBCO weak links have been fabricated by depositing an YBCO - Ag bilayer on a step in a $LaAlO_3$ substrate [DiIorio *et al.* (1991)]. An SNS structure was isolated by photolithography [Figure 6.1 (c)]. They observed a supercurrent up to 87 K and the ac Josephson effect up to 80 K. They found reasonable reproducibility and I_cR_N products of order 100 μV. The I_cR_N product (where I_c is the critical current of the junction and R_N is the slope of the I-V curve for $V > 2\Delta/e$) is a figure of merit of superconducting junctions. Junctions fabricated in parallel showed SQUID behavior in an applied magnetic field. Results with Ag - Au alloy bridges using the same junction fabrication procedure [Ono *et al.* (1991)] have also been encouraging. Junctions with I_cR_N products over 1 mV have been made.

Edwards *et al.* (1992) have deposited weak links by growing epitaxial YBCO over a step in a MgO substrate. Since they found that the c-axis is normal to the substrate (even over the step), two tilt grain boundaries are formed [Figure 6.1 (d)]. They observed Josephson currents up to 89 K and resistively shunted junction (RSJ) like I-V curves. (In the RSJ model, the I-V curve of a junction is calculated by assuming the junction behaves as a simple junction in parallel with a capacitance and a voltage dependent conductance.) Finally, SQUID's fabricated using these junctions showed clear modulation of critical current in an applied magnetic field.

Weak links have also been successfully formed by controlling the in-plane epitaxy of YBCO [Char *et al.* (1991)]. Figure 6.1 (e) shows the processing used to fabricate a 45° grain boundary as a weak link. Note that the film had the c-axis perpendicular to the substrate on both sides of the grain boundary. The critical current density of the boundary was 3 to 4 orders of magnitude less than

the rest of the film. Junctions showed RSJ-like behavior. Current-biased SQUID's showed modulation of voltage vs. magnetic field up to 88 K.

Barner *et al.* (1991) have been able to take advantage of the longer coherence length in the Cu-O planes by growing YBCO films with the a-axis normal to the substrate. a-axis YBCO films can be nucleated on a-axis PBCO films which can be grown at lower temperatures [Inam *et al.* (1990)]. Figure 6.1 (f) shows a schematic of their devices. PBCO with the a-axis normal to the substrate was grown on $SrTiO_3$. An YBCO - PBCO - YBCO trilayer was grown *in situ* on this. The barrier layer thickness was varied from 300 - 1500 Å. The device shown in Figure 6.1 (f) was then patterned using standard photolithography. Typical device area was 200 square microns. Junctions showed RSJ like behavior. The ac Josephson effect was observed up to 80 K. I_c scaled with area and device resistance scaled with the inverse of the area. Similar junctions have also been fabricated by Hashimoto *et al.* (1992). They too observe RSJ-like behavior. They also observe Fraunhofer-like magnetic field dependence of the critical current of their junctions.

Some work has also been done on studying SIS junctions. This is more difficult because of fabrication problems and because of the short coherence length of YBCO. Results have not been conclusive. However, one group [Hirata *et al.* (1990)] has reported results for YBCO - Y_2O_3 - YBCO c-axis oriented films. They found that plots of differential tunnel conductance vs. voltage show an energy gap whose magnitude and temperature dependence compare reasonably with BCS predictions. Other candidates for an insulator in a SIS YBCO junction currently being investigated include $PrBa_2Cu_{3-y}Nb_yO_{7-z}$, $SrTiO_3$, MgO, and CeO_2.

C. Device Design/Fabrication Progress

1. Device Design

It is our desire to fabricate a high quality superconducting device. We are able to grow high quality YBCO films *in situ* in a versatile system. We decided to take advantage of this versatility to fabricate a SNS (or even eventually a SIS) junction *in situ* using mechanical contact masks without the need for any post-deposition processing. In many other processes either the patterning and/or the exposure to atmosphere between process steps is a major source of degradation of the device.

Figure 6.2 shows the necessary processing steps of our proposed technique. Figure 6.3, which is described later, shows the shapes of the masks. First an YBCO strip is deposited through the first mask. Then an insulator is deposited in the pattern shown through a second mechanical mask. This defines one of the dimensions of the junctions. The insulator could be $SrTiO_3$ which is a good insulator and a good epitaxial match to YBCO [Kingston *et al.* (1990)]. Next, a cross strip of the weak link (for example, PBCO) with a narrow neck is deposited using a third mask. With this same mask in place, the counterelectrode of YBCO is then deposited. These four layers would be grown epitaxially. Finally, four Ag contact pads for the current and voltage leads are deposited using the last mask. This too can be done *in situ*.

2. Advantages and Disadvantages

The main advantages to this approach as opposed to others that have been tried are that all levels are grown *in situ* and there is no need for post-

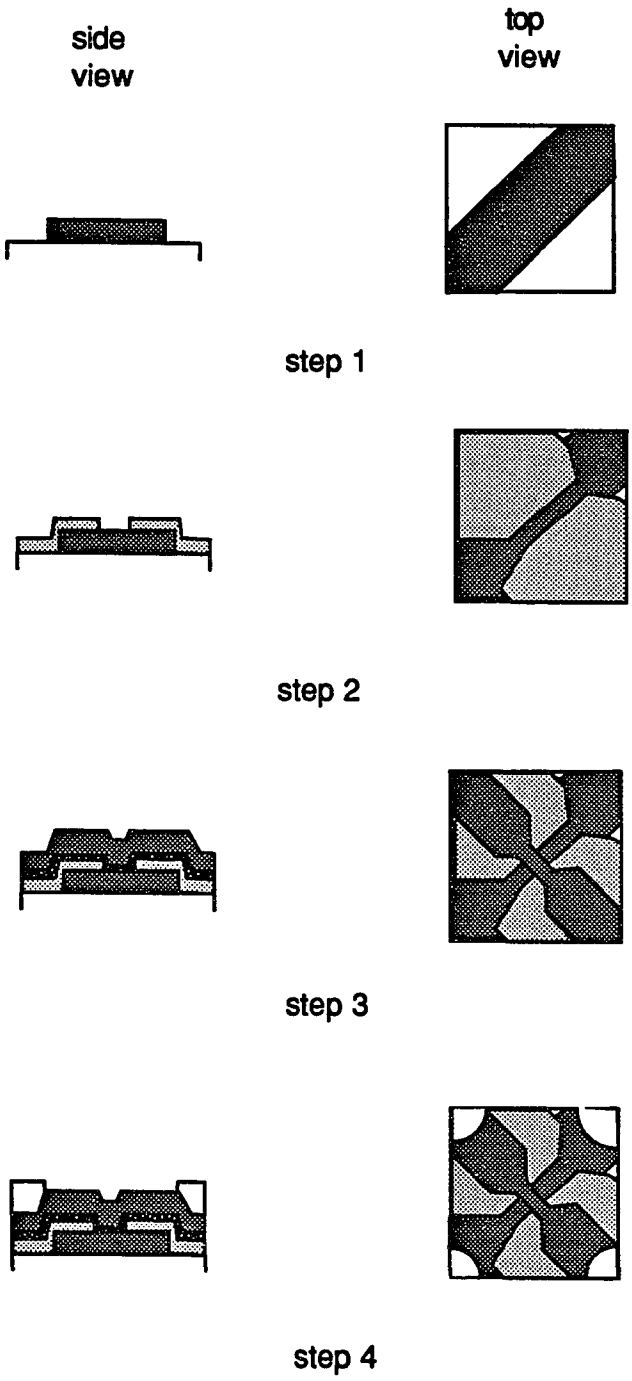

Figure 6.2: Fabrication steps for all in situ junction. Films are grown through mechanical masks which are rotated in situ. The shaded regions represent YBCO, the dotted regions represent an insulator,the black regions represent the barrier, and the white regions represent the contact metal.

deposition processing. *In situ* growth leads to cleaner interfaces. Since there is no processing after deposition, there is less degradation of the films. The obvious disadvantage of this approach is that it can not easily be scaled to devices on several substrates grown at once or to other devices on the same substrate. Since our goal is to study the physical properties of the superconductors as opposed to large scale applications, this was not a primary concern.

Dimensions can be scaled by making different mechanical masks. Substrates are typically 1/4" squares. It is possible to machine a mask such that the junction dimensions would be as small as about 100 μm. If need be, the area can be made even smaller with minimal post-deposition processing (by etching part of the junction area).

The choice of weak links can easily be changed. First, PBCO could be tried to form a SNS weak link. Also, $SrTiO_3$ has a good lattice match and is an insulator [Kingston *et al.* (1990)], so it can be tried to form a SIS junction. Similarly MgO has favorable properties [Tanaka et al. (1990)] and can be tried.

3. Progress

Although we have not yet fabricated such a device, progress towards making it has been made. Successful film growth has already been described, the mechanical mask has been designed and tested, the *in situ* changing of masks has been successful, and a slit of superconducting YBCO has been grown *in situ* through the mask.

The four mechanical masks are all located on a two-inch flat stainless steel disc which is shown in Figure 6.3 (shown roughly double size). The dotted

lined squares represent where the substrate would be under the mask. The solid lines outline the holes in the mask. The 1/4-inch square, 25-mil thick substrate on which the device would be grown sits in a recessed well milled into the pallet. It is slightly off the center of the pallet so that the four stations (a, b, c, and d) shown in Figure 6.3 can be sequentially rotated in front of it. These four stations are the steps shown in Figure 6.2. The pallet rests on the mask but is free to rotate with respect to the mask. This rotation is achieved by securing the mask to the rotating shaft (Figure 4.1) and having the pallet sit freely on it. It is then possible to rotate the pallet relative to the mask using the transfer arm and the ability to rotate the shaft. Three other substrates are in similarly recessed wells of the pallet such that isolated films of each processing layer can be grown through station e of Figure 6.2 and be characterized separately.

Alignment is achieved by lining up scores etched onto the rotatable pallet and the fixed pallet holder which are seen through the view ports. Taking into account uncertainty in lining up the scores and the slightly loose fit of the pallet in its holder, alignment to better than 40 mils is expected. Based on mask design, even if the mask is misaligned by about 75 mils, junction fabrication would be successful. Based on practice alignment runs using Ag and Au, alignment was reliable.

After several iterations, we were able to grow superconducting patterned films through the mechanical mask. The optimum temperature for the thermocouple in the heater box was about 75 °C lower when the mechanical mask was in place compared to its optimum temperature when the mask was not used. This is not surprising since the mask acts as a thermal radiation shield during growth. Therefore it is likely that the substrate temperature is the

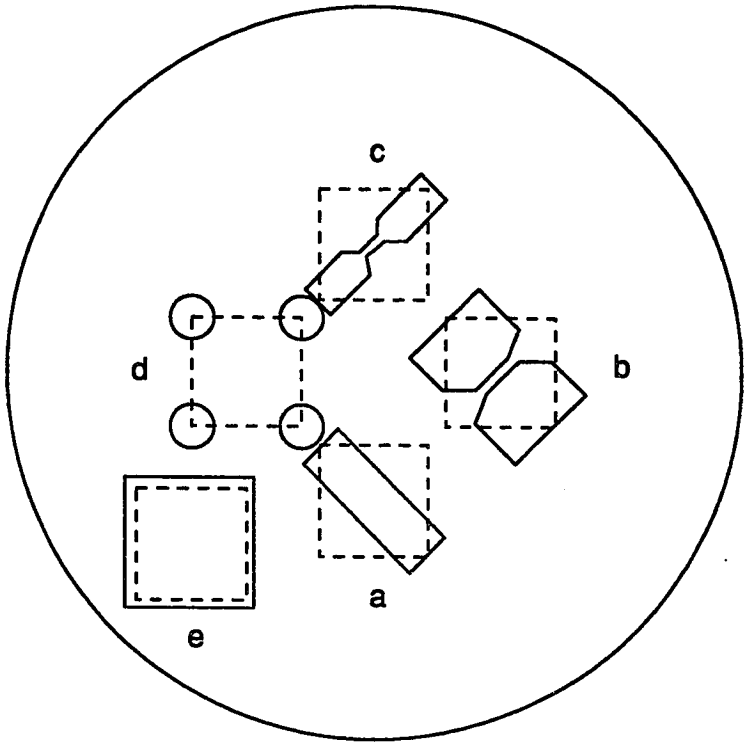

Figure 6.3: Mechanical mask described in the text. Solid lines represent holes. Dotted lines represent substrate location under the mask. One substrate rotates sequentially under stations a,b,c, and d.

same in the two cases. After accounting for this we were able to grow a 125-mil wide superconducting stripe through a mechanical mask. Figure 6.4 shows the resistive transition of an YBCO strip. Figure 6.5 shows an inductive transition of the same strip. These transitions are very encouraging.

One other problem we had at first was shadowing due to the thickness of the mask. We found that, in particular for station c of Figure 6.3, the film was visibly a different color in the thin slit region compared to the rest of the structure. This problem was alleviated by thinning the mask and sloping the mask hole in the vicinity of the slit.

4. Remaining Work

We have been able to grow high quality YBCO thin films by off-axis composite target sputtering. We have also been able to grow these films through a mechanical mask to make patterns as well as rotate the mask *in situ* for potential multilayer structure fabrication. The next step in the process just outlined would be to grow and characterize PBCO and $SrTiO_3$ thin films. As already described, these processes are well studied and would not likely be a problem. Finally we would perform the steps to fabricate a junction described in the previous section and characterize its properties.

For reasons discussed in the conclusion, we have not yet been able to perform these next steps. Our stated goal being to fabricate and characterize YBCO superconducting devices, it became more attractive in the near term to continue this effort solely in a Yale-Westinghouse collaboration described briefly in the conclusion. This had been conducted in parallel to the work described in this thesis since the spring of 1991.

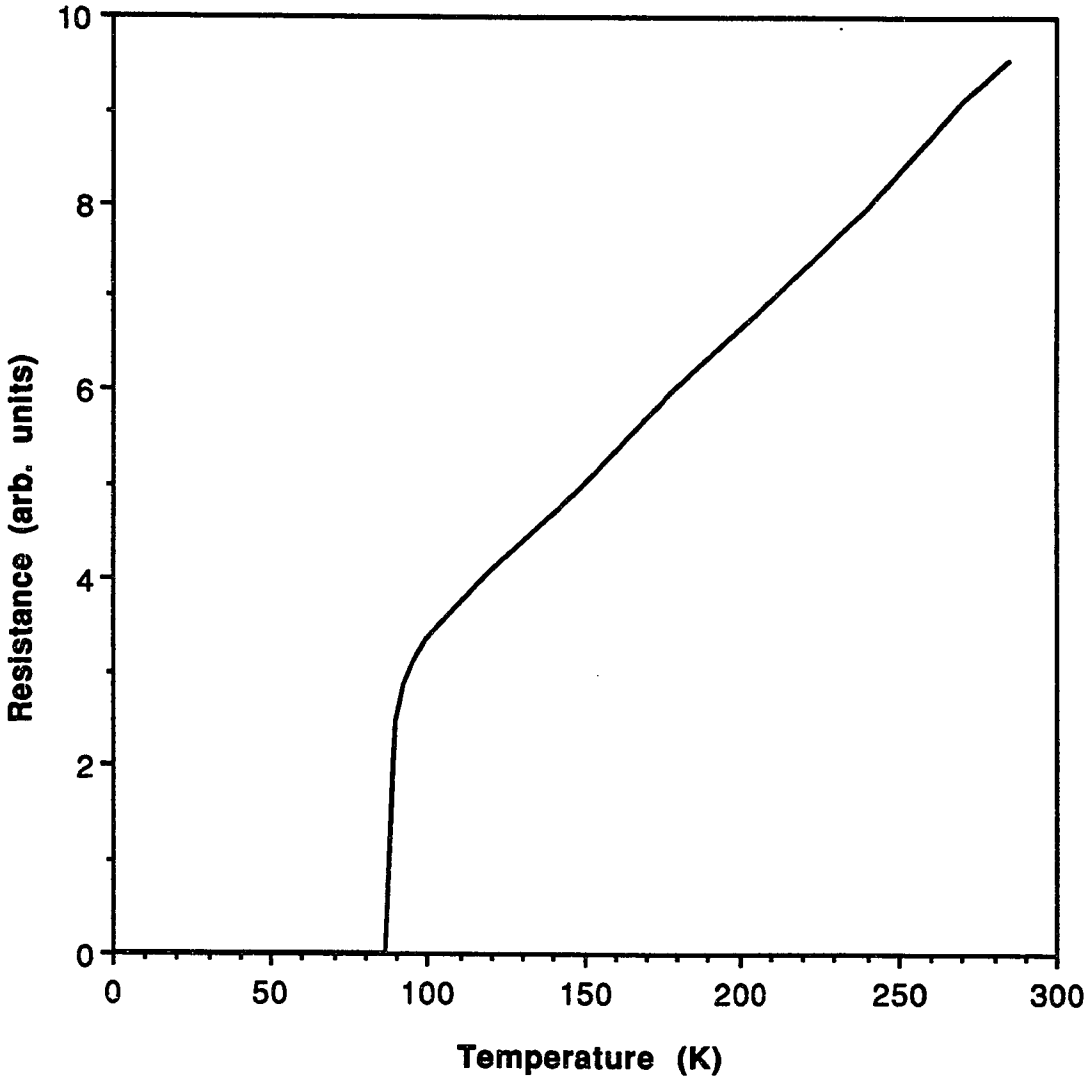

Figure 6.4: Resistance vs. temperature for a YBCO stripe grown through a mechanical mask (sample B53-1).

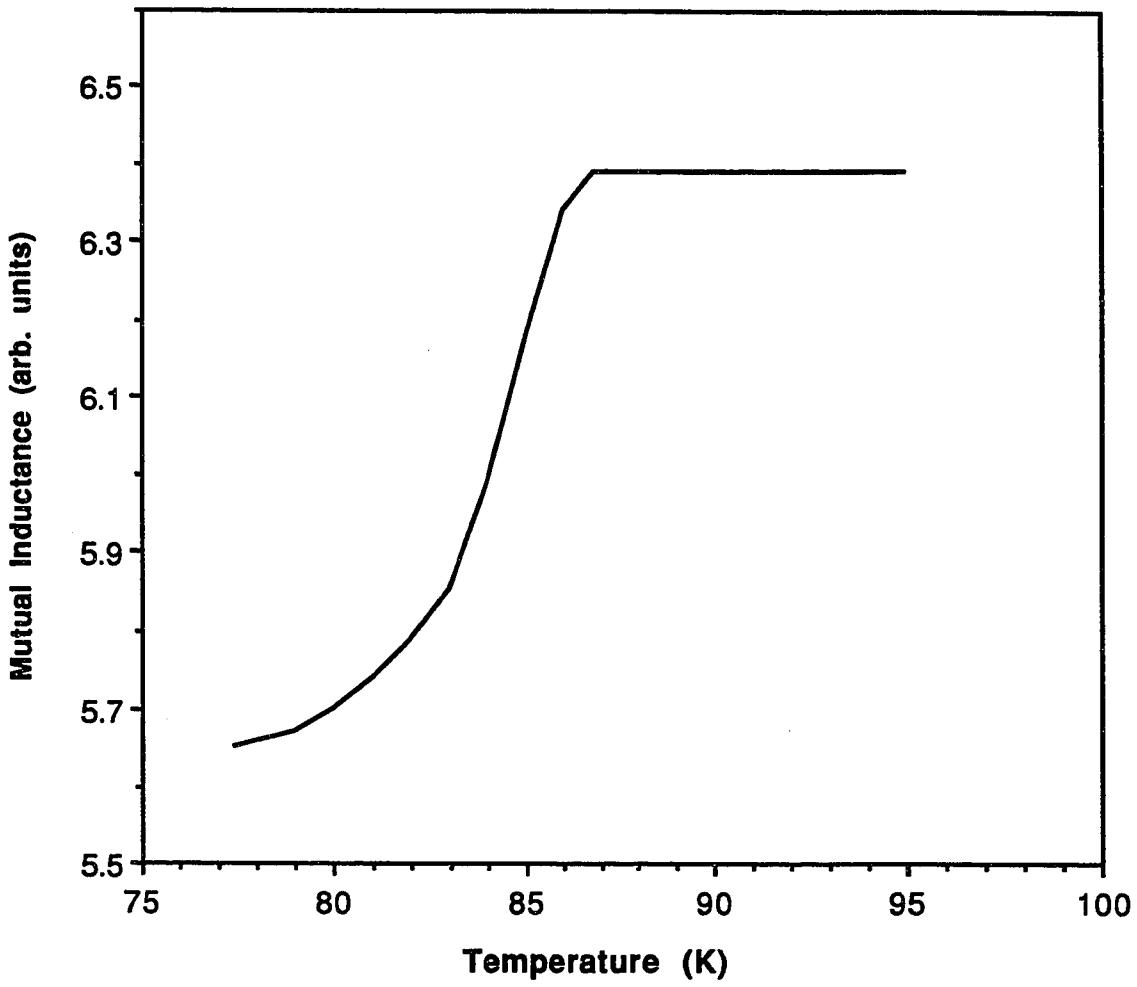

Figure 6.5: Inductive transition for a YBCO stripe grown through a mechanical mask (sample B53-1).

VII. CONCLUSIONS

Superconductivity is a field rich in scientifically interesting and unique phenomena, and superconductors are being exploited for ever-improving applications. The discovery of superconductivity at higher temperatures in a new class of materials in 1986 has resulted in increased attention and activity in the field. Unfortunately, it has proven extremely difficult to fabricate and understand these new superconductors. In this thesis, I have reported the results of synthesis and characterization of $YBa_2Cu_3O_7$ (YBCO) thin films for the purpose of fabricating high temperature superconducting devices.

We have fabricated the highest quality as grown YBCO films by cosputtering from metallic targets and described issues of film growth. The key to this success was differentially pumping the deposition chamber to minimize the oxygen partial pressure at the targets and to maximize the oxygen partial pressure at the growing films. Because of apparent damage to the growing YBCO film due to resputtering, we found it necessary to point the sputter guns away from the substrate. Our films are among the better grown *in situ* by any codeposition technique. A major drawback to this approach, though, was irreproducibility.

Based on a published report, we have investigated deposition of YBCO films by sputtering from a single composite target with a high strength magnet in place of the standard one in the sputter gun. We have established that this technique is unlikely to yield quality YBCO films.

We have grown superconducting YBCO films by off-axis composite target sputtering. Based on resistive transition measurements, inductive transition measurements, x-ray diffraction results, and estimation of critical current density as determined by a remnant magnetic field technique, the films are of high quality.

The long term goal of our work has been to fabricate YBCO superconducting devices. We have demonstrated the ability to grow YBCO films. Furthermore, we have demonstrated the ability to grow these films through a contact mechanical mask. We have shown that we can rotate this mask *in situ*. One possible technique based on these capabilities to grow a YBCO device *in situ* without any post-deposition processing has been outlined. Also described are other techniques by which YBCO devices have been fabricated elsewhere (and which could be tried here). As of now, for reasons discussed below, we have not yet fabricated a junction.

The deposition system used for the work covered in this thesis has unavoidably served many functions. In particular, the station with two sputter guns shown in Figure 4.2 has been used to deposit Nb and Ta thin films for a project unrelated to our work on high temperature superconductivity. Despite mechanical shielding to prevent cross-deposition, we found that the quality of our films deteriorated immediately after deposition of Ta. Unfortunately, this correlation was not made until all the films we grew contained Ta, as confirmed by ICP and EDS measurements at Olin. Replacing the YBCO target did not help, implying the problem arose from energetic ion bombardment of the inside of the chamber during YBCO growth. The problem persisted even though time appeared to improve the situation.

The work currently being conducted jointly by researchers in our group, primarily Jim McCambridge, with researchers at the Westinghouse Science and Technology Center (7) involves fabrication of SNS YBCO junctions. The process is similar to that of DiIorio *et al.* (1991) [see Figure 6.1 (c)]. This is done at Westinghouse where they reproducibly grow high quality YBCO films by off-axis composite target sputtering [Gavaler *et al.* (1991)]. Junctions show both the dc and ac Josephson effect. Current biased SQUID's show the expected modulation of voltage in applied magnetic fields. Currently, to improve quality and reproducibility, other substrates and normal metals are being considered. Also, an improved measurement setup is being constructed at Yale.

APPENDIX A: Measurements of Superconductivity in Small Samples

When we began our work in the field of high T_c superconductivity, we wanted to be able to measure transitions of small samples. The main motivation for this was that at the time, no large single crystals were available. The technique we used could measure samples of order of 100 μm in size. The technique is described in detail in Bruce Dalrymple's Ph. D. thesis (1983) and is now summarized. A block diagram of the apparatus is shown in Figure A.1. The sample was placed on a sapphire rod which was thermally mounted to the variable temperature part of the cryostat. Sapphire is a good thermal conductor but a poor electrical conductor and is hence ideal. The sample was placed in a coil which was the inductor of a high-Q resonant circuit. The capacitor C was kept at the bath temperature to limit variations in this capacitance. The capacitor C_1 = 1 pF biased the resonant circuit with a constant current. This rf current $I_1 \approx i\omega C_1 V_g$ was shifted 90° out of phase relative to the rf generator voltage V_g. The voltage across the resonant circuit was:

$$V_{LC} = Z_{LC} I_1 = (-Z_2 + iZ_1)\omega C_1 V_g \qquad (A.1)$$

where $Z_{LC} = Z_1 + iZ_2$ was the impedance of the resonant part of the circuit. This voltage was amplified and mixed with the generator voltage. Therefore, after this signal was fed through a low pass filter and amplified, the resultant voltage V_0 was dc and proportional to Z_2.

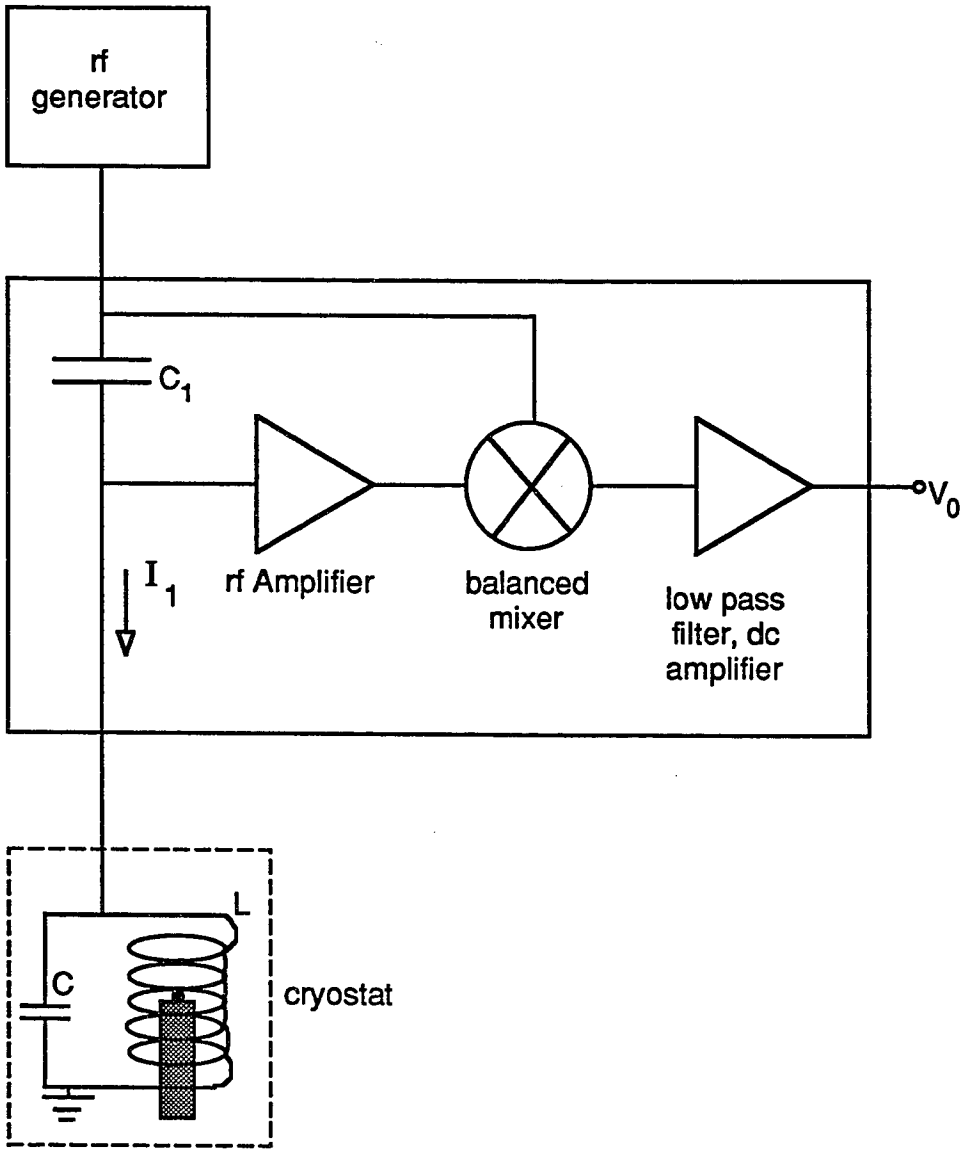

Figure A.1: Block diagram of apparatus used to measure superconducting transitions [Dalrymple (1983)].

The shape of Z_2 (and hence V_0) as a function of frequency is shown in Figure A.2. The value is zero at resonance and has a slope which is roughly proportional to Q^2. In the normal state, the ac magnetic field penetrates the sample the normal state skin depth:

$$\delta = (2/\omega\mu\sigma)^{1/2} \qquad (A.2)$$

With $f \approx 0.5$ MHz and $\sigma < 1$ $(m\Omega\text{-cm})^{-1}$, δ is greater than 0.2 cm. In the superconducting state, the field penetrates the sample $\lambda \approx 1$ μm, which is much less than both δ and the size of the sample. Therefore, there was a change in the coil inductance, and hence a small shift in the resonant frequency, when the sample entered the superconducting state. This is depicted in Figure A.2 by the dotted curve. During the measurement, the frequency was fixed between the two resonant frequencies and the temperature was varied. Therefore, there was a change in V_0 at the transition temperature. V_0 was plotted vs. temperature. The transition of a sample grown at Olin is shown in Figure A.3. This shows an onset to superconductivity at 87 K.

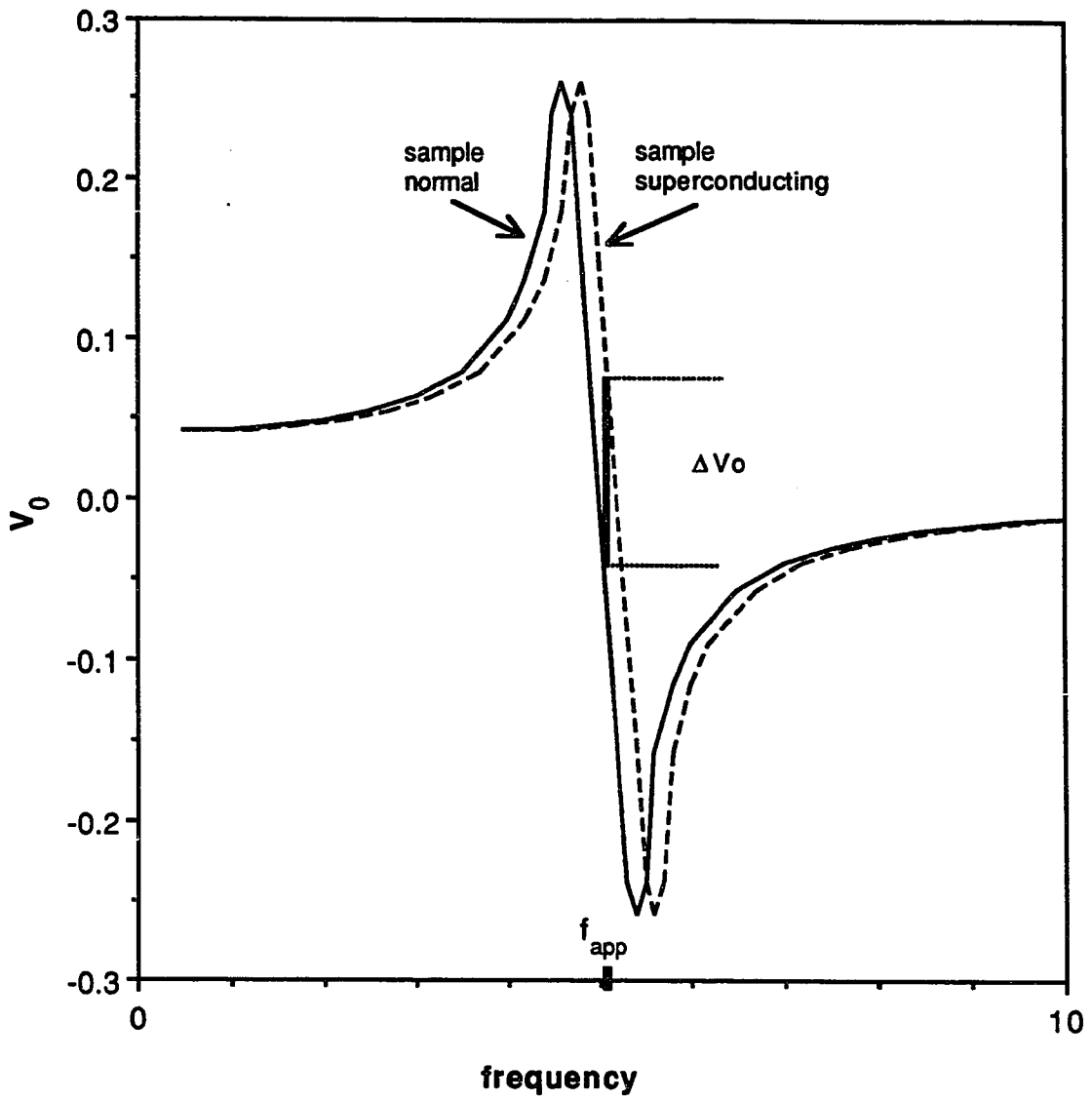

Figure A.2: Output voltage vs. frequency. When the sample goes superconducting, the shift in resonant frequency causes a shift in a dc output voltage which is recorded.

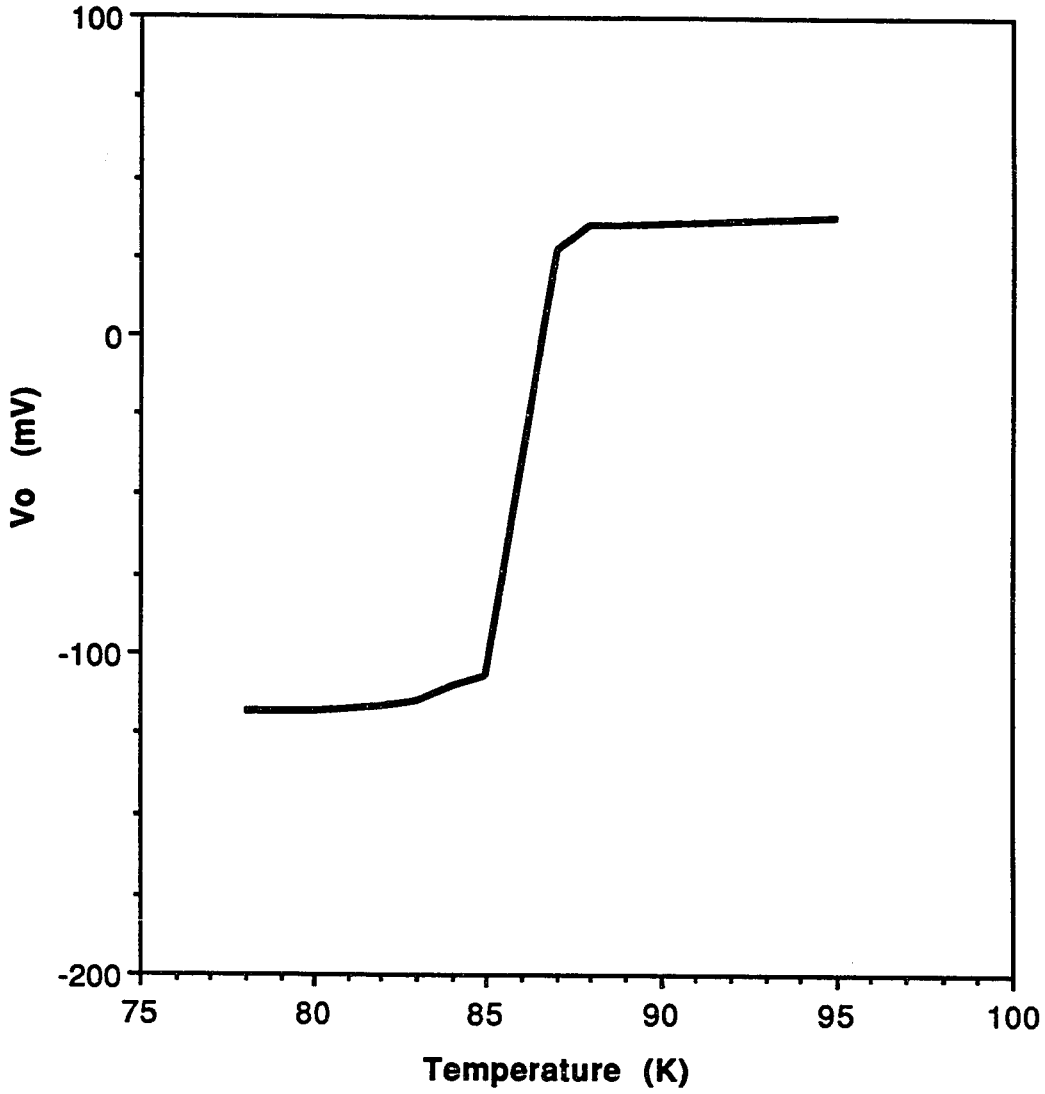

Figure A.3: Superconducting transition of bulk sample MRL 12A using the method described in the text.

APPENDIX B: Cryostat Design

A schematic of the cryostat used to perform the measurements on our high T_c films is shown in Figure B.1. A 3/4-inch, vacuum-sealed brass can was immersed in a liquid cryogen, usually liquid nitrogen. A stainless steel tube served as a mechanical support, as a conduit for electrical wires, and as a vacuum line. A Cu bar, which comes through the top of the can, was at the temperature of the bath. This bar was weakly thermally connected to a second piece of Cu by a stainless steel screw. The temperature of this piece of Cu could be raised above the temperature of the bath by running current through a resistor which served as a heater. Temperature was measured with a calibrated Si diode thermometer which was thermally anchored to the Cu. All samples being measured were also thermally anchored to the Cu. Measurements were made as the sample was cooled and as it was warmed with the average of the two runs reported.

Electrical contact to the samples was made using Pogo Contacts (Augat-Pylon). These are spring loaded pressure contacts. Eight of these pins were fed through an insulating piece of phenolic so 4-point measurements of two different samples could be made.

On the bottom of the cryostat was a tapped hole such that one of several stations could be mounted. Shown is the mutual inductance arrangement. Here, the sample was thermally anchored to a sapphire rod. The sample rested between 2 coils. Other stations which could be installed at this location include

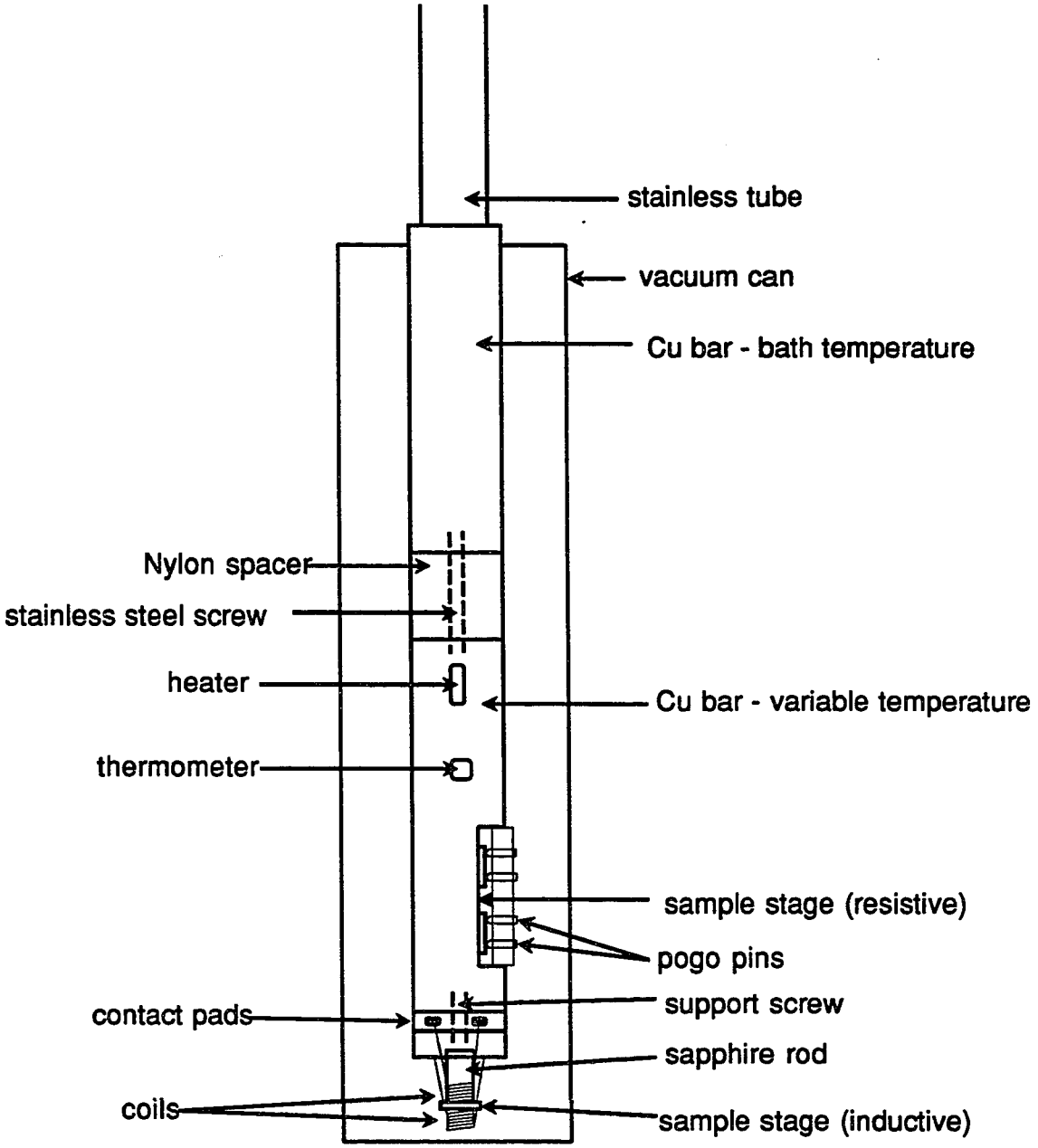

Figure B.1: Schematic of sample measurement cryostat

a third resistive measurement sample holder and the sample holder for J_c measurements described in the Chapter V.

The thermal link between the bath temperature and the variable temperature Cu bar was stainless steel. This was chosen because of its thermal resistance. The thermal resistivity of stainless steel at 77 K is 12.5 K-cm/W. For the size screw used, this corresponds to a thermal resistance of about 200 K/W. With 1/4 W of power dissipated in the heater, this means there would be a convenient temperature increase of roughly 50 K. In practice, the temperature increased about two thirds of this amount because of other thermal links between the Cu bar and the bath.

This rig was modified from the one originally reported in Bruce Dalrymple's thesis (1983). Initially, to do the measurements reported in Appendix A, the stainless weak link was installed and an appropriate sample holder was in place of the variable temperature Cu bar shown. As described in Appendix A, a capacitor was attached to the bath temperature Cu bar. Films were large enough to be measured by more conventional techniques so the rig was modified into the one shown in Figure B.1.

APPENDIX C: Post-Annealed Cosputtered Films

Table C.1 on the following pages contains a summary of the deposition runs performed by cosputtering at ambient temperature followed by a post-deposition anneal in oxygen. The first part of the sample number refers to the number of the run. The second part (after the dash) refers to the number of the sample within the run. Individual rates are as determined from the gun calibration. The thickness estimate is based on this rate. "Anneal T" and "Anneal t" refer to the post-deposition temperature and time. The "onset Tc" and "R=0 Tc" refer to the resistive transition temperatures. The different techniques attempted to measure the stoichiometry along with the results are given. EDS (energy dispersive spectroscopy) performed both here and at Olin was inaccurate. ICP (inductively coupled plasma spectroscopy) has proven to be very reliable. Films listed in Table C.1 were grown on MgO.

Sample	Y rate	BC rate	C rate	Thk est	Anneal	Anneal	onset	R=0	Stoich.	%Y	%Ba	%Cu	Comments
	(Å/m)	(Å/m)	(Å/m)	Å	T (C)	t (hrs)	Tc(K)	Tc (K)	Technique				
3-one	10.6	22	10.7	10000	500-850	6.5	75	28	EDS (Olin)	17	26	57	melted BC targ.
16-1	7.4	20.6	4.7	3800	500-850	23							
17-1	13.4	29	9.5	6200	500-850	21	80	43					
18-1	16.9	34.2	16.1	8000	500-850	6							
18-2					none	0							
19-1	13.4	26.6	12.2	4200	none	0							P=15 um Ar
21-1	17	34.6	17.1	5400	500-850	6	60	15					
22-1	13.6	29	11.9	4400	500-850	4.5			EDS (Olin)	2.4	3.5	4.8	P=15 um Ar
23-1	17.4	39	16.8	6600	500-850	4.5			EDS (Olin)	7.2	9.2	14.1	
23-2					none	0							
23-3					500-850	4.5	50	<10	EDS (Yale)	17	31	52	
									EDS (Yale)	13	33	55	counting Mg
24-1	16.5	38.6	15.1	8400	500-850	21	75	30	EDS (Yale)	13	36	51	
24-2													
25-1	16.5	38.6	15.1	4200	500-850	21			EDS (Yale)	13	31	55	
25-2													

Table C.1: Post-annealed cosputtered films

Sample	Y rate	BC rate	C rate	Thk est	Anneal	Anneal	onset	R=0	Stoich.	%Y	%Ba	%Cu	Comments
	(Å/m)	(Å/m)	(Å/m)	Å	T (C)	t (hrs)	Tc(K)	Tc (K)	Technique				
26-1	9.4	38.6	9.2	11000	450-850	20							BC shutter off
28-1	13	40	12	5100	450-850	6.5			ICP	11	56	33	
28-2													
28-3													

Table C.1: Post-annealed cosputtered films

APPENDIX D: *In situ* Cosputtered Films

Table D.1 on the following pages contains a summary of the deposition runs performed by *in situ* cosputtering at elevated temperatures, followed by a slow cool in oxygen. "Samp" uses the same notation as Appendix C. Substrates used were MgO, $SrTiO_3$ (STO), and sapphire (AlO). Powers to the three separate guns are given in watts. The thickness reported is usually as determined from ICP. "P (mT)" is the deposition pressure in mT. "Ar Flo" and "O2 Flo" are the flow rates of argon and oxygen during deposition in sccm. "Tdep" is the deposition temperature of the heater box in °C. The substrate is roughly 125 °C lower temperature. "R on" and "R=0" refer to the onset and zero resistance transition temperatures. The different techniques attempted to measure the stoichiometry along with the results are given. As described in Appendix C, EDS refers to energy dispersive spectroscopy and ICP is for inductively coupled plasma spectroscopy. "EDS-Hyp" refers to EDS measurements performed at Hypres, with thanks to Dr. Elie Track. RBS is for Rutherford Backscattering Spectroscopy performed either at the University of Connecticut (UC) or at the University of Arizona (UA). The ratio of Y:Ba:Cu is also given. All runs starting with number 52 were done in the off-axis geometry. Investigated but not shown in this summary are different cool-down parameters, different substrate mounting and cleaning procedures, and unsuccessful attempts to improve films by post-annealing them in oxygen.

Samp	Subs	Y	BC	C	Thick	P	Ar Flo	O2 Flo	Tdep	R on	R=0	Meas	Y:Ba:Cu	Sample	Run
		(W)	(W)	(W)	Å	(mT)	(sccm)	(sccm)	C	(K)	(K)	Tech		Comments	Comments
27-1	MgO	25	100	7	4000	6	58-56	0.4	700						
29-1	MgO	35	150	11	5000	6	51-50	0.4	700						
29-2	MgO														
30-1	MgO	35	175	12	7500	6	57-55	0.4	700						
															Thru target?
31-1	MgO	35	150	11	6000	6	53-51	0.4	700						Thru target!
															switch target
33-1	MgO	60	125	22	4000	6	58-54	1	750	<10		RBS-UC	just Cu		
34-1	MgO	60	125	25	7500	6	56-54	1	750			ICP	1.00:1.89:1.82	1/2" subs	
												re-ICP	1.00:1.99:1.99	should be same	
35-1	MgO	57	125	70	4500	6	63-59	1	750	80	46				
35-2	MgO									81	48	ICP	1.00:2.53:4.99		
36-1	STO	66	125	47	4500	6	62-59	1	750	86	43	RBS-UC	1.0:4.0:3.6	broken	
36-2	MgO									84	34	ICP	1.00:1.99:3.67		
36-3	MgO									84	30				
36-4	MgO													dbl side polish	
37-1	STO	65	125	34	4500	6	49-48	0.8	750			RBS-UC	just Cu		heater shut off
37-2	MgO														

Table D.1: In situ cosputtered films

Samp	Subs	Y	BC	C	Thick	P	Ar Flo	O2 Flo	Tdep	R on	R=0	Meas	Y:Ba:Cu	Sample	Run
		(W)	(W)	(W)	Å	(mT)	(sccm)	(sccm)	C	(K)	(K)	Tech		Comments	Comments
37-3	MgO														
37-4	MgO									80	<10				
38-1	MgO	68	125	38	4000	6	49-48	1.2	775	<5		ICP	1.00:1.90:0.78		
38-2	MgO													was 37-3	
38-3	MgO									75	5		1.00:1.92:0.59		
38-4	STO														
														was 37-1	
39-1	MgO	72	125	71	4500	6	44-43	1.1	775				1.00:1.98:3.55		
39-2	MgO														
39-3	MgO												1.00:1.94:3.41		
39-4	MgO														
40-1	MgO	69*	125	57	4000	6	42-41	1.1-1.0	775					S impurity	
40-2	MgO													S impurity	V jump at end
40-3	STO											ICP	1.00:2.27:3.44		
40-4	STO														
40-5	MgO									50	<5				
41-1	MgO	69	125	57	5400	6	44-43	1.2-1.1	775	85	59				
41-2	MgO									80	<20				all nonuniform
41-3	STO									90	65				in color
41-4	MgO														
42-1	MgO	73	125	65	4500	6	45-44	1.3	825			ICP	1.00:1.90:3.26		
42-2	MgO									85	58	EDS-Hyp	1.00:3.17:2.83	S impurity	
42-3	MgO									87	57				

Table D.1: In situ cosputtered films

Samp	Subs	Y	BC	C	Thick	P	Ar Flo	O2 Flo	Tdep	R on	R=0	Meas	Y:Ba:Cu	Sample	Run
		(W)	(W)	(W)	Å	(mT)	(sccm)	(sccm)	C	(K)	(K)	Tech		Comments	Comments
43-1	MgO	70	125	55	4500	6	44-43	1.3	825						
43-2	MgO									?	<5				
43-3	MgO									?	<5				
43-4	MgO											ICP	1.00:2.01:3.18		
43-5	AlO														
44-1	MgO	71	125	60	4500	6	42-41	1.3-1.2	825						
44-2	MgO											ICP	1.00:2.04:3.52		
44-3	MgO														
44-4	MgO									35	10				
44-5	MgO														
															No more MoS
45-1	MgO	73	125	65	5000	6	40-39	1.2	825			RBS-UA	1.00:1.67:3.06		
45-2	MgO														
45-3	MgO														
45-4	MgO									84	67	ICP	1.00:1.72:3.41		
45-5	MgO									84	67	ICP	1.00:1.71:3.35		
45-6	MgO									83	<20				
46-1	MgO	73	125	65	1000	6	43	1.3	825			RBS-UA	1.00:1.64:3.15		
46-2	MgO														
46-3	MgO											ICP	1.00:1.71:3.52		
46-4	MgO											ICP	1.00:1.74:3.92		
46-5	MgO														

Table D.1: In situ cosputtered films

Samp	Subs	Y	BC	C	Thick	P	Ar Flo	O2 Flo	Tdep	R on	R=0	Meas	Y:Ba:Cu	Sample	Run
		(W)	(W)	(W)	Å	(mT)	(sccm)	(sccm)	C	(K)	(K)	Tech		Comments	Comments
47-1	MgO	100	125	100	5000	6	49	1.5	825	89	78			no Sulfur	
47-2	MgO														
47-3	MgO									88	79	EDS-Hyp	1.00:2.01:4.07	no Sulfur	
47-4	MgO											ICP	1.00:1.05:3.21		
48-1	MgO	85	150	85	2500	7	91-89	3.2-3.1	800			ICP	1.00:1.71:4.01	1/2" subs	
48-2	MgO									81	45	ICP	1.00:1.74:4.23		
49-1	STO	78	150	65	3000	7	98-92	3.4-3.2	800	86	40				heatr shut off
49-2	MgO									81	37	ICP	1.00:1.85:4.31		during cool
49-3	MgO									80	42			no Sulfur	
49-4	MgO														
50-1	STO	110	150	100	2500	7	89-84	3.1-3.0	825	85	70				
50-2	MgO									85	62				
50-3	MgO									85	60				
50-4	MgO														
50-5	MgO														
51-1	STO	70	150	40	3000	7	93-90	3.2	825						
51-2	MgO														
51-3	MgO														
51-4	MgO														
51-5	MgO														

Table D.1: In situ cosputtered films

Samp	Subs	Y	BC	C	Thick	P	Ar Flo	O2 Flo	Tdep	R on	R=0	Meas	Y:Ba:Cu	Sample	Run
		(W)	(W)	(W)	Å	(mT)	(sccm)	(sccm)	C	(K)	(K)	Tech		Comments	Comments
															Rotated Guns
															Wired Grid
52-1	MgO	80	125	80	1100	7.5	88-87	1.9	825			ICP	1.00:0.71:2.90	1/2" sub	grid grounded
53-1	MgO	80	125	80	1500	7.5	85-84	1.8	825			ICP	1.00:0.67:4.00	1/2" sub	-70 V on grid
54-1	STO	48	125	45	1200	7.5	85-83	1.9-1.8	825	93	83	ICP	1.00:1.60:3.38		-70V on grid
54-2	MgO				1250					88	79	ICP	1.00:1.39:3.24		
54-3	MgO				1500					91	81	ICP	1.00:1.35:3.58		
54-4	MgO									90	80				
55-1	MgO	50	125	50		7.5	86-85	1.9-1.8	825	91	74				grid grounded
55-2	STO				1200					94	84	ICP	1.00:1.82:3.28		
55-3	MgO				1250					88	71	ICP	1.00:1.47:3.77		
55-4	MgO									86	77				
55-5	MgO									86	71				
56-1	STO	50	140	43		7.5	84	1.9-1.8	825						grid grounded
56-2	STO				850					90	83	ICP	1.00:1.65:4.60		Y plsma flicker
56-3	MgO													samp fell	
56-4	MgO				900					86	55	ICP	1.00:1.72:3.55		
56-5	MgO														
56-6	MgO													samp fell	

Table D.1: In situ cosputtered films

Samp	Subs	Y	BC	C	Thick	P	Ar Flo	O2 Flo	Tdep	R on	R=0	Meas	Y:Ba:Cu	Sample	Run
		(W)	(W)	(W)	Å	(mT)	(sccm)	(sccm)	C	(K)	(K)	Tech		Comments	Comments
57-1	STO	46	140	38	1050	7.5	83-81	1.8-1.7	825		80?	ICP	1.00:1.83:4.72		grid grounded
57-2	MgO				1300						35?	ICP	1.00:2.00:5.34		Y plsma flicker
57-3	MgO														
57-4	MgO													samp fell	
57-5	STO														
57-6	MgO														
58-1	STO	41	140	32	950	7.5	81-79	1.7	825		75?	ICP	1.00:4.26:8.77		
58-2	MgO													samp fell	
58-3	STO										80?	ICP	1.00:5.00:10.3		
58-4	MgO										40?	ICP	1.00:4.55:10.2		
59-1	STO	44	140	29	1650	7.5	75-73	1.5-1.4	810	84	61	ICP	1.00:2.50:3.69		
59-2	MgO				2100					80	40	ICP	1.00:2.47:3.67		
59-3	MgO														
59-4	STO									82	59				
60-1	STO	51	140	31	2100	7.5	74-71	1.4	810	83	62	ICP	1.00:2.63:3.45		
60-2	MgO									82	52	ICP	1.00:2.41:3.94		
60-3	MgO														
60-4	MgO														
60-5	STO									85	60				
61-1	STO	61	140	37		7.5	72-70	1.4	810						
61-2	MgO				2300					87	40	ICP	1.00:1.90:3.82		
61-3	MgO														
61-4	STO													samp fell	

Table D.1: In situ cosputtered films

Samp	Subs	Y	BC	C	Thick	P	Ar Flo	O2 Flo	Tdep	R on	R=0	Meas	Y:Ba:Cu	Sample	Run
		(W)	(W)	(W)	Å	(mT)	(sccm)	(sccm)	C	(K)	(K)	Tech		Comments	Comments
61-5	MgO														
62-1	STO	63	140	35	1550	7.5	70-69	1.3	*810	90	30	ICP	1.00:1.89:3.91		thrmcpl prblm
62-2	MgO				2050							ICP	1.00:1.89:4.23		
62-3	STO														
62-4	MgO														
63-1	STO	66	140	29	1400	7.5	77-74	1.5-1.4	815	85	55	ICP	1.00:1.80:3.45		
63-2	MgO				1350							ICP	1.00:1.79:2.78		
63-3	MgO														
64-1	STO	67	140	29		7.5	73-71	1.4	835						
64-2	MgO														
64-3	MgO														
65-1	STO	68	140	28		7.5	75-74	1.5-1.4	835						
65-2	MgO														
65-3	MgO														

Table D.1: In situ cosputtered films

APPENDIX E: Off-axis composite target sputtering

Table E.1 on the following pages contains a summary of the deposition runs performed by off-axis sputtering using a composite YBCO target. "Samp" uses the same notation as Appendices C and D. Substrates used were Si, MgO, $SrTiO_3$ (STO), and $LAlO_3$ (LAO). "Rate," "P (mT)," and "Ar flow" are the same as in Appendices C and D. "Gun Watts" refers to the power to the single sputter gun. As explained in Chapter V, the first 12 runs were sputtered with a dc voltage and the rest were rf sputtered. Beginning with run B19, most runs were performed at 125 Watts and the amount the gun was rotated from its on-axis position was systematically varied. "Gun Angle" is the number of degrees the gun was rotated. "Tdep" is again the deposition temperature of the heater box (about 125 °C higher than the substrate). All films were slow cooled in oxygen. "% oxy" is the oxygen flow divided by the Ar flow (which is less than the oxygen flow divided by the total flow). "R on" and "R=0" are as before. "Tons mag" and "Tcmp mag" are the onset and final transition temperatures as determined by the mutual inductance technique. Film thickness and stoichiometry are as determined by ICP. "Mask" refers to the mechanical contact mask described in Chapter VI.

Samp	Subs	Rate	P	Ar	Gun	Tdep	%	R on	R=0	Tons	Tcmp	thick	Y:Ba:Cu	Sample	Other
		Å/hr	(mT)	flow	Watts	(C)	oxy	(K)	(K)	mag	mag	(A)		comments	Comments
B1-1	Si	65	75	32	100	775	15					423	1.00:2.14:4.66		
B1-2	Si											343	1.00:2.23:3.93		
B2-1	MgO	80	75	29	90	840	25					388	1.00:2.21:8.34		
B2-2	MgO											452	1.00:2.23:8.54		
B2-3	Si											286	1.00:2.16:3.96		
B3-1	MgO	45	125	64	90	775	5					278	1.00:2.03:7.49		
B3-2	MgO											318	1.00:1.97:7.12		
B3-3	Si											266	1.00:2.00:5.48		
B3-4	Si											275	1.00:1.92:5.68		
															Heater sleeves
															added
B4-1	MgO	27	175	89	100	840	5					216	1.00:4.45:11.2		
B4-2	MgO											286	1.00:2.01:8.32		
B4-3	Si											206	1.00:2.01:4.50		
B4-4	Si											202	1.00:2.02:4.42		
B5-1	MgO	45	125	51	100	915	25					394	1.00:2.05:9.12		
B5-2	MgO											373	1.00:2.07:9.44		
B5-3	Si											231	1.00:2.00:3.70		
B5-4	Si											193	1.00:1.99:2.57		
															Target is toast
B6-1	MgO	95	75	34	100	775	15					616	1.00:2.09:10.3		
B6-2	MgO											613	1.00:2.02:11.6		
B6-3	Si											714	1.00:1.98:11.0		
B6-4	Si											538	1.00:2.17:8.29		

Table E.1: Off-axis composite target sputtering

Samp	Subs	Rate	P	Ar	Gun	Tdep	%	R on	R=0	Tons	Tcmp	thick	Y:Ba:Cu	Sample	Other
		Å/hr	(mT)	flow	Watts	(C)	oxy	(K)	(K)	mag	mag	(A)		comments	Comments
B7-1	MgO	61	75	31	90	840	25					376	1.00:3.50:11.9		
B7-2	MgO											471	1.00:2.08:8.05		
B7-3	Si											304	1.00:2.07:4.44		
B7-4	Si											307	1.00:2.02:4.28		
B8-1	MgO	67	75	35	80	915	5					512	1.00:1.71:6.19		
B8-2	MgO											354	1.00:2.62:7.54		
B8-3	Si											456	1.00;1.65:4.20		
B8-4	Si											383	1.00:2.52:5.32		
B9-1	MgO	39	125	59	80	840	15					265	1.00:1.87:9.55		
B9-2	MgO											241	1.00:1.94:9.33		
B9-3	Si											156	1.00:2.02:8.75		
B9-4	Si											218	1.00:2.07:11.2		
B10-1	MgO	31	125	66	90	775	5					200	1.00:1.80:8.40		
B10-2	MgO											192	1.00:1.85:8.20		
B10-3	Si											200	1.00:2.16:10.3		
B10-4	Si											209	1.00:1.86:9.44		
B11-1	MgO	65	75	34	100	775	15					381	1.00:1.94:6.82	not on well	T is all over
B11-2	Si											399	1.00:1.92:6.00		
B11-3	Si											417	1.00:1.92:6.53		
B12-1	MgO	47	125	55	100	915	25					335	1.00:1.91:9.50		
B12-2	Si											206	1.00:1.88:4.06		
															rf plsma, raise gun

Table E.1: Off-axis composite target sputtering

Samp	Subs	Rate	P	Ar	Gun	Tdep	%	R on	R=0	Tons	Tcmp	thick	Y:Ba:Cu	Sample	Other
		Å/hr	(mT)	flow	Watts	(C)	oxy	(K)	(K)	mag	mag	(A)		comments	Comments
B13-1	MgO		150	65	100	840	25								
B13-2	MgO														
B13-3	STO														
B14-1	MgO		150	69	100	amb	25							post annealed	plasma prblms
B14-2	MgO														
B14-3	STO														
B15-1	MgO		150	74	85	650	10							post annealed	
B15-2	MgO														
B15-3	STO														
															Gun twisted
															less
B16-1a	MgO	113	150	74	85	840	10					1467	1.00:1.99:5.03		
B16-1b															
B16-2	MgO													film nonunfrm	
B16-3	STO							91	86	88	86				
B17-1a	MgO		100	45	85	840	10					1800	1.00:1.61:2.22		
B17-1b	MgO											1612	1.00:1.76:2.66		
B17-2a	MgO														
B17-2b	MgO														
B17-3	STO							85	73						
B18-1	STO		175	88	85	840	10								
B18-3	MgO														
B18-4	LAO														

Table E.1: Off-axis composite target sputtering

Samp	Subs	Rate	P	Ar	Gun	Tdep	%	R on	R=0	Tons	Tcmp	thick	Y:Ba:Cu	Sample	Other
		Å/hr	(mT)	flow	Angle	(C)	oxy	(K)	(K)	mag	mag	(A)		comments	Comments
															new target
															new gun
B19-1	STO	279	150	75	5	775	15	84	28			3214	1.00:1.67:2.41		
B19-2	STO														
B20-1	STO	215	175	77	5	880	25	87	74?			1981	1.00:1.71:2.50		
B20-2	STO							85	74			1825	1.00:1.77:2.44		
B20-3	STO							86	74			1807	1.00:1.72:2.47		
B20-4	LAO							87	82						
B21-1	STO	247	200	110	5	840	5	85	65			2399	1.00:2.19:2.88		
B21-2	STO														
B21-3	STO													fell off	
B22-1	STO	242	150	73	5	775	15	84	19			1974	1.00:1.67:2.49		
B22-2	STO											2045	1.00:1.68:2.52		
B22-3	STO														
															moved gun
B23-1	STO	188	150	66	15	840	25	79	66						
B23-2	STO							87	72						
B23-3	STO							84	69			1864	1.00:1.74:2.34		
B24-1	STO		175	90	15	775	5	86	68						*cool dwn
B24-2	STO	181						85	70			1850	1.00:1.77:2.72		failure
B24-3	STO														
B25-1	STO	153	200	100	15	880	15					1889	1.00:1.90:3.16		
B25-2	STO							85??	14			3094	1.00:1.65:2.47	??	

Table E.1: Off-axis composite target sputtering

Samp	Subs	Rate	P	Ar	Gun	Tdep	%	R on	R=0	Tons	Tcmp	thick	Y:Ba:Cu	Sample	Other
		Å/hr	(mT)	flow	Angle	(C)	oxy	(K)	(K)	mag	mag	(A)		comments	Comments
B25-3	STO											1573	1.00:1.92:2.63		
B26-1	STO	158	175	95	15	775	5	84	67			2038	1.00:2.03:2.87		
B26-2	STO														
B26-3	STO											1931	1.00:2.04:2.86		
															moved gun
B27-1	STO	164	150	78	25	880	15					1354	1.00:1.97:2.44		
B27-2	STO							84	81			1531	1.00:1.89:2.36		
B27-3	STO							84	82						
B28-1	STO	150	175	85	25	840	15					1279	1.00:1.89:2.53		
B28-2	STO							83	78			1485	1.00:1.91:2.51		
B28-3	STO														
B29-1	STO	144	200		25	775	25	86	69			1499	1.00:1.91:2.82		
B29-2	STO											1499	1.00:1.91:2.82		
B29-3	STO														
															moved gun
B30-1	STO	97	250		35	820	20	73	56						
B30-2	STO											1166	1.00:2.08:2.96		
B30-3	STO														
B31-1	STO		250	130	35	800	20								
B31-2	STO	95						82	65			1150	1.00:2.07:2.77		
B31-3	STO							83	66						
B32-1	STO		250	120	35	820	30	88	78						

Table E.1: Off-axis composite target sputtering

Samp	Subs	Rate	P	Ar	Gun	Tdep	%	R on	R=0	Tons	Tcmp	thick	Y:Ba:Cu	Sample	Other
		Å/hr	(mT)	flow	Angle	(C)	oxy	(K)	(K)	mag	mag	(A)		comments	Comments
B32-2	STO	75*										900*	1.00:1.94:2.80	* cracked	
B33-1	STO		250	135	35	820	20								
B33-2	STO	91*										600*	1.00:2.00:2.90	* cracked	
B34-1	STO		250	125	35	800	30	76	62						
B34-2	STO	110*						85	69			1250	1.00:2.03:2.90		
B35-1	STO		250		35	810	50								system fail
B35-2	STO														
B36-1	STO	57	250	108	35	810	60	78	75						
B36-2	STO											687	1.00:2.14:3.03		
B36-3	STO														
B37-1	STO	57	250	94	35	810	80	90	79						
B37-2	STO											641	1.00:2.17:2.95		
B37-3	STO														
B38-1	STO	58	250	107	35	840	60	87	76						
B38-2	STO											773	1.00:2.24:3.01		
B38-3	STO											787	1.00:2.37:3.19		
B39-1	STO	48	250	95	35	840	80	85	79						
B39-2	STO							83	80			684	1.00:2.31:3.25		
B39-3	STO														

Table E.1: Off-axis composite target sputtering

Samp	Subs	Rate	P	Ar	Gun	Tdep	%	R on	R=0	Tons	Tcmp	thick	Y:Ba:Cu	Sample	Other
		Å/hr	(mT)	flow	Angle	(C)	oxy	(K)	(K)	mag	mag	(A)		comments	Comments
B40-1	STO		250	92	35	860	80								thru target
B40-2	STO														
B41-1	STO		250	90	35	860?	60	89	86						
B41-2	STO							90	86						
B42-1	STO		250	93	35	850	60	89	86						
B42-2	STO														
B42-3	LAO							91	89						
B42-4	MgO							85	50			1654	1.00:1.99:2.96	big, 2.2%Fe	
B43-1	STO		250	93	35	850	60								
B43-2	STO							88	76						
B43-3	LAO									90	80				
B43-4	MgO														
															system changed?
B44-1	STO	76	250	91	35	825	60								
B44-2	STO														
B44-3	LAO														
B44-4	LAO									72	65				
B44-5	LAO											1199	1.00:1.89:2.68	big, Fe<0.6%	
B44-6	LAO														
B45-1	LAO		250	91	35	850	60								
B45-2	LAO							85	77						
B45-3	LAO														
B45-4	LAO													EDS shows Fe	

Table E.1: Off-axis composite target sputtering

Samp	Subs	Rate	P	Ar	Gun	Tdep	%	R on	R=0	Tons	Tcmp	thick	Y:Ba:Cu	Sample	Other
		Å/hr	(mT)	flow	Angle	(C)	oxy	(K)	(K)	mag	mag	(A)		comments	Comments
B45-5	LAO									81	78	1204	1.00:2.10:2.80	Fe<3.0%	
															dark space
															distance lessened
B46-1	LAO	82	250		35	850	60								
B46-2	LAO							90	85			1336	1.00:1.98:2.94	Fe<0.9%	
B46-3	LAO														
B46-4	LAO									87	84				
B47-1	LAO		250		35	865	60	88	85						
B47-2	LAO							91	87						
B47-3	LAO									86	84				
B47-4	LAO														
B48-1	LAO		250		35	880	60	89	86						
B48-2	LAO									88	83				
B49-1	LAO	68	250		35	895	60	88	85			1051	1.00:2.19:3.07	Fe<1.0%	
B49-2	LAO														
B49-3	LAO									85	81				
B49-4	LAO														
B50-1	LAO	101	150		35	850	60					1481	1.00:1.85:2.76	1% Fe ??	
B50-2	LAO														
B50-3	LAO														
B50-4	LAO									<77					
B51-1	LAO	49	250		35	865	60			91	89	837	1.00:2.20:2.52		new pallet

Table E.1: Off-axis composite target sputtering

Samp	Subs	Rate	P	Ar	Gun	Tdep	%	R on	R=0	Tons	Tcmp	thick	Y:Ba:Cu	Sample	Other
		Å/hr	(mT)	flow	Angle	(C)	oxy	(K)	(K)	mag	mag	(A)		comments	Comments
B51-2	LAO							92	90	90.5	89				
B52-1	LAO	25	250		35	865	60			87	77			stripe	w/ mask
B52-2	LAO									91	80?	393	1.00:2.31:3.32	no stripe	
B53-1	LAO		250		35	865	60	90	86	87	77			stripe	w/ mask
B53-2	LAO													no stripe	
															through target
B54-1	LAO	100	250		35	850	60			81	77?	1623	1.00:1.95:2.64	3.6%Ta	
B54-2	LAO														
B54-3	LAO														
B54-4	LAO														
B54-5	LAO														
B55-1	LAO		250		35	850	60			82	79				new pallet
B55-2	LAO														
B55-3	LAO														
B55-4	LAO														
B56-1	LAO		250		35	875	60			89	85?				
B56-2	LAO														
B56-3	LAO														
B57-1	LAO	109	250		35	900	60			86	84				
B57-2	LAO											1731	1.00:1.98:2.97		
B57-3	LAO														
B57-4	LAO							87	84						

Table E.1: Off-axis composite target sputtering

Samp	Subs	Rate	P	Ar	Gun	Tdep	%	R on	R=0	Tons	Tcmp	thick	Y:Ba:Cu	Sample	Other
		Å/hr	(mT)	flow	Angle	(C)	oxy	(K)	(K)	mag	mag	(A)		comments	Comments
B58-1	LAO		250		35	875	60								back of new
B58-2	LAO									84	82				pallet
B58-3	LAO														
B59-1	LAO	28	250		35	825	60			<78				stripe (dark)	w/ mask
B59-2	LAO													slit(lite,fuzzy)	
B59-3	LAO									<78		460	1.00:2.14:0.22	no stripe (dark)	lots of Ta
B60-1	LAO	72	250		35	865	60								
B60-2	LAO														
B60-3	LAO									84	80				
B60-4	MgO											1181	1.00:2.03:2.92	1.9% Ta	
															improve mask
B61-1	LAO	23	250		35	850	60							stripe (lite)	
B61-2	LAO													slit(lite,sharp)	
B61-3	LAO									83	77	389	1.00:2.12:0.16	no stripe (mid)	lots of Ta
B62-1	LAO		250		35	775	60			90	77?				
B62-2	LAO									90	78?				
B62-3	LAO									<78					
B63-1	LAO	71	250		35	860	60			82	78				
B63-2	LAO														
B63-3	LAO														
B63-4	MgO											1070	1.00:2.08:3.20	<1.2% Ta	
B64-1	LAO		250		35	750	60			<78					

Table E.1: Off-axis composite target sputtering

Samp	Subs	Rate	P	Ar	Gun	Tdep	%	R on	R=0	Tons	Tcmp	thick	Y:Ba:Cu	Sample	Other
		Å/hr	(mT)	flow	Angle	(C)	oxy	(K)	(K)	mag	mag	(A)		comments	Comments
B64-2	LAO									<78					
B64-3	LAO														
B65-1	LAO	100	250		35	860	60			<78					
B65-2	LAO														
B65-3	LAO														
B65-4	MgO											1607	1.00:2.10:3.06	<1.2% Ta	
B66-1	LAO		250		35	860	60			<78					
B66-2	LAO														
B66-3	LAO														
B67-1	LAO		250		35	775	60			<78					
B67-2	LAO														
B67-3	LAO														
															new target
															system changes
B68-1	LAO	51	250			865	60			81	<78				
B68-2	MgO											703	1.00:2.10:2.53		
B69-1	LAO		250			880	60			82	78				
B69-2	LAO														
B69-3	LAO														
B70-1	LAO		250			800	60			73?					w/ mask
B70-2	LAO														
B70-3	LAO									79					

Table E.1: Off-axis composite target sputtering

Samp	Subs	Rate	P	Ar	Gun	Tdep	%	R on	R=0	Tons	Tcmp	thick	Y:Ba:Cu	Sample	Other
		Å/hr	(mT)	flow	Angle	(C)	oxy	(K)	(K)	mag	mag	(A)		comments	Comments
B71-1	LAO		250			880	60			80	<78				
B71-2	LAO														
B71-3	LAO														
B72-1	LAO		250			775	60			76					w/ mask
B72-2	LAO														
B72-3	LAO									66					
															twist gun more
B73-1	LAO		250			880	60			76	70				
B73-2	LAO											530	1.00:2.14:2.77		
B73-3	MgO														
															twist gun less
B74-1	LAO		250			880	60			<78					
B74-2	LAO														
B74-3	MgO											877	1.00:2.18:2.87		
															switched guns
B75-1	LAO		250			880	60			<78					plasma
B75-2	STO									<78					failure
B76-1	LAO		250			880	60			79					
B76-2	STO									<78					
B77-1	LAO		365			880	60			67					
B77-2	LAO														
B78-1	LAO		250			880	60								
B78-2	LAO														

Table E.1: Off-axis composite target sputtering

References

(1) Olin Metals Research Laboratories, New Haven, CT.

(2) Kurt J. Lesker Co., Clairton, PA.

(3) Advanced Energy Industries, Fort Collins, CO.

(4) Haynes International, Inc., Kokomo, IN.

(5) CTI Cryogenics, Waltham, MA.

(6) Leybold Inc., San Jose, CA.

(7) Westinghouse Science and Technology Center, Pittsburgh, PA.

Akutsu, N., M. Fukutomi, K. Katoh, H. Takahara, Y. Tanaka, T. Asano, and H. Maeda, Jpn. J. App. Phys. **29**, L604 (1990).

Anderson, A., private communication.

Anderson, P.W., *Supercurrents*, Aug, p. 2 (1988).

Anderson, P.W. and Z. Zou, Phys. Rev. Lett. **60**, 132 (1988).

Bardeen, J., L.N. Cooper, and J.R. Schrieffer, Phys. Rev. **108**, 1175 (1957).

Barner, J.B., C.T. Rogers, A. Inam, R. Ramesh, S. Bersey, Appl. Phys. Lett. **59**, 742 (1991).

Batlogg, B., R.J. Cava, A. Jayaraman, R.B. van Dover, G.A. Kourouklis, S. Sunshine, D. W. Murphy, L.W. Rupp, H.S. Chen, A. White, K.T. Short, A.M. Mujsce, and E.A. Rietman, Phys. Rev. Lett. **58**, 2333 (1987).

Batlogg, B., *Physics Today*, Jun, p. 44 (1991).

Bean, C.P., Rev. Mod. Phys. **36**, 31 (1964).

Beasley, M., Proc. IEEE **77**, 1155 (1989).

Bednorz, J.G. and K.A. Mueller, Z. Phys. B **64**, 189 (1986).

Bednorz, J.G. and K.A. Mueller, Rev. Mod. Phys. **60**, 585 (1988).

Beyers, R. and T. M. Shaw, in Solid State Physics Vol. 42, H. Ehrenreich and D. Turnbull, Eds., Academic Press, Inc., New York, p. 135 (1989).

Bormann, R., and J. Nolting, Appl. Phys. Lett. **54**, 2148 (1989).

Bourne, L.C., M.F. Crommie, A. Zettl, H.C. Loye, S.W. Keller, K.L. Leary, A.M. Stacy, K.J. Chang, M.L. Cohen, and D.E. Morris, Phys. Rev. Lett. **58**, 2337 (1987).

Brandt, N.B., S.V. Kuoshiunikov, A.P. Rusakov, and V.M. Semenor, JETP Lett. **27**, 33 (1978).

Cava, R.J., B. Batlogg, R. B. van Dover, D. W. Murphy, S. Sunshine, T. Siegrist, J. P. Remeika, E. A. Rietman, S. Zahurak, and G. P. Espinosa, Phys. Rev. Lett. **58**, 1676 (1987).

Chang, C.C., X. D. Wu, A. Inam, D. M. Hwang, T. Venkatesan, P. Barboux, and J. M. Tarascon, Appl. Phys. Lett. **53**, 517 (1988).

Char, K., A. D. Kent, A. Kapitulnik, M. R. Beasley, and T. H. Geballe, Appl. Phys. Lett. **51**, 1370 (1987).

Char, K., M.S. Colcloigh, S.M. Garrison, N. Newman, and G. Zaharchuk, Appl. Phys. Lett. **59**, 733 (1991).

Chaudhari, P., R. H. Koch, R. B. Laibowitz, T. R. McGuire, and R. J. Gambino, Phys. Rev. Lett. **58**, 2684 (1987).

Clark, G.J., F. K. LeGoues, A. D. Marwick, R. B. Laibowitz, and R. Koch, Appl. Phys. Lett. **51**, 1462 (1987).

Dalichaouch, Y., M.S. Torikachvili, E.A. Early, B.W. Lee, C.L. Seaman, K.N. Yang, H. Zhou, and M.B. Maple, Solid State Commun. **65**, 1001 (1988).

Dalrymple, B.J., Ph. D. Thesis, Yale University (1983).

Dimos, D., P. Chaudhari, J. Mannhart, and F. LeGoues, Phys. Rev. Lett. **61**, 219 (1988).

DiIorio, M.S., S. Yoshizumi, K.-Y. Yang, J. Zhang, and M. Maung, Appl. Phys. Lett. **58**, 2552 (1991).

Dinger, T.R., T.K. Worthington, W.J. Gallagher, and R.L. Sandstrom, Phys. Rev. Lett. **58**, 2687 (1987).

Edwards, J.A., J.S. Satchell, N.G. Chew, R.G. Humphreys, M.N. Keene, and O.D. Dosser, Appl. Phys. Lett. **60**, 2433 (1992).

Ekin, J.W., A.J. Panson, and B.A. Blankenship, Appl. Phys. Lett. **52**, 331 (1988).

Enami, H., T. Shinohara, N. Kawahara, S. Kawabata, H. Hoshizaki, and T. Imura, Jpn. J. App. Phys. **29**, L782 (1990).

Eom, C.B., J. Z. Sun, K. Yamamoto, A. F. Marshall, K. E. Luther, T.H. Geballe, and S. S. Laderman, Appl. Phys. Lett. **55**, 595 (1989).

Fardnanesh, M., K. Scoles, A. Rothwarf, E. Sanchez, E. Brosha, and P. Davies, AIP Conf. Proc. **251**, 283 (1991).

Fiory, A.T., A.F. Hebard, P.M. Mankiewich, and R.E. Howard, Appl. Phys. Lett. **52**, 2165 (1988).

Forrester, M.G., J. Talvacchio, J.R. Gavaler, M. Rooks, and J. Lindquist, IEEE Trans. Magn. **27** No. 2, 3098 (1991).

Freeman, A.J., J. Yu, S. Massidda, in Mechanisms of High Temperature Superconductivity, H. Kamimura and A. Oshiyama, Eds., Springer-Verlag, Berlin, p. 99 (1989).

Fueki, K., K. Kitazawa, K. Kishio, T. Hasegawa, S. Uchida, H. Tagagi, and S. Tanaka, in Chemistry of High Temperature Superconductors, D.L. Nelson, M.S. Whittingham, and T.F. George, Eds., American Chemical Society, Washington D.C., p. 38 (1987).

Fujimori, A., in Mechanisms of High Temperature Superconductivity, H. Kamimura and A. Oshiyama, Eds., Springer-Verlag, Berlin, p. 176 (1989).

Gavaler, J.R., Appl. Phys. Lett. **23**, 480 (1973).

Gavaler, J.R., J. Talvacchio, T.T. Braggins, M.G. Forrester, and J. Greggi, J. Appl. Phys. **70**, 4383 (1991).

Gergis, I.S., J.T. Cheung, T.N. Trinh, E.A. Sovero, and P.H. Kobrin, Appl. Phys. Lett. **60**, 2026 (1992).

Giaever, I., Phys. Rev. Lett. **5**, 147 (1960).

Ginzburg, V.L., and L.D. Landau, JETP **20**, 1064 (1950).

Gor'kov, L.P., JETP **9**, 1364 (1959).

Hashimoto, T., M. Sagoi, Y. Mizutani, J. Yoshida, and K. Mizushima, Appl. Phys. Lett. **60**, 1756 (1992).

Hass, K.C., in Solid State Physics Vol. 42, H. Ehrenreich and D. Turnbull, Eds., Academic Press, Inc., New York, p. 213 (1989).

Hawley, M., I. D. Raistrick, J.G. Beery, and R. Houlton, Science **251**, 1587 (1991).

Hebard, A.F., M.J. Rosseinsky, P.C. Haddon, D.W. Murphy, S.H. Glarum, T.T.M. Palstra, A.P. Ramirez, and A. R. Kortan, Nature **350**, 600 (1991).

Hewat, E.A., M. Dupuy, A. Bourret, J.J. Capponi, and M. Marezio, Solid State Commun. **64**, 517 (1987).

Hirata, K., K. Yamamoto, K. Iijima, J. Takada, T. Terashima, Y. Bando, and H. Mazaki, Appl. Phys. Lett. **56**, 683 (1990).

Hirsch, J.E., in Mechanisms of High Temperature Superconductivity, H. Kamimura and A. Oshiyama, Eds., Springer-Verlag, Berlin, p. 34 (1989).

Inam, A., C.T. Rogers, R. Ramesh, K. Resching, L. Farrow, D. Hart, and T. Venkatesan, Appl. Phys. Lett. **57**, 2484 (1990).

Jorgenson, J.D., M.A. Beno, D.G. Hinks, L. Soderholm, K.J. Volin, R.L. Hitterman, J.D. Grace, I.K. Schuller, C.U. Segre, K. Zhang, and M.S. Kleefisch, Phys. Rev. B **36**, 3608 (1987).

Josephson, B.D., Phys. Letters **1**, 251 (1962).

Kingston, J.J., F.C. Wellstood, P. Lerch, A.H. Miklich, and J. Clarke, Appl. Phys. Lett. **56**, 189 (1990).

Kirlin, P., AIP Conf. Proc. **251**, 175 (1991).

Kozlowski, G., C.E. Oberly, J. Ho, and R. Leese, IEEE Trans. Magn. **27** No. 2, 901 (1991).

Kubinski, D.J., D.W. hoffman, R.E. Soltis, and E.M. Logothetis, J. Appl. Phys. **71**, 1860 (1992).

Kuroda, K., K. Kojima, M. Tanioka, K. Yokoyama, and K. Hamanaka, Jpn. J. App. Phys. **28**, 1797 (1989).

Kwo, J., M. Hong, D.J. Trevor, R.M. Fleming, A.E. White, R.C. Farrow, A.R. Kortan, and K.T. Short, Appl. Phys. Lett. **53**, 2683 (1988).

Lathrop, D.K., S. E. Russek, and R. A. Buhrman, Appl. Phys. Lett. **51**, 1554 (1987).

Li, H.C., G. Linker, F. Ratzel, R. Smithey, and J. Geerk, Appl. Phys. Lett. **52**, 1098 (1988).

Li, Q., O. Meyer, X.X. Xi, J.Geerk, and G. Linker, Appl. Phys. Lett. **55**, 310 (1989).

Liu, J.Z., G.W. Crabtree, A. Umezawa, and Li Zongquan, Phys. Lett. A **121**, 305 (1987).

Maeda, M., Y. Tanaka, M. Fukutomi, and A. Asano, Jpn. J. App. Phys. **27**, L209 (1988).

Mattheiss, L.F., E.M. Gyorgy, and D.W. Johnson Jr., Phys. Rev. B **37**, 3745 (1988).

Matijasevic, V., P. Rosenthal, K. Shinohara, A. F. Marshall, R. H. Hammond, and M. R. Beasley, J. Mater. Res. **6**, 682 (1991).

Meissner, W. and R. Ochsenfeld, Naturwiss. **21**, 787 (1933).

Micnas, R., J. Ranninger, and S. Robaszkiewicz, Rev. Mod. Phys. **62**, 113 (1990).

Migliuolo, M., R. M. Belan, and J. A. Brewer, Appl. Phys. Lett. **56**, 2572 (1990).

Missert, N., R. H. Hammond, J. E. Mooij, V. Matjasevic, P. Rosenthal, T. H. Geballe, A. Kapitulnik, M. R. Beasley, S. S. Laderman, C. Lu, E. Garwin, and R. Barton, IEEE Trans. Magn. **25**, 2418 (1989).

Neal, M.J. and V.M. Pathare, IEEE Trans. Magn. **27** No. 2, 1652 (1991).

Neiser, R.A., J.P. Kirkland, W.T. Elam, H. Herman, S. Rangaswamy, V.M. Letourneau, and M. Osofsky, Mat. Res. Soc. Symp. Proc. **99**, 689 (1988).

Numata, K., K. Hoshino, Y. Yoshida, K. Inoue, H. Maeda, Y. Kamekawa, and M. Suzuki, AIP Conf. Proc. **251**, 418 (1991).

Ogg, R.A., Phys. Rev. **69**, 243 (1946).

Ogushi, T., K. Obara, and T. Anayama, Jpn. J. App. Phys. **22**, L523 (1983).

Oh, B., M. Naito, S. Arnason, P. Rosenthal, R. Barton, M. R. Beasley, T. H. Geballe, R. H. Hammond, and A. Kapitulnik, Appl. Phys. Lett. **51**, 852 (1987).

Oh, B., R. H. Koch, W. J. Gallagher, R. P. Robertazzi, and W. Eidelloth, Appl. Phys. Lett. **59**, 123 (1991).

Onnes, H.K., Leiden Comm. 120b, 122b, 124c (1911).

Ono, R.H., J.A. Beall, M.W. Cromar, T.E. Harvey, M.E. Johansson, C.D. Reintsemn, and D.A. Rudman, Appl. Phys. Lett. **59**, 1126 (1991).

Oseroff, S.B., D.C. Vier, J.F. Smyth, C.T. Salling, S. Schultz, Y. Dalichaouch, B.W. Lee, M.B. Maple, Z. Fisk, J.D. Thompson, J.L. Smith, and E. Zirngiebl, Solid State Commun. **64**, 241 (1987).

Ozhogin, V., private communication.

Parks, R.D. (ed.), Superconductivity, vols I and II, Marcel Dekker, Inc., New York (1969).

Phillips, J., to appear in Superconducting Engineering in the AIChE Symposium Series (1992).

Pickett, W.E., Rev. Mod. Phys. **61**, 433 (1989).

Rice, C.E., R.B.van Dover, and G.J. Fisanick, Appl. Phys. Lett. **51**, 1842 (1987).

Rogers, C.T., A. Inam, M.S. Hegde, B. Dutta, X.D. Wu, and T. Venkatesan, Appl. Phys. Lett. **55**, 2032 (1989).

Rossnagel, S.M., and J. J. Cuomo, AIP Conf. Proc. **165**, 106 (1988).

Sagoi, M., Y. Terashima, K. Kubo, Y. Mizutani, T. Miura, J. Yoshida, and K. Mizushima, Jpn. J. App. Phys. **28**, L444 (1989).

Scharen, M.J., A.H. Cardona, J.Z. Sun, L.C. Bourne, and J.R. Schrieffer, Jpn. J. App. Phys. **30**, L15 (1991).

Scheuermann, M., C. C. Chi, C. C. Tsuei, D. S. Yee, J. J. Cuomo, R. B. Laibowitz, R. H. Koch, B. Braren, R. Srinivasan, and M. M. Plechaty, Appl. Phys. Lett. **51**, 1951 (1987).

Sheng, Z.Z. and A.M. Hermann, Nature **332**, 138 (1988).

Shinohara, K., F. Munukata, M. Yamanaka, V. Matijasevic, P. Rosenthal, R. Hammond, M. Beasley, Jpn. J. App. Phys. **31**, L160 (1992).

Silver, R.M., A. B. Berezin, M. Wendman, and A. L. deLozanne, Appl. Phys. Lett. **52**, 2174 (1988).

Simon, R., Sol. St. Tech. **32** No. 9, 141 (1989).

Simon, R., *Physics Today*, Jun, p. 64 (1991).

Sleight, A., *Physics Today*, Jun, p. 24 (1991).

Specht, E.D., C.J. Sparks, A.G. Dhere, J. Brynestad, O.B. Cavin, D.M. Kroeger, and H.A. Oye, Phys. Rev. B **37**, 7426 (1988).

Steinberg, R.N., J.D. McCambridge, D.E. Prober, and B.M. Guenin, AIP Conf. Proc. **251**, 146 (1991).

Tanaka, S., H. Nakanishi, K. Higaki, and H. Itozaki, Jpn. J. App. Phys. **29**, 1059 (1990).

Tarascon, J.M., W.R. McKinnon, L.H. Greene, G.W. Hull, and E.M. Vogel, Phys. Rev. B **36**, 226 (1987).

Terashima, T., K. Iijima, K. Yamamoto, Y. Bando, and H. Mazaki, Jpn. J. App. Phys. **27**, L91 (1988).

Tinkham, M., Introduction to Superconductivity, Robert E. Krieger Publishing Co., Huntington, New York (1975).

Tozer, S.W., A.W. Kleinsasser, T. Penney, D. Kaiser, and F. Holtzberg, Phys. Rev. Lett. **59**, 1768 (1987).

Tranquada, J.M., A.H. Moudden, A.I. Goldman, P. Zolliker, D.E. Cox, G. Shirane, S.K. Sinha, D. Vaknin, D.C. Johnston, M.S. Alvarez, A.J. Jacobson, J.T. Lewandowski, and J.M. Newsam, Phys Rev B **38**, 2477 (1988).

Tzeng, Y., A. Holt, R. Ely, Appl. Phys. Lett. **52**, 155 (1988).

Uemura, Y. J., L.P. Le, G.M. Luke, B.J. Sternleib, W.D. Wu, J.H. Brewer, T.M.Riseman, C.L. Seaman, M.P. Maple, M. Ishikawa, D.G. Hinks, J.D. Jorgenson, G. Saito, and H. Yamochi, Phys. Rev. Lett. **66**, 2665 (1991).

Valles, Jr., J.M., A. E. White, K. T. Short, R. C. Dynes, J. P. Garno, A. F. J. Levi, M. Anzlowar, and K. Baldwin, Phys. Rev. B **39**, 11599 (1989).

Van Duzer, T. and C.W. Turner, Principles of Superconducting Devices and Circuits, Elsevier North Holland, New York (1981).

Vossen, J.L. and J.J. Cuomo, in Thin Film Processess, J.L. Vossen and W. Kern, Eds., Academic Press, Inc., New York, p. 12 (1978).

Weinberger, B.R., L. Lynds, J. Van Valzah, H.E. Eaton, J.R. Hull, T.M. Mulcahy, S.A. Basinger, IEEE Trans. Magn. **27** No. 2, 2415 (1991).

Witanachchi, S., H. S. Kwok, X. W. Wang, and D. T. Shaw, Appl. Phys. Lett. **53**, 234 (1988).

Wu, M.K., J.R. Ashburn, C.J. Torng, P.H. Hor, R.L. Meng, L. Gao, Z.J. Huang, Y.Q. Wang, C.W. Chu, Phys. Rev. Lett. **58**, 908 (1987).

Xi, X.X., T. Venkatesan, Q. Li, X.D. Wu, A. Inam, C.C. Chang, R. Ramesh, D. M. Hwang, T.S. Ravi, A. Findikoglu, D. Hemmick, S. Etemad, J. A. Martinez, and B. Wilkens, IEEE Trans. Magn. **27** No. 2, 912 (1991).

Yin, G.Z., and D.W. Jillie, Sol. St. Tech. **30** No. 5, 127 (1987).

Zhang, K., B. Dabrowski, C.U. Segre, D.G. Hinks, I.K. Schuller, J.D. Jorgenson, and M. Slaski, J. Phys. C. **20**, L935 (1987).

Zhou, L., P. Zhang, P. Ji, K. Wang, and X. Wu, IEEE Trans. Magn. **27** No. 2, 912 (1991).